OPTICAL SYSTEMS TO EVALUATE VOLUME OF MEDICAL SAMPLES IN OPAQUE TEST TUBES

by

Xin Liu

A dissertation submitted to the faculty of
The University of Utah
in partial fulfillment of the requirements for the degree of

Doctor of Philosophy

Department of Mechanical Engineering

The University of Utah

August 2011

ProQuest LLC.
789 East Eisenhower Parkway
P.O. Box 1346
Ann Arbor, MI 48106 - 1346

The University of Utah Graduate School

STATEMENT OF DISSERTATION APPROVAL

The dissertation of **Xin Liu**

has been approved by the following supervisory committee members:

Eberhard Bamberg	, Chair	**05/11/2011** Date Approved
Stacy Morris Bamberg	, Member	**05/11/2011** Date Approved
Bruce Gale	, Member	**05/11/2011** Date Approved
William Roberts	, Member	**05/11/2011** Date Approved
Douglas A. Christensen	, Member	**05/11/2011** Date Approved

and by **Tim Ameel**, Chair of the Department of **Mechanical Engineering**

and by Charles A. Wight, Dean of The Graduate School.

ABSTRACT

Measuring volume in medical samples without removing the cap of the tube is an important first step in highly automated biomedical laboratories. The variations of liquid properties, tube material, and number as well as location of labels attached to the outside of the test tube are the key points that prevent use of most traditional methods. Research into optical level detection was conducted to resolve the above issues. The research focuses on the optical detection of liquid level and volume of medical samples in the test tubes that are covered by an unknown number of labels. It has been carried out at the Precision Design Laboratory in the Department of Mechanical Engineering at University of Utah since 2006. The project is funded by the ARUP Institute for Clinical and Experimental Pathology® (ARUP).

This research mainly investigates optical methods that detect the liquid level through the side of the test tube. By analyzing the change of power of transmitted light, which passes through the sample, the location of the interface between air and liquid inside the test tube is determined.

To study the effect of loss of light through sample tubes, the propagation process is modeled and simulated through a ray tracing method. Experiments were conducted to verify the modeling and simulation.

In this research, two detection principles based on the light propagation principle were developed, and their application systems were prototyped. The first one is a Max/Min Level Detection System, which can verify the minimum and maximum liquid levels in test tubes by computing the power ratio of two wavelengths. The second system is referred to as a Volume Detection System, which takes into account the volume of the meniscus by identifying the height and position of the meniscus.

In order to determine the liquid volume in different types of test tubes by the liquid level, a machine vision system was developed to identify the type of tube and retrieve the relevant geometric data from a database. An experimental prototype was set up and experiments were conducted to verify the functionality of the system.

TABLE OF CONTENTS

LIST OF TABLES

Table Page

ACKNOWLEDGMENTS

I would like to heartily thank the guidance and support from my advisor, Dr. Eberhard Bamberg. His ideas, patience, and encouragement have allowed me to finish this work.

I would also like to thank the other members of my committee, Dr. Stacy Bamberg, Dr. William Roberts, Dr. Bruce Gale and Dr. Douglas Christensen, whose guidance led me to develop a main part of this work, the modeling of the meniscus and its effect on the level detection process.

I have been very fortunate to work with many outstanding graduate students in the Precision Design Lab. I would also like to thank Dinesh Rakwal, Sumet Heamawatanachai, and Sangju Lee for their help and many useful discussions related to this work. I would like to thank Brendan Corbin and Tom Ross for their help in the area of fabrication and equipment. I would like to extend heartfelt thanks for their friendship.

I would like acknowledge the financial support of the project from the ARUP Institute for Clinical and Experimental Pathology®. Particular thanks go to Dr. Charles Hawker and Dr. William Roberts for their expertise in testing medical samples as well as William Owen for providing and characterizing the medical samples used in this research.

I wish to express my love and gratitude to my parents, sisters and wife. Their understanding and endless love let me persevere with my dream/ideals. All my success belongs to them.

Lastly, I offer my regards and blessings to all of those who supported me in any respect during the study in Utah.

CHAPTER 1

INTRODUCTION

1.1 Background and significance of the research

This research focuses on the optical detection of liquid level and volume of medical samples in test tubes that are covered by an unknown number of labels, which are attached the outside of test tubes to identify samples. It has been carried out at the Precision Design Lab in the Department of Mechanical Engineering at University of Utah since 2006. The project is funded by the ARUP Institute for Clinical and Experimental Pathology® (ARUP). All technical requirements and medical samples used in this project are provided by ARUP.

ARUP is a national clinical and anatomic pathology reference laboratory. It offers more than 2,000 tests and test combinations to hospital clinical laboratories and other reference laboratories throughout the United States and several other countries. Approximately 40–45,000 specimens are sent to ARUP every day. In order to meet the increasing demands of testing patient samples and reduce the costs, ARUP decided to develop fast, automated testing lines to analyze the liquid medical samples in tubes. The largest section is called the Automated Core Laboratory, which deals with approximately 25% of specimens (Hawker *et al.* 2007; Hawker *et al.* 2002a, b).

To ensure the safety and reliability of testing, it is necessary to verify the volume level of the liquid without removing the tube cap prior to testing. If the liquid level is too high or too low it could cause problems in the subsequent testing process. For example, if the liquid level is above the maximum allowable level, the liquid in the tubes might spill over when the caps are removed. This is potentially dangerous because the liquid may present a biohazard. On the other hand, if the liquid level is below the minimum level required, there will not be enough volume for the tests. Furthermore, if the automated tester is programmed to advance the probe until it contacts the liquid, the probe might touch the bottom of the tube and damage the detection system. To avoid these problems and to guarantee that the testing system works effectively and safely, it is important to determine whether the liquid level in the tubes is below a minimum or above a maximum allowable level before the samples are tested.

To meet the above basic requirement and to improve the efficiency of the testing facility, a detection system called Max/Min Level Detection System, which can verify the minimum and maximum liquid levels in test tubes, is desired. This system will be able to determine whether the volume of liquid in the test tubes is too low or too high to be subjected to automated testing. The test tubes with too much or too little liquid are removed from automatic testing and tested by manual inspection. This avoids the unexpected damage that might occur if the probe touches the bottom of tubes, or the spillage of the liquid.

To further improve the automatic testing system, a Volume Detection System was developed. Compared with the Max/Min Level Detection System, this system can detect the actual liquid volume in test tubes. By obtaining the value of liquid volume, the

automatic testing system can also directly assign the probe a specific position to imbibe in a required volume of liquid for the next step of the analysis.

1.2 Objectives and scope of the research

There are two main objectives that need to be met in this research. The final result should be delivered as a product that can be used in the actual testing facility. Because the system will be used to detect medical samples in testing labs, there will be additional safety requirements in addition to the technical requirements.

1.2.1 Objective 1 and requirements

The first main objective of this research is to develop a novel opto-mechanical system that can detect if a medical sample in a labeled test tube is at the correct level. This new system is called Max/Min Level Detection System. It must meet the following safety requirements from ARUP.

1.2.1.1 Measurement uncertainty

For the Max/Min Level Detection System, ARUP sets that the maximum allowable volume can be adjusted from 3.9 to 4.0 mL with an uncertainty ±0.1 mL, and the acceptable minimum volume is adjustable from 0.3 to 0.4 mL with an uncertainty ±0.1 mL. As illustrated in Fig. 1-1, the measurement uncertainty of volume for both levels translates to a maximum height uncertainty of ±0.75 mm for standard tubes with a diameter of 13.0 mm.

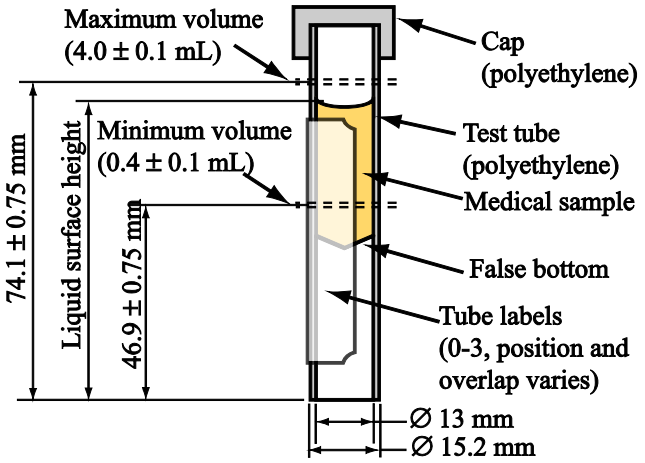

Fig. 1-1 The allowable minimum and maximum volume translates to two distinct liquid levels at 46.9 ±0.75 mm and 74.1 ±0.75 mm (Liu *et al.* 2008).

In this research, the maximum allowable volume is set to 4.0 mL, and the acceptable minimum volume is 0.4 mL to verify the system. The Max/Min Level Detection System determines the results by the volume/level of liquid (see Table 1-1).

The test tubes detected as low or high are picked out for manual inspection. Others will be sent to the automatic tester.

1.2.1.2 Unknown number of labels

The cylindrical test tubes have labels attached to their sides to identify the samples. In order to meet ARUP requirements, a detection system must be able to inspect test tubes with multiple labels.

Table 1-1 The detection result based on liquid volume

Volume of liquid (mL)	Height of level (mm)	Result of detection
<0.3	<46.15	Low
0.3~0.5	46.15~47.65	Low/OK
0.5~3.9	47.65~73.35	OK
3.9~4.1	73.35~74.85	OK/High
>=4.1	>=74.85	High

In practice, the number of labels can range from one to three[1]. In addition, the labels may or may not overlap, as shown in Fig. 1-2, resulting in anywhere from zero to six layers that can obstruct the optical path of the measurement. These labels also absorb light, and the absorption is affected by the thickness of layers. As a result, the effect of labels must be considered at the time of measurement. Because a standard sample or a predetermined curve method is not practical, the Max/Min Volume Detection System uses the power ratio of two wavelengths to verify the presence of liquid.

1.2.1.3 Short detection time

The ARUP's desired throughput of the system is 2,000 tubes per hour, allowing only 1.8 seconds to measure the volume of each tube.

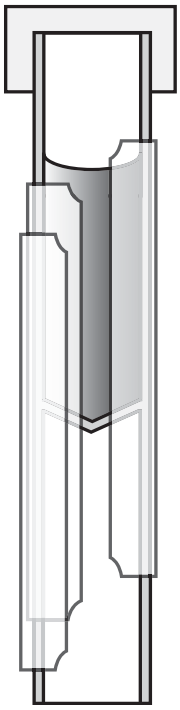

Fig. 1-2 Labels are attached to the outside of the test tube at different heights

[1] New requirement reduces to one to two labels.

This time, however, includes the time required to handle the tube, which is estimated at 1.0 seconds. As such, the Max/Min Level Detection System makes a determination in no more than 0.8 seconds.

1.2.1.4 Safety for operators and samples

To guarantee the safety of the operators and the purity of the samples, ARUP requires that biological materials contained in the samples should neither taint the test device nor be tainted by the device. Also, the detection process must not affect the sample properties or its bioactivity.

To meet these requirements, the Max/Min Volume Detection System detects test tubes through noncontact detection. Considering the biological effect of electromagnetic fields, this system uses an optical detection method, rather than a capacitance- or inductance-based detection.

Other ARUP requirements such as reliability, life time and structural strength are also met by the Max/Min Volume Detection System as well.

1.2.2 Objective 2 and requirements

The second objective of this research is to determine the volume of the medical sample in tubes to which an unknown number of labels have been attached. This new system, referred to as the Volume Detection System, will use two light wavelengths to scan the entire height of tubes that are covered by an unknown number of labels. By detecting the shape and position of the meniscus that is formed at the liquid/air interface,

the system can determine the volume of liquid in the tube. Because the test tubes include nonstandard tubes that vary in size and shape, it will be necessary for this system to identify the type of tube as part of the volume detection. The Volume Detection System needs to meet the following system requirements:

1.2.2.1 Uncertainty of measurement

As with the Max/Min Level Detection System, the measurement uncertainty of volume of this measurement system must be less than ±0.1 mL. By taking the volume of the meniscus into account, this system can reach a ±0.06 mL measurement uncertainty.

1.2.2.2 Labels and prints

As with the Max/Min Level Detection System, the Volume Detection System is based on the power change of transmitted light during the scanning process. The unknown numbers of labels presents two potential problems for detecting the volume of the liquid.

First, the absorption of labels and print reduces the power of the light reaching the detector and may result in detection error. This must be considered at the time of the measurement. This system use infrared light sources to eliminate the effect of the print.

Second, the thickness of the labels must be considered when the type of test tube is determined. The number of labels attached to the test tubes can range from 1 to 4. Therefore even for the same type of test tubes, their outside diameter may be different. When using the geometrical size of tubes to determine their type, the tolerance of

diameter must be considered. To solve this problem, a Fuzzy Logical Determination is applied in the identification process.

1.2.2.3 Operator and sample safety

The biological characters of samples require that tube caps not be removed during the test process.

1.3 Introduction about detection methods

The detection of liquid levels in containers is one of the most important steps in the modern industry process. Numerous methods have been developed and are widely used in many fields. In terms of detection styles, they are divided into contact (invasive) and noncontact (noninvasive) methods. Based on the physical principle of detection, the detection methods can be sorted as capacitive, conductance, hydrostatic head, radar/microwave, ultrasonic (Vass 2000) and optical detection, etc. All these methods detect the liquid's appearance by measuring the physical properties of the liquid and the media around it. The liquid and the media have different values for properties such as capacitance, conductivity, etc., and by measuring these properties, the methods described above can determine the liquid's location.

1.3.1 Capacitive

The capacity method is based on the relative dielectric constant of the detected material, which changes with the quantity and properties of material filled between the electrodes. The level of liquid can be measured by analyzing the value of capacitance.

The most common capacity sensor consists of two insulated coaxial tubes, which will be immersed in liquid partly during the detection (Medeova *et al.* 1998). Casanella *et al.* (2007) and Toth *et al.* (1997) developed planar capacitive liquid-level sensors to measure the level of liquid in a tank. The core part of the sensors is a planar electrode structure, which consists of an electrode array. This kind of sensor must also be partly immersed in liquid.

To avoid immersing the sensor in the liquid, Goekler (1991) mounts the electrodes the outside of the vessel. Bera *et al.* (2006) used hydrostatic leveling to measure the liquid level by a cylindrical shaped sensor.

In addition to the work on the capacitance sensor structure, some researchers also investigated measurement methods of capacity. Medeova *et al.* (1998) found that high linearity and good stability measurement results can be obtained by the phase-locked loop technique. Bera *et al.* (2006) measured it using a modified De' Sauty bridge network.

While the capacitance is a low-cost way to detect the liquid in a tank, the large parasitic capacitances of wire and the noise of the environment decrease its accuracy when it is used to measure liquids in a small container.

1.3.2 Radar/microwave

Radar/microwave is one of the most widely used methods to measure the level of liquid in a tank. It detects the level of the liquid by measuring the time it takes for a wave emitted from a signal source mounted on a reference plane to travel to the detection surface and be reflected to a sensor (Di Sante 2005; Nemarich 2001). Three types of radar are discussed in the literature.

The first is frequency-modulated continuous wave (FMCW), which sends out a singular continuous wave. The phase difference between the emitted wave and reflected wave is used to determine the distance of an object. Its performance depends on the bandwidth and the applied signal processing strategy (Vass 2000). Significant work has been done to improve the signal processing strategy. Chen *et al.* (2008) showed that the measurement resolution of the system was about 5 mm using Fast Fourier Transformations (FFT), and it can reach up to l mm when the AR spectral estimation is used. Liu *et al.* (2006) developed a different fast frequency estimation algorithm based on FFT as well. This is a time saving signal processing that is more precise. The simulation results show a 0.5 mm root mean squared error. Instead of FFT, Gulden *et al.* (2003) used the State-Space Frequency Estimation (SSFE) to analyze the signal received by radar. When testing the level of liquid in a tank, the SSFE can obtain two to three times better resolution compared to the classical FFT algorithm.

The second type of sensor is called the multiple-frequency continuous wave radar (MFCW). Compared with FMCW, MFCW is more accurate (Stuchly *et al.* 1971). Park and Nguyen (2006) developed a new sensor using a stepped frequency radar technique to monitor continuously varying liquid levels in a tank with less than ±1 mm error. In this system, a wave source sends out several waves with different frequencies. The distance of an object is calculated by the phase difference of reflection waves.

All the above methods require an expensive signal processing that limits their application in the industrial field (Kielb and Pulkrabek 1999).

The third one is pulsed radar. It is a less costly way to measure the distance compared with the two above mentioned methods. It sends out a pulse signal, and the

travel time of this signal (pulsed time of flight) (Stuchly *et al.* 1971) is measured to calculate the position of the liquid level.

To reduce the interference of outside noise, rods or cables are used to guide the microwave in guided-wave radar (GWR) systems (Bialkowski and Stuchly 1994; Vass 2000).

The industrial field is tending toward a wider application of the microwave for detection of liquid levels in tanks because it reduces costs. But it is not suitable for measuring the level of liquid in a small container (Manik *et al.* 2001).

1.3.3 Ultrasonic

The ultrasonic detection method is another common way to measure the liquid level in a tank. It measures the time that ultrasound travels down to the reflecting surface and returns back. Its accuracy is apparently affected by environmental factors such as temperature, humidity, air pressure, etc. The noise caused by multiple reflections on the liquid surface or reflection by the container walls also leads to inaccurate measurements of liquid levels, especially in small vessels. These two drawbacks restrict the application of ultrasonic detection in many conditions (Vass 2000; Kielb and Pulkrabek 1999).

Efforts have been taken to solve these problems. Bachur *et al.* (2010) mounted the system at the bottom of a container. Others have guided the ultrasonic wave by immersing a tube into the liquid (Olmos 2002). Meribout *et al.* (2004) developed a method that can detect the interface position of oil and water by inserting two stands in the detected liquid.

As shown above, the ultrasonic method is not suitable for measuring the liquid level in a small container without physical contact with the liquid.

1.3.4 Optical fiber sensors

The optical fiber sensors are widely applied in dangerous or harsh environments because of their nonconductive and corrosion resistant properties (Chandani and Jaeger 2007; Yakymyshyn and Pollock 1987). The principle of optical fiber is based on the total internal refection occurring at the interface of two media with different refractive indices. The fiber may work as light transmission parts or transducers in optical fiber sensors too. Normally, these sensors detect the liquid level by contact (invasive) methods.

Morris and Pollock (1987), Wang *et al.* (1992), Betta *et al.* (1998), Perez-Ocon *et al.* (2006), Romo-Medrano *et al.* (2006), Yun *et al.* (2007), and Chandani *et al.* (2007) have all developed different systems that can detect liquid by immersing optical fibers into the containers and detecting the power change when the liquid is at different levels. Based on the same principle of optical fiber, Weiss (2000) developed a fluorescent optical liquid-level sensor, which must also be lowered into the liquid. Raatikainen *et al.* (1997), Ilev and Waynant (1999), Yang *et al.* (2001), Golnabi (2004), and Nath *et al.* (2008), developed systems that are based on the principle of total internal reflection. When the tips of the sensors touch the liquid, the media surrounding the sensors are changed from air to liquid. Partial reflection replaces the total internal reflection, because the refractive index changes. Thus, the liquid level can be detected by inspecting the change in power received.

1.3.5 Optical methods

Many different methods have been investigated to detect the level of liquid based on its optical properties. They use a light beam emitted from laser diodes or other sources to illuminate the detected liquid. By analyzing the change of transmitted or reflected light, the level of liquid is obtained. Some methods emit the light beam vertically to illuminate the sample from the top or bottom when detecting the liquid level.

Maatta and Kostamovaara (1997) detected the distance between the light source and the liquid surface by measuring the travel time of light. Jaramillo-Nunez and Lucero-Alvarez (2006) developed an instrument for measuring the level of a liquid surface based on the change in distance between the light reflected from the top surface of the liquid and the laser source. Bachur *et al*. (2010) proposed a similar method to measure the liquid level in bottles. Ghosh *et al*. (2000) used four different combinations of light sources and detectors that utilize the transmission and reflectivity properties of the liquid to establish the liquid level. All four methods require the removal of the cap of the containers before the measurement. Yakymyshyn and Pollock (1987) invented a method that establishes the liquid height by measuring the absorption of two wavelengths of light that pass through the liquid vertically. Manik *et al.* (2001) floated a reflector on the liquid surface. By measuring the power of the reflected light, the level of liquid is determined. All of the above methods require that there are no obstructions between the detected liquid surface and the detection system.

Others detect the liquid level by illuminating the samples from the side. These systems are effective when the test tubes are sufficiently transparent.

Frank (2004) presented a method that can detect if the sensor immersed in liquid based on the amount of reflected light received. Musayev and Karlik (2003) developed a method that can detect the liquid level by recording the power of transmitted light, which depends on the amount of light reflected away from the detector by the liquid surface. Other methods by Bachur *et al.* (2010), Fine and Shvartsman (2008), Cadell and Samsoondar (2002) and Hendee *et al.* (2004) detected levels of liquid samples by measuring the power of transmitted light that passes through a sample and comparing the results either to the light power that passes through a reference sample or to the known results of a similar sample. Since all these methods detect the liquid using light in the visible spectrum, unobstructed visual access to the liquid is critical.

As for liquids filled in a translucent container, considering the different absorption coefficient of liquids, McNeal *et al.* (2004) invented a method to detect the liquid level height by moving the sample containers vertically past a fixed optical system while recording the light power, which will change at the interface of the two liquids.

Recently, Liu *et al.* (2008) developed an optical system with the ability to distinguish between a liquid and air through an unknown number of labels attached to the outside of the tube. The system performed this measurement at two fixed positions, namely the minimum required lower level and the maximum allowable upper level with an uncertainty of ±0.1 mL and better than 99.73% level of confidence.

While all of the above listed systems can detect the liquid level from the side, none of the systems consider the shape of the liquid level. In general, the level of liquid inside a container is not flat but forms a meniscus due to the surface tension forces. The

curvature of the meniscus, given that liquids typically have a much greater refractive index than air, will affect the amount of light transmitted.

A few methods use the optical effect of the liquid meniscus to find the surface of the liquid. Lee (1993) developed a method to detect liquid at a specific position by inspecting the power unbalance of two light sources, when they are reflected by the meniscus. Ondris *et al.* (1994) utilized the optical effect of the meniscus to measure the level of a liquid surface. This method used a CCD line image sensor to capture the power change in the vertical direction. The measurement range and accuracy were dependent on the size and quantity of the CCD sensors. The light source system needed to emit rays that were parallel to the plane that passed through the center line of the tube and sensor. The light also had to be orthogonal to the tube center line.

1.3.6 Other methods

Some other methods, such as conductance and hydrostatic, also appear in detection systems based on the particular properties of liquid.

The principle of conductance method is based on the principal that a liquid, such as ordinary water, is a conductor with some resistance. When the probe is located in air, which is considered a nonconductor, the resistance of the media is infinite. When it touches the liquid surface, the resistance of the media will drop dramatically. By inspecting the position of change, the level of liquid can be acquired (Onacak and Yurur 2007; Onacak 2007).

Hydrostatic methods use the hydrostatic pressure of liquid to measure the height of liquid in a vessel. When the height of the liquid in a vessel changes, the pressure on the

sensor placed on the bottom of the vessel will change proportionally. By measuring the pressure, the level of liquid is identified (Lu and Yang 2007; Wang *et al.* 2007).

A computer vision system is also used in liquid level detection systems. Yuan and Li (2004) used edge detection technology to find the interface between liquid and air or two liquids. This method requires that the test tubes are sufficiently transparent for the camera to take a clean image from the side of the tubes.

1.4 Method comparison and selection

Although most of the methods mentioned above work well in an industrial environment, each of them has drawbacks.

Radar/microwave and ultrasonic methods emit a signal vertical to the surface. It is more suitable for detecting liquid in a bigger container and without obstruction between the signal source/receiver and the detected surface.

Capacitance, conductance, hydrostatic pressure, and optical fiber sensors are intrusive methods, which need to be immersed into or be in contact with the liquid.

Methods detecting the liquid surface vertically require that there are no obstructions between the sensor and the detected surface. The system detecting the liquid level from the side by visible light and machine vision methods can detect only in containers with transparent walls or windows.

Both Lee (1993) and Ondris *et al*. (1994) used the optical effect of the meniscus to detect the level of liquid. Only the method of Ondris *et al.* considers the volume error caused by the meniscus, while its application is limited by the size and cost of CCD sensors and the parallel laser source.

The purpose of this research is to detect the volume of medical liquids in opaque test tubes accurately. Because of the biohazard properties of samples, intrusive methods will not be appropriate. Such methods require the removal of tube caps, which risks spills where the tubes are overfilled. Also, since the sensors make physical contact with the liquid, they will have to be replaced or sterilized after each measurement.

At the same time, methods using the visible spectrum will not be considered because the various numbers of labels at different positions lead to the opaqueness of test tubes.

Because the top surface of the liquid forms a meniscus, a small volume of liquid will appear above the lowest level. It is called the volume of the meniscus part. When the container has a small diameter and its total volume is limited, the liquid remaining in the meniscus plays an important role for the accuracy of measurement. All of the abovementioned systems detect the liquid volume by measuring the liquid level but ignore the volume of the meniscus. To acquire more accurate results, the volume of the meniscus part should be taken into consideration, while a system using a CCD sensor with the same length as the test tube is not a reasonable problem-solving strategy, considering the costs of CCD sensors.

The optical method detecting the liquid level from the side of a test tube is a more appropriate way to meet the ARUP requirements. Because the unknown layers of labels may lead to a detection error, the infrared lights with distinct wavelengths, to which labels have similar absorption coefficients, are chosen as light sources. Due to their long lifetime, and spectral and power stability, laser diodes are used as light sources to

guarantee the accuracy of the detection system (Kobtsev *et al.* 2007; Meier and Graf 1996).

In sum, the system developed in this research will be an optical detection system. The test process is a noncontact detection, which avoids potential biohazards. The system uses two distinct light wavelengths to eliminate the influence of the unknown number of labels, which will cover the tubes and make them opaque. A higher accuracy of measurement will be acquired by considering the volume of the meniscus.

1.5 Contributions

The following is a list of contributions made in this dissertation.

Research on optical systems to evaluate volume of medical samples in opaque test tubes

1. Measuring and calculating the optical properties of the test tube wall, labels and ink

2. Developing a novel method for detecting the liquid level by analyzing the power ratios of transmitted lights

3. Modeling and simulating the optical detection process

4. Improving the accuracy of level–based volume detection method by including the optical effect of the meniscus

The research has been applied to and verified by the following application devices:

1. Max/Min Level Detection System has been mounted and tested in the ARUP Institute for Clinical and Experimental Pathology® (ARUP).

2. Variable Volume Detection System has been verified and demonstrated at the Abbott Laboratories.

The research resulted in the following journal publications:

1. Liu, X., Corbin, B.J., Morris Bamberg, S.J., Provancher, W.R. and Bamberg, E. "Optical system to detect volume of medical samples in labeled test tubes," *Optical Engineering*, **47**(9), 094402 (094406 pp.), 2008.

2. Liu, X., Bamberg, S.J.M. and Bamberg, E. "Increasing the accuracy of level-based volume detection of medical liquids in test tubes by including the optical effect of the meniscus," *Measurement*, **44**(4), 750-761, 2011.

The following US Patent has issued:

Eberhard Bamberg, Brendan Corbin, Stacy Bamberg, Charles Hawker, William Roberts, "Through-Container Optical Evaluation System," Issued Mar. 31, 2010 as US Patent #7,688,448

1.6 Outline of the dissertation

The content presented in this dissertation is organized into several chapters as outlined below.

Chapter 1 covers the objectives and scope of this research. A brief overview of the previous work and current development in this field is presented. This chapter also compares methods and justifies this study's selection of methods.

Chapter 2 describes the physical fundamentals of the Max/Min Level Detection System and the Volume Detection System. The properties of detected samples are checked by the literature reviews and experiments.

Chapter 3 reports an optical detection method of Max/Min Level Detection System.

Chapter 4 presents the Variable Volume Detection System. By scanning the entire length of samples, this system can calculate the volume of liquid by finding the level and length of liquid in test tubes.

Chapter 5 reports an improvement of the Variable Volume Detection System, which increases the accuracy of volume detection by including the optical effect of the meniscus. The effect of liquid condition on the power of transmitted light is studied. Prototypes of systems based on the methods are set up. A series of experiments are discussed to verify the methods.

Chapter 6 shows a machine vision system, which is used to identify the type of test tubes through edge detection technology and Fuzzy determination. The modification of image aberration is also presented in this chapter.

1.7 References

Bachur, J., Nicholas, R., Foley, J., and Timothy, G. (2010). "System and Method for Determining Fill Volume in a Container." Becton, Dickinson and Company (Franklin Lakes, NJ, US), United States Patent Application #20100003714.

Bera, S. C., Ray, J. K., and Chattopadhyay, S. (2006). "A low-cost noncontact capacitance-type level transducer for a conducting liquid." *IEEE Transactions on Instrumentation and Measurement*, 55(3), 778-786.

Betta, G., Pietrosanto, A., and Scaglione, A. (1998). "A gray-code-based fiber optic liquid level transducer." *IEEE Transactions on Instrumentation and Measurement*, 47(1), 174-178.

Bialkowski, M. E., and Stuchly, S. S. (1994). "A study into a microwave liquid level gauging system incorporating a surface waveguide as the transmission medium." *Proc., Proceedings of ICCS '94*, IEEE, 939-943.

Cadell, T. E., and Samsoondar, J. (2002). "Apparatus and method for rapid spectrophotometric pre-test screen of specimen for a blood analyzer." United States Patent Application #20020180964.

Casanella, R., Casas, O., and Pallas-Areny, R. (2007). "Continuous liquid level measurement using a linear electrode array." *Measurement Science and Technology*, 18(2007), 1859-1866.

Chandani, S. M., and Jaeger, N. A. F. (2007). "Optical fiber-based liquid level sensor." *Optical Engineering*, 46(11),114401-7

Chen, H., Li, Y., and Wang, X.-M. (2007). "Digital signal processing for a level measurement system based on FMCW radar." *Proc., 2007 IEEE International Conference on Control and Automation, ICCA,* , Institute of Electrical and Electronics Engineers Inc., 2843-2847.

Di Sante, R. (2005). "Time domain reflectometry-based liquid level sensor." *Review of Scientific Instruments*, 76(9),0951071-5

Fine, I., and Shvartsman, L. (2008). "Method of optical measurements for determining various parameters of the patient's blood." Orsense Ltd. (Rehovot, IL), United States Patent #7,319,939.

Frank, P. L., GB) (2004). "Level sensors." United States Patent Application #20100003714.

Ghosh, A. K., Bedi, N. S., and Paul, P. (2000). "Package design for low-cost optical liquid-level sensors." *Optical Engineering*, 39(5), 1405-1412.

Goekler, L. E. C., OH) (1991). "Capacitive liquid level sensor." Standex International Corporation (Cincinnati, OH), United States Patent #5,017,909.

Golnabi, H. (2004). "Design and operation of a fiber optic sensor for liquid level detection." *Optics and Lasers in Engineering*, 41(5), 801-812.

Gulden, P., Vossiek, M., Pichler, M., and Stelzer, A. (2003). "Application of state-space frequency estimation to a 24-GHz FMCW tank level gauging system." *Proc., 33rd European Microwave Conference Proceedings,* Horizon House Publications, 995-998.

Hawker, C. D., Garr, S. B., Hamilton, L. T., Penrose, J. R., Ashwood, E. R., and Weiss, R. L. (2002). "Automated transport and sorting system in a large reference laboratory: Part I. Evaluation of needs and alternatives and development of a plan." *Clinical Chemistry*, 48(10), 1751-1760.

Hawker, C. D., Roberts, W. L., DaSilva, A., Stam, G. D., Owen, W. E., Curtis, D., Choi, B. S., and Ring, T. A. (2007). "Development and validation of an automated thawing and mixing workcell." *Clinical Chemistry*, 53(12), 2209-2211.

Hawker, C. D., Roberts, W. L., Garr, S. B., Hamilton, L. T., Penrose, J. R., Ashwood, E. R., and Weiss, R. L. (2002). "Automated transport and sorting system in a large reference laboratory: Part 2. Implementation of the System and performance measures over three years." *Clinical Chemistry*, 48(10), 1761-1767.

Hendee, S. P., Jones, H. D. T., Birnkrant, D. A., Johnson, R. D., Abbink, R. E., and Messerschmidt, R. G. (2004). "Analyte determinations." United States Patent Application #20040241736.

Ilev, I. K., and Waynant, R. W. (1999). "All-fiber-optic sensor for liquid level measurement." *Review of Scientific Instruments*, 70(5), 2551-2554.

Jaramillo-Nunez, A., and Lucero-Alvarez, M. (2006). "Optical laser level." *Optical Engineering*, 45(9),093601-6

Kielb, J. A., and Pulkrabek, M. O. (1999). "Application of a 15 GHz FMCW radar for industrial control and process level measurement." *Proc., 1999 IEEE MTT-S International Microwave Symposium Digest*, IEEE, 281-284.

Kobtsev, S., Kandrushin, S., and Potekhin, A. "New approach to long-term frequency stabilisation of radiation of single-frequency lasers." *Proc., International Conference on Lasers, Applications, and Technologies 2007: Advanced Lasers and Systems*, SPIE - The International Society for Optical Engineering, 67312-67311.

Lee, T. E. S. D. A., Chicago, IL, 60637) (1993). "Optical liquid level detector using dual varying light emitters." United States, Patent #5,274,245.

Liu, J., Chen, X. Z., and Zhang, Z. (2006). "A novel algorithm in the FMCW microwave liquid level measuring system." *Measurement Science & Technology*, 17(1), 135-138.

Liu, X., Corbin, B. J., Morris Bamberg, S. J., Provancher, W. R., and Bamberg, E. (2008). "Optical system to detect volume of medical samples in labeled test tubes." *Optical Engineering*, 47(9), 094402 -094406

Lu, T., and Yang, S. P. (2007). "Extrinsic Fabry-Perot cavity optical fiber liquid-level sensor." *Applied Optics*, 46(18), 3682-3687.

Maatta, K. E., and Kostamovaara, J. T. (1997). "High-accuracy liquid level meter based on pulsed time of flight principle." *Proc., Sensors, Sensor Systems, and Sensor Data Processing*, Society of Photo-Optical Instrumentation Engineers, 268-277.

Manik, N. B., Mukherjee, S. C., and Basu, A. N. (2001). "Studies on the propagation of light from a light-emitting diode through a glass tube and development of an optosensor for the continuous detection of liquid level." *Optical Engineering*, 40(12), 2830-2836.

Mc Neal, J. D., Liu, Y., and Adzich, M. S. (2004). "Sample level detection system." Beckman Coulter, Inc. (Fullerton, CA), United States Patent Application #20020180964.

Medeova, M., Pavlik, V., and Skyba, P. (1998). "Simple continuous level meter for cryogenic liquids." *Cryogenics*, 38(3), 289-291.

Meier, H. P., and Graf, V. (1996). "Research lab converts to diode-laser manufacturer." *Laser Focus World*, 32(10), 51.

Meribout, M., Habli, M., Al-Naamany, A., and Al-Busaidi, K. (2004). "A new ultrasonic-based device for accurate measurement of oil, emulsion, and water levels in oil tanks." *Proc., Proceedings of the 21st IEEE Instrumentation and Measurement Technology Conference, IMTC/04,* Institute of Electrical and Electronics Engineers Inc., 1942-1947.

Morris, J. A., and Pollock, C. R. (1987). "A digital fiber-optic liquid level sensor." *Journal of Lightwave Technology*, LT-5(7), 920-925.

Musayev, E., and Karlik, S. E. (2003). "A novel liquid level detection method and its implementation." *Sensors and Actuators a-Physical*, 109(1-2), 21-24.

Nath, P., Datta, P., and Sarma, K. C. (2008). "All fiber-optic sensor for liquid level measurement." *Microwave and Optical Technology Letters*, 50(7), 1982-1984.

Nemarich, C. P. (2001). "Time domain reflectometry liquid level sensors." *IEEE Instrumentation Measurement Magazine*, 4(4), 40-44.

Olmos, P. (2002). "Extending the accuracy of ultrasonic level meters." *Measurement Science & Technology*, 13(4), 598-602.

Onacak, T., and Yurur, M. T. (2007). "A new high precision pluviometer system." *Instrumentation Science & Technology*, 35(5), 551-561.

Onacak, T. (2007). "Micron resolution electromechanical liquid level measurement system." *Instrumentation Science & Technology*, 35(5), 563-569.

Ondris, L., Trnovec, M., Keppert, M., Rusina, V., and Buzasi, J. (1994). "An optoelectronic hydrolevelling system." *Measurement Science Technology*, 5(10), 1287-1293.

Park, J., and Nguyen, C. (2006). "Development of a new millimeter-wave integrated-circuit sensor for surface and subsurface sensing." *IEEE Sensors Journal*, 6(3), 650-655.

Perez-Ocon, F., Rubino, A., Abril, J. M., Casanova, P., and Martinez, J. A. (2006). "Fiber-optic liquid-level continuous gauge." *Sensors and Actuators a-Physical*, 125(2), 124-132.

Raatikainen, P., Kassamakov, I., Kakanakov, R., and Luukkala, M. (1997). "Fiber-optic liquid-level sensor." *Sensors and Actuators a-Physical*, 58(2), 93-97.

Romo-Medrano, K. E., and Khotiaintsev, S. N. (2006). "An optical-fibre refractometric liquid-level sensor for liquid nitrogen." *Measurement Science Technology*, 17(5), 998-1004.

Stuchly, S. S., Hamid, M. A. K., and Andres, A. (1971). "Microwave surface level monitor." *IEEE Transactions on Industrial Electronics and Control Instrumentation*, IECI-18 (3), 85-92.

Toth, F. N., Meijer, G. C. M., and vanderLee, M. (1997). "A planar capacitive precision gauge for liquid-level and leakage detection." *IEEE Transactions on Instrumentation and Measurement*, 46(2), 644-646.

Vass, G. (2000). "The principles of level measurement." *Sensors*, 2000 (17), 55-64.

Wang, A., Gunther, M. F., Murphy, K. A., and Claus, R. O. (1992). "Fiber-optic liquid-level sensor." *Sensors and Actuators, A: Physical*, 35(2), 161-164.

Wang, Q., Liu, Z., Zhang, J., and Wu, Q. (2007). "Optical liquid level measurement system based on DSP." *Embedded System & SOC*, 22(23), 177-178.

Weiss, J. D. (2000). "Fluorescent optical liquid-level sensor." *Optical Engineering*, 39(8), 2198-2213.

Yakymyshyn, C. P., and Pollock, C. R. (1987). "Differential absorption fiber-optic liquid level sensor." *Journal of Lightwave Technology*, LT-5(7), 941-946.

Yang, C. N., Chen, S. P., and Yang, G. G. (2001). "Fiber optical liquid level sensor under cryogenic environment." *Sensors and Actuators a-Physical*, 94(1-2), 69-75.

Yuan, W., and Li, D. (2004). "Measurement of liquid interface based on vision." *Proc., Proc. of Fifth World Congress on Intelligent Control and Automation WCICA 2004*, Zhejiang Univerisity, 3709--3713.

Yun, B. F., Chen, N., and Cui, Y. P. (2007). "Highly sensitive liquid-level sensor based on etched fiber Bragg grating." *IEEE Photonics Technology Letters*, 19(21-24), 1747-1749.

CHAPTER 2

FUNDAMENTALS OF DETECTION

In this chapter, the principle fundamentals of the Max/Min Volume Detection System and Volume Detection System are presented and the physical proprieties of samples are investigated.

2.1 Detection principle

Numerous methods have been developed to detect the volume or level of liquid in a container, and all of them are based on proprieties of the liquid. Most of the methods using optical properties are based on the liquid's reflection, refraction and absorption of the detection beam. Because the samples detected by the Max/Min Level Detection System and the Volume Detection System are test tubes filled with medical liquid, the volume detection process must be a noncontact detection to avoids potential biohazards. Thus, the optical measurement detecting from the side of the test tube is used as the detection method for these two systems. Because an unknown number of labels covered the tubes and make them opaque to visible light, infrared light is chosen as light source. Considering the obvious absorption difference of air and liquid to light, the absorption is one of the most convenient ways to be used as a detection method.

The physical fundamental of the Max/Min Level Detection System and the Volume Detection System is based on the absorption of samples to transmitted light and the light refraction occurring at the interface of different media. The basic principle is that a light source illuminates the sample from one side of a container, while a detector measures the power of the transmitted light on the other side at a specific position. Different liquids will produce different absorption and refraction effects, which will result in different amounts of power reaching the detector. By analyzing the power change, the condition of the liquid at the measured position will be identified. Furthermore, the level of the liquid can be determined by inspecting the condition of the liquid along the whole height of the container.

Because the absorption coefficients of test tubes, the liquid and labels change with the variation of the light wavelength, a detection method using a combination of different wavelengths is introduced. The system based on this method will be robust, and can detect the liquid level in test tubes covered by labels at different position.

2.2 Light source

Corbin (2007) and Liu *et al.*(2008) chose two lasers with 980 and 1550 nm peak wavelengths respectively as the light source. These wavelengths have small differences in attenuation to empty tubes but large differences in attenuation to tubes filled with aqueous medical samples. To empty tubes, the attenuation degree of both wavelengths is similar, while the attenuation degree of 1550 nm for tubes filled with aqueous medical sample is very large. Because of the above described properties of the two wavelengths,

the Max/Min Level Detection System and the Volume Detection System are based on 980 and 1550 nm as the wavelengths of light source.

Monti De Sopra *et al*. (2001) showed that a 780 nm laser diode shifts 75 GHz in spectral frequency after 600 days of aging under several rigors conditions created in the laboratory. The wavelength shift is transferred to about 0.15 nm away from the peak wavelength. Meier and Braf (1996) pointed out that the reliability of their laser diodes can reach a mean time to failure of 1.1 million hours (125.6 years). Because of their longer life spans and long-term spectral stability, laser diodes are used as light sources for the Max/Min Level Detection System and the Volume Detection System.

2.3 Physical properties of samples

A typical sample detected by the Max/Min Level Detection System and the Volume Detection System is a test tube filled with a certain volume of medical liquids and covered by printed labels. To prove and explain the principle of the two systems in theory, this study had to determine the physical properties of four types of materials: test tubes, labels, ink used in printing the labels, and the biomedical liquids.

2.3.1 Test tubes

The test tubes are made of polypropylene, whose refractive index is given by Shabana (2004) as about 1.52 at room temperature. The absorption coefficient could not be obtained from the literature but was determined using an optical spectrum analyzer (AQ6315E) to measure the loss of transmitted light emitted from a light source. This

experiment passed white light through a sample of test tubes and captured the transmitted light with an optical spectrum analyzer.

When light passes through an interface between air and a test tube with refractive indexesn_1 and n_2 respectively, part of it may be reflected by the surface. When the incident light is normal to the interface, the transmission coefficient can be calculated by the equitation $T = 4n_1n_2/(n_1 + n_2)$ (Sharma 2006). When the refractive index of air n_1 is 1 and that of the test tube n_2 is 1.52, the transmission coefficient is 96%. If the absorption is zero and the effect of the second reflections at internal interfaces is ignored, the power of the transmitted part of light is $I_T = I_I \cdot T^2$, where I_I is the power of the incident light. This allows the absorption coefficient of the test tube wall α to be calculated based on the thickness of the tube material and the power measurement values of transmitted light though air and the tube material (Robertson and Williams 1971).

$$\alpha = -\ln\left[I_{T,tube}/\left(I_{T,air} \cdot T^2\right)\right]/L \tag{2.1}$$

Here, $I_{T,tube}$ and $I_{T,air}$ are the power of transmitted light through the tube and air, respectively, and L is the thickness of the tube material.

As shown in Fig. 2-1, an experimental device was set up to conduct the measurements for the experiment. A halogen bulb (Fiber-Lite) served as a light source in this project. The output beam was focused and collimated using one set of lenses at the beam entry side and another at the exit side.

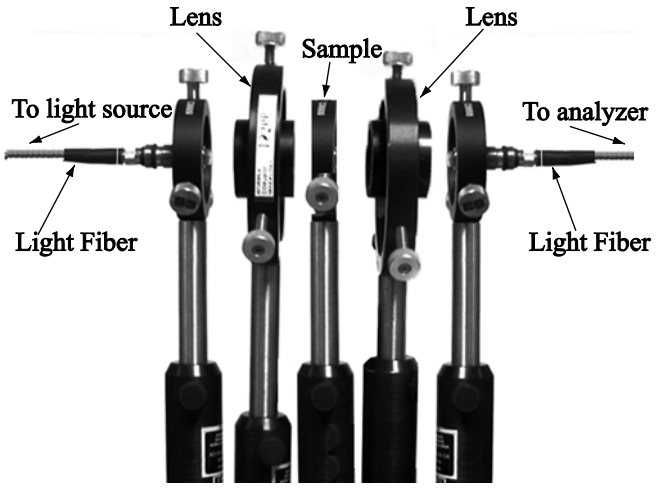

Fig. 2-1 Experimental setup to measure the absorption coefficient of the test tube wall.

A section of the tube wall was cut from a tube and flattened as much as possible and was mounted between the collimating lenses. An optical spectrum analyzer (not shown in Fig. 2-1) was used to measure the power change of the wavelength emitted by the light source. The analyzer can scan the transmitted light from 350 to 1750 nm.

When the testing began, the initial power value of the light source was measured when the sample was not placed in the system. The powers of different wavelengths from 350 to 1750 nm were measured by the optical spectrum analyzer. The values are the initial power of the light source. Then the samples of the test tube wall were mounted at the inspection position. The analyzer scanned the powers over the same spectrum range again. The powers were measured by the spectrum analyzer and recorded to a computer. These values are the power of the transmitted light after being absorbed and reflected.

The measured powers absorbed and reflected by the tube wall are normalized with the powers of air and shown in Fig. 2-2. It is clear that, at wavelengths of 980 and 1550 nm, the tube wall has similar power absorption.

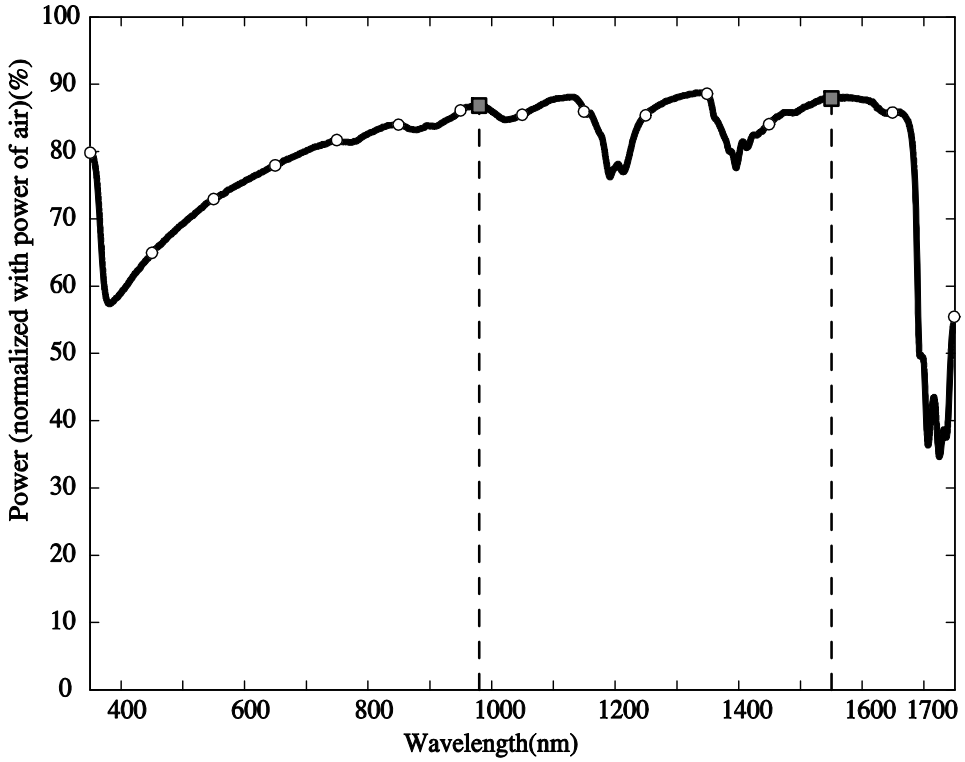

Fig. 2-2 Power of transmitted light through a test tube wall.

Using equation (2.1), the absorption coefficient α can be calculated by measuring the thickness of the sample and determining the difference in power between the air and the tube material (Robertson and Williams 1971). The thickness of each layer tube wall is 1.0 mm. Based on the measurement with a resolution of 1 nm, and considering the loss due to the reflection from both sides of the test tube wall, the absorption coefficient for polypropylene was identified to be 0.6 cm^{-1} and 0.48 cm^{-1} for 980 nm and 1550 nm, respectively.

2.3.2 Labels

The labels are made of polyurethane, which makes the test tubes opaque. The labels absorb a significant amount of light when an optical detection method is conducted

to measure the volume of liquid in samples from the side. There is no discussion in the literature of the wavelength absorption of labels. This property must be obtained through experimentation.

The white surfaces of labels will reflect a lot of light when the beam illuminates them. When detecting the absorption coefficient of labels, it is necessary to consider the attenuation of power due to surface reflection.

Robertson and Williams (1971) developed a method that can eliminate the power loss caused by reflection at the interface between air and the tested material. Since the reflection happens on the surface of the first layer, the absorption coefficient, α, can be calculated from the power ratio of two lights that have a different path length when transmitted through the same type of medium.

$$\alpha = -\ln(I_1/I_2)/(L_2 - L_1) \tag{2.2}$$

Here, I_1 and I_2 are the power of light transmitted through labels of different thicknesses. L_1 and L_2 are the thickness of the tested material, respectively, and $\alpha(\lambda)$ is the absorption coefficient of the material.

For this project, an experiment was conducted to determine the absorption coefficients of labels based on Robertson's method.

This test uses the same experiment setup (as shown in Fig. 2-1) that was used to measure the absorption coefficient of the test tube wall. A label sample replacing the test tube wall was mounted between the optical fibers of the light source and the spectrometer.

The labels were attached together to create a sample to be measured. The test examined from 0 to 5 layers of labels. The path lengths of the transmitted light through particular label samples are expressed by the number of layers.

The spectrometer measured the power of different wavelengths with a 1 nm resolution 30 times for every thickness. After the power loss reflected at the surface of the label sample is eliminated, the transmitted powers with one layer of label from 350 to 1750 nm are measured and normalized with the power of air shown in Fig. 2-3. At the wavelengths of 980 and 1550 nm, the polyurethane labels have a similar power absorption coefficient.

Equation (2.2) is used to calculate the absorption coefficient of labels at 980 and 1550 nm. Because a label is very thin, the layer number is used to represent the thickness instead of a unit of distance (mm). The absorption coefficients of the test tube wall are 0.801 $layer^{-1}$ and 0.769 $layer^{-1}$, when the wavelength of the light source, λ, is equal to 980 nm, or 1550 nm, respectively. Fig. 2-4 shows the power change of transmitted light following the variation in the number of labels. From Fig. 2-4, the experimental results show good agreement with the calculation results.

2.3.3 Ink of barcode

In laboratories, samples are identified through labels printed with barcodes. When beams of detection systems scan a sample, they may encounter a printed part of a label, an unprinted part or both. Because the system uses an infrared light source, its robustness will not be affected by the presence of ink. The details of this verification are presented in Chapter 5.

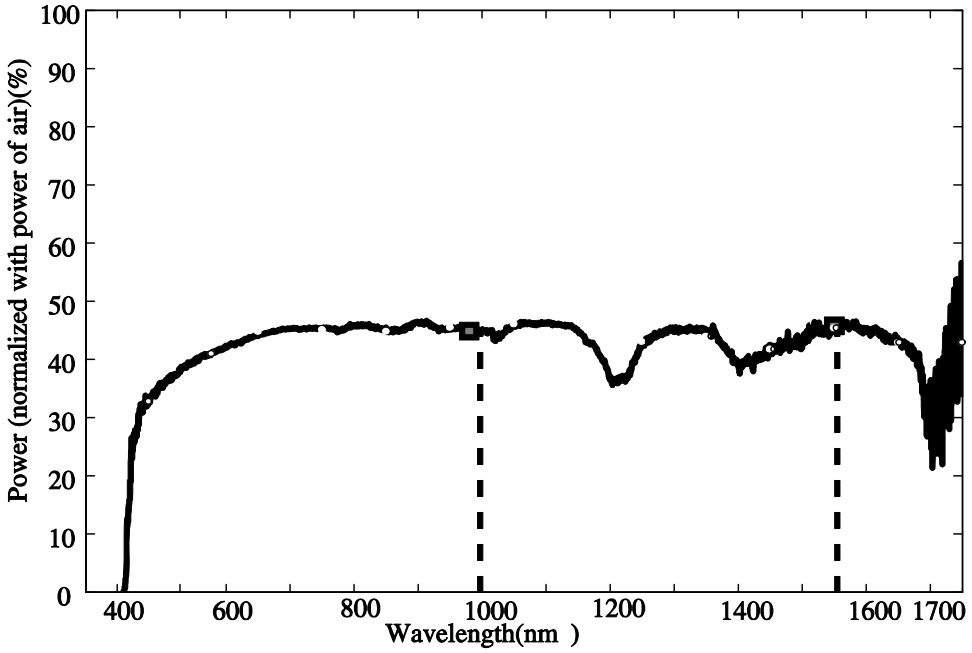

Fig. 2-3 Power absorption of transmitted light through a label.

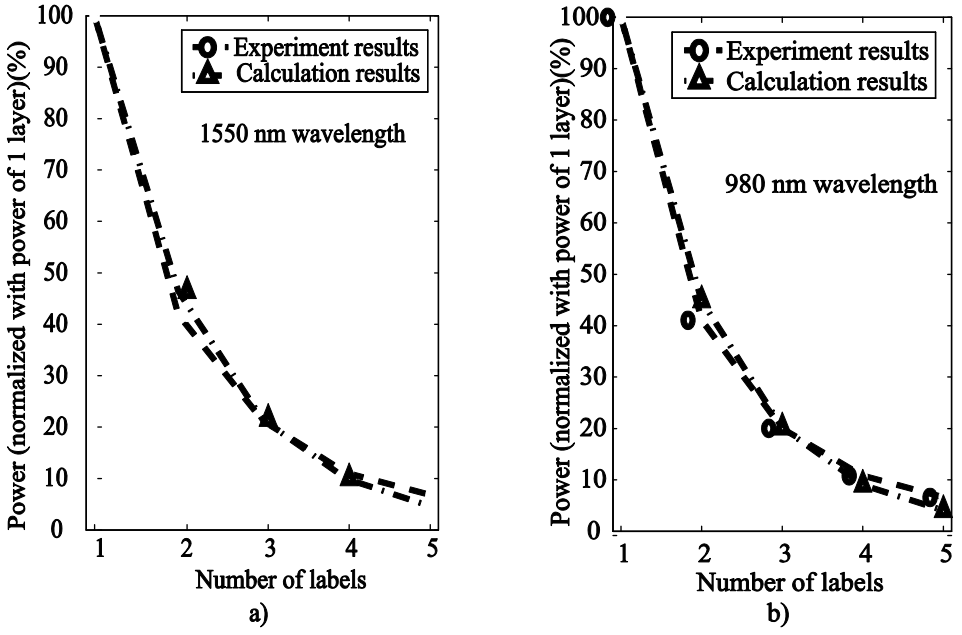

Fig. 2-4 The transmitted power is attenuated as the number of labels is increased from 1 to 5 layers. (a) The absorption with 1550 nm wavelength; (b) The absorption with 980 nm wavelength.

2.3.4 Liquid

To design a method for detecting liquids, it is necessary to investigate the properties of the liquids. In this case, the most important parameters are the optical properties of the liquids, in particular the absorption coefficients and the refractive indices.

In the verification experiments, water is used in place of a medical liquid. Its density is 1.0 g/cm^3 at room temperature. Its surface tension is 0.07275 N/m when the temperature is 20°C (Vargaftik *et al.* 1983). The optical properties of water as a function of wavelength and temperature are well documented in the literature (Kou *et al.* 1993; Hale and Querry 1973; Harvey *et al.* 1998). For a wavelength of 980 nm at 20°C, the refractive index of water is given as 1.327 and the absorption coefficient is 0.46 cm^{-1}; while at 1550 nm, the literature shows 1.319 and 11.92 cm^{-1}, respectively.

Serum is one of the most common liquids in the Core lab. It potentially may be contaminated with hemolysis, icterus and lipemia. Serum can be seen as the remains after fibrinogen is removed from plasma. Because the plasma consists of 90% water and 10% proteins, the major constituent of serum is water. Thus, water plays a major role in the physical properties of serum (El-Kashef and Atia 1999; Meinke *et al.* 2007). The density of serum can be regarded as the same as that of plasma: 1.0239-1.025 g/cm^3 (Mody and King 2007; Rhoades and Bell 2008). Its surface tension is about 0.05872 N/m at 20ºC (Rosina *et al.* 2007). Because the wavelength of 980 nm is close to the visible range, its refractive index can be calculated approximately by the Sellmeier approximation with two parameters, in which B=0.7914, c=9865.04463. Based on this fit equation, the

refractive index of serum is computed as 1.342 at room temperature (20ºC) (Meinke *et al.* 2007). Because the major constituent of serum is water, the refractive index of serum for the wavelength 1550 nm is set to 1.319, which is the refractive index of water. The absorption coefficient is estimated at about 0.2 cm^{-1} when the wavelength is at 980 nm (Meinke *et al.* 2007). At 1550 nm, the absorption coefficient can be regarded as the same as that of that of water (Kasemsumran *et al.* 2004). Thus the absorption coefficient of serum can be approximated as 12 cm^{-1}.

Urine is another common liquid in the lab. Normally, the density of urine of a healthy human is about 1.022 g/cm^3 at 16ºC. The average surface tension of urine of a healthy human at 16ºC is about 0.0691 N/m, which is a little lower than that of water. The refractive index of urine of a healthy human at 18ºC is measured as about 1.34 (Donnan and Donnan 1905).

Beside the serum and urine, cerebrospinal fluid (CSF) also appears in the lab frequently. Its density is 1.00 g/cm^3 at room temperature (Lui *et al.* 1998). Its surface tension has a range of 0.046 to 0.060 N/m for its normal condition (Brydon *et al.* 1995). Levinson tested 115 samples obtained from 93 patients, and obtained a refractive index of CSF ranging between 1.334 and 1.336 (Levinson and Serby 1926).

Corbin (2007) examined the attenuation of white light transmitted through a test tube with medical samples. The experiment shows that urine and CSF have the same absorption coefficient with water at 980 and 1550 nm. Their absorption coefficient at 980 nm is 0.46 cm^{-1}; while at 1550 nm, the experiment shows 11.92 cm^{-1}.

2.4 Conclusions

In this chapter, the fundamentals of the optical detection method are presented. The properties of the test tubes, labels, ink and medical liquids are investigated. These properties will be used in the next chapter to simulate the propagation process of laser beams in samples.

2. 5 References

Brydon, H. L., Hayward, R., Harkness, W., and Bayston, R. (1995). "Physical-properties of cerebrospinal-fluid of relevance to shunt function .2. The effect of protein upon csf surface-tension and contact-angle." *British Journal of Neurosurgery*, 9(5), 645-651.

Corbin, B. J. (2007). "Design of optical scanning system to detect volume and interferences in blood specimen in test tubes." M S Thesis, University of Utah, Salt Lake City , UT.

Donnan, W., and Donnan, F. (1905). "The surface tension of urine in health and disease: with special reference to icterus." *British Medical Journal*, 2(2347), 1636.

El-Kashef, H., and Atia, M. A. (1999). "Wavelength and temperature dependence properties of human blood-serum." *Optics and Laser Technology*, 31(1999), 181-189.

Hale, G. M., and Querry, M. R. (1973). "Optical constants of water in the 200-nm to 200-mu m wavelength region." *Applied Optics*, 12(3), 555-563.

Harvey, A. H., Gallagher, J. S., and Sengers, J. (1998). "Revised formulation for the refractive index of water and steam as a function of wavelength, temperature and density." *Journal of Physical and Chemical Reference Data*, 27(4), 761-774.

Kasemsumran, S., Du, Y. P., Murayama, K., Huehne, M., and Ozaki, Y. (2004). "Near-infrared spectroscopic determination of human serum albumin, [gamma]-globulin, and glucose in a control serum solution with searching combination moving window partial least squares." *Analytica Chimica Acta*, 512(2), 223-230.

Kou, L., Labrie, D., and Chylek, P. (1993). "Refractive indices of water and ice in the 0.65- to 2.5 micrometer spectral range." *Applied Optics*, 32(19), 3531-3540.

Levinson, A., and Serby, A. (1926). "The refractometric and viscosimetric indexes of cerebrospinal fluid." *Archives of Internal Medicine*, 37(1), 144.

Liu, X., Corbin, B. J., Morris Bamberg, S. J., Provancher, W. R., and Bamberg, E. (2008). "Optical system to detect volume of medical samples in labeled test tubes." *Optical Engineering*, 47(9), 094402 -6 .

Lui, A. C. P., Polis, T. Z., and Cicutti, N. J. (1998). "Densities of cerebrospinal fluid and spinal anaesthetic solutions in surgical patients at body temperature." *Canadian Journal of Anaesthesia-Journal Canadien D Anesthesie*, 45(4), 297-303.

Meier, H. P., and Graf, V. (1996). "Research lab converts to diode-laser manufacturer." *Laser Focus World*, 32(10), 51-53.

Meinke, M., Mueller, G., Helfmann, J., and Friebel, M. (2007). "Optical properties of platelets and blood plasma and their influence on the optical behavior of whole blood in the visible to near infrared wavelength range." *Journal of Biomedical Optics*, 12(1), 014024-1-6.

Mody, N. A., and King, M. R. (2007). "Influence of Brownian motion on blood platelet flow behavior and adhesive dynamics near a planar wall." *Langmuir*, 23(11), 6321-6328.

Monti De Sopra, F., Gauggel, H. P., Brunner, M., Hovel, R., Moser, M., and Zappe, H. P. (2001). "Long-term spectral stability of singlemode VCSELs." *Electronics Letters*, 37(2001), 832-834.

Rhoades, R., and Bell, D. (2008). *Medical physiology: principles for clinical medicine*, Lippincott Williams & Wilkins.

Robertson, C. W., and Williams, D. (1971). "Lambert absorption coefficients of water in the infrared." *Journal of the Optical Society of America*, 61(10), 1316-1320.

Rosina, J., Kvasnak, E., Suta, D., Kolarova, H., Malek, J., and Krajci, L. (2007). "Temperature dependence of blood surface tension." *Physiological Research*, 56, S93-S98.

Shabana, H. M. (2004). "Determination of film thickness and refractive index by interferometry." *Polymer Testing*, 23(6), 695-702.

Sharma, K. K. (2006). *Optics : principles and applications*, Boston : Academic Press, Amsterdam.

Vargaftik, N. B., Volkov, B. N., and Voljak, L. D. (1983). "International tables of the surface tension of water." *Journal of Physical and Chemical Reference Data*, 12(1984), 817-820.

CHAPTER 3

OPTICAL SYSTEM TO DETECT VOLUME OF MEDICAL SAMPLES IN LABELED TEST TUBES

Liu, X., Corbin, B. J., Bamberg, S. J. M., Provancher, W. R., and Bamberg, E. (2008). "Optical system to detect volume of medical samples in labeled test tubes." *Optical Engineering*, 47(9), 094402 -094406

Optical Engineering 47(9), 094402 (September 2008)

Optical system to detect volume of medical samples in labeled test tubes

Xin Liu
Brendan J. Corbin
Stacy J. Morris Bamberg
William R. Provancher
Eberhard Bamberg
University of Utah
Department of Mechanical Engineering
Salt Lake City, Utah 84112
E-mail: e.bamberg@utah.edu

Abstract. A novel system for liquid-level detection is reported. The system uses two different wavelengths of light to detect the liquid level of medical samples in tubes that are covered by an unknown number of paper labels. By measuring the intensity of the transmitted light at two distinct wavelengths and computing their ratio, which is compared to a threshold value, a system was developed that is self-compensating for the number of tube labels and the type of medical sample to be analyzed. A laboratory prototype was built, and the test results were analyzed using different types of medical samples. Based on a series of experiments, the system was found to detect the liquid level of 0.4 mL with a maximum allowable tolerance of ±0.1 mL with better than 99.73% reliability and a total test time of 0.5 s. These results were achieved with test tubes that had up to six layers of labels attached to the outside of the tube, thereby making the tube completely opaque. [DOI: 10.1117/1.2978953]

Subject terms: volume measurement; optics; optoelectronics; liquid level sensors; laser diode.

Paper 080125RR received Feb. 13, 2008; revised manuscript received Jul. 18, 2008; accepted for publication Jul. 22, 2008; published online Sep. 18, 2008.

1 Introduction

An increasing number of biotechnology companies use automated testing facilities to test liquid medical samples in tubes. In order to perform these tests safely and reliably, it is necessary to verify the minimum required and maximum allowable volume levels without removing the cap of the tube.

Many different methods have been investigated to detect the level of liquids in tubes. Jaramillo-Nunez and Lucero-Alvarez[1] developed an instrument for measuring the level of a liquid surface based on the distance change between the light reflected from the top surface and the laser source. Similarly, Maatta and Kostamovaara[2] detected the distance between the light source and the liquid surface by measuring the flight time of light. Yakymyshyn and Pollock[3] invented a method that established the liquid height by measuring the absorption of two wavelengths of light that pass through the liquid vertically. Ghosh et al.[4] used four different combinations of light sources and detectors that utilized the liquid's transmission and reflectivity properties to establish the liquid level. All four methods required the removal of the tube cap before the measurement, thereby risking spills for the case where the tubes are overfilled.

Methods that do not require the removal of the tube cap include the computer vision system developed by Yuan and Li[5] that detected the liquid levels through edge detection at the interface between two liquids. Similarly, McNeal et al.[6] invented a method to detect the liquid level height by moving the samples vertically past an optical system while recording the light intensity, which will change at the interface of two liquids. Other methods by Bachur and Foley,[7] Fine and Shvartsman,[8] Cadell and Samsoondar,[9] and Hendee et al.[10] detected levels of liquid samples by comparing the light intensity that passes through a sample with the light intensity that passes through a reference sample or to known results of a similar sample. Musayev and Karlik[11] developed a method using a light source and a detector whose optical axes are shifted relative to each other. The liquid level was detected by recording the shift in position of the light reflected of the liquid surface with a photodetector. Because all the methods detected the liquid using light in the visible spectrum, unobstructed visual access to the liquid is critical.

In this paper, a novel volume detection system is presented that is based on detecting the presence of liquids by measuring the intensity of light that has passed across a standard tube. Two distinct light sources are used to compensate for an unknown number of paper labels attached to the outside of the tube. The system is located at two distinct heights that correspond to the minimum required and maximum allowable liquid level. For increased robustness and simplicity, the system has no moving parts.

2 System Requirements

The medical samples to be tested are contained in test tubes as shown in Fig. 1. The tubes are made from polyethylene and may have from zero to three labels attached to the outside. These labels may or may not overlap and also vary in height and width, resulting in a number of layers (which can vary between zero and six) that obstruct the optical path of the measurement. The labels also absorb light, and the absorption is affected by the thickness of the layer. Because of the high variability of this setup, the effect of the labels must be considered in the design of the system.

0091-3286/2008/$25.00 © 2008 SPIE

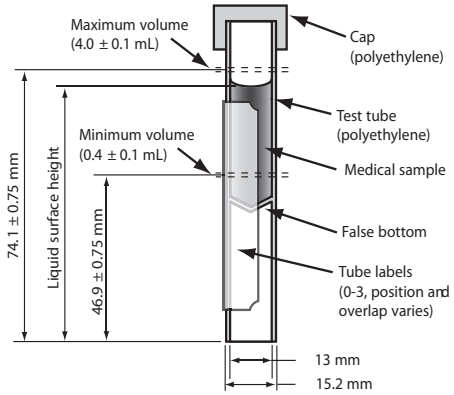

Fig. 1 Test tube made from polyethylene. The allowable minimum and maximum volume translates to two distinct liquid levels at 46.9±0.75 and 74.1±0.75 mm from the base of the tube.

For the tubes used in this system, the minimum required volume is 0.4 ± 0.1 mL, and the acceptable maximum volume is 4.0 ± 0.1 mL. As illustrated in Fig. 1, the volume tolerances for both levels translate to a maximum height tolerance of ± 0.75 mm.

3 Detecting Media Based on Spectral Absorption

To meet the above-listed requirements, a new system was developed based on the spectral absorption of medical samples, which are serum or plasma that potentially are contaminated with hemolysis, icterus, or lipemia. Other sample types encountered may contain urine or cerebrospinal fluid. The spectra were obtained by passing white light through the specimen and capturing the transmitted light with an optical spectrum analyzer (Ando AQ-6315E).

The spectrum analyzer scans the transmitted light from 350 to 1750 nm with a 0.5-nm resolution and outputs the average intensities of 100 scans. Using this method, the optical response of various samples as well as water was collected. Figure 2 shows the intensities of the transmitted light that has been normalized with the spectrum of the light source. As can be seen in Fig. 2, all liquids follow a similar absorption pattern in the range from 950 to 1700 nm. Of particular interest is the range from 1400 to 1600 nm, where all liquids exhibit a dramatically increased absorption compared to the 950–1250 nm range. Because water and the medical samples of interest exhibit a very similar behavior in this range, liquid detection in this range can be performed with water instead of the actual medical samples. For final system verification, the actual medical samples were used.

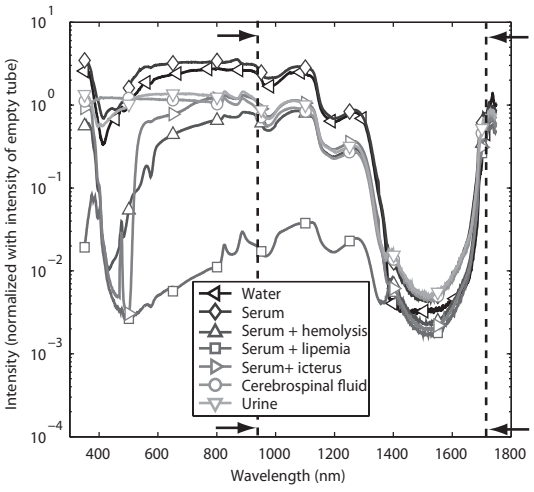

Fig. 2 Absorption spectrum of various medical samples and water.

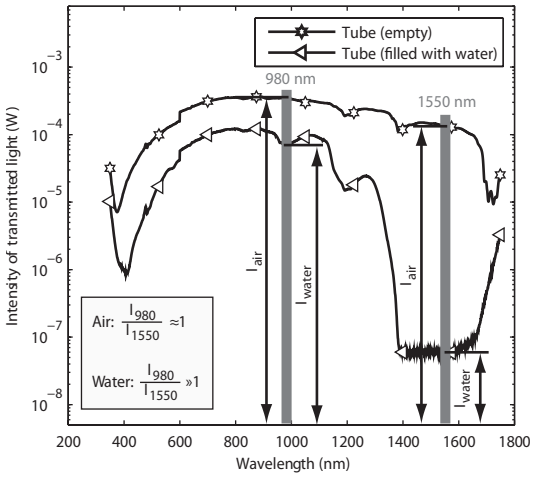

Fig. 3 Intensity of transmitted light through an unlabeled empty tube and an unlabeled tube filled with water.

An empty tube and a tube with water were tested, both without labels, and the measured intensities are shown in

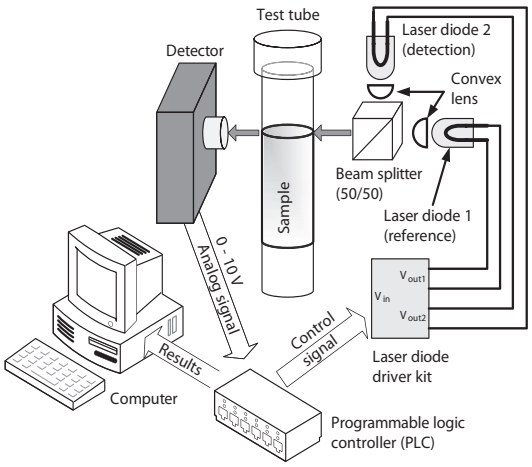

Fig. 4 Schematic of the volume detection system. The detection system features two laser diodes and a beamsplitter that creates the common optical path for both light sources. A photodetector measures the intensity of the transmitted light, and a PLC controller computes the intensity ratio based on the analog output of the detector.

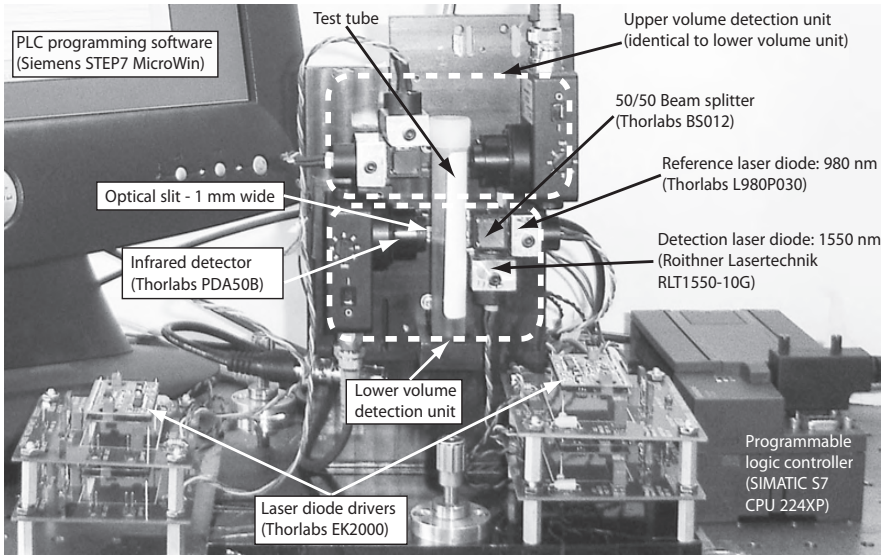

Fig. 5 Prototype of volume detection to verify minimum and maximum allowable volume levels in medical samples.

Fig. 3. In the range from 350 to 1100 nm, the tube with water has an intensity distribution that follows the shape of an empty tube but at a slightly lower level. Between 1400 and 1600 nm, the light intensity drops dramatically for the tube with water. Direct comparison between the empty tube and the tube filled with water shows that the drop in intensity is a result of increased absorption by the water and not by the tube material. Therefore, the range of 1400 to 1600 nm is well suited for differentiating between a liquid and air. Similarly, in order to be able to compensate for the effects of an unknown number of paper labels, a reference wavelength is selected in a range where liquids and air absorb light at a similar rate, in this case within the range of 900–1100 nm.

4 Volume Detection Prototype

The principle of the detection system is demonstrated in Fig. 4. The system features two light sources in the form of laser diodes, which are mounted on a common plane at 90 deg relative to each other. The detection laser diode has a peak wavelength of 1550 nm and an optical output of 30 mW (RLT1550-10G from Roithner Lasertechnik). The reference laser diode peak wavelength is located at 980 nm and also has an optical output of 30 mW (L980P030 from ThorLabs). The output of both diodes is passed through a 50/50 beamsplitter, which creates a common optical path through the sample. The rectangular output of the laser diodes is focused with planoconvex lenses to create rectangular beams with a width of 10 mm and a height of 1 mm.

The measurement of the intensities is performed sequentially. First, the reference light is turned on and the intensity of the transmitted light is measured by the detector (PDA50B from ThorLabs) in the form of an analog voltage that ranges between 0 and 10 V. The PDA50B has a builtin amplifier, which was set to 70 dB, a range of 800–1800 nm, and reaches peak sensitivity at 1550 nm. The programmable logic controller (PLC, SIMATIC S7 CPU 224XP) samples the analog output digitally with a 16-bit resolution and stores the mean value of the voltage in memory. Next, the detection light is turned on, its intensity is measured, and the mean value of the voltage is stored in the PLC memory. The final step is for the PLC controller to compute the ratio between the two stored intensities in terms of their respective voltages,

$$R = \frac{I_{980\ \mathrm{nm}}}{I_{1550\ \mathrm{nm}}} = \frac{I_{\mathrm{REF}}}{I_{\mathrm{DET}}}. \tag{1}$$

This ratio R is compared to a threshold value R_{th}, which takes into consideration the relevant optical characteristics of all elements involved, which include the output of the light sources, the sensitivity of the detector, as well as the

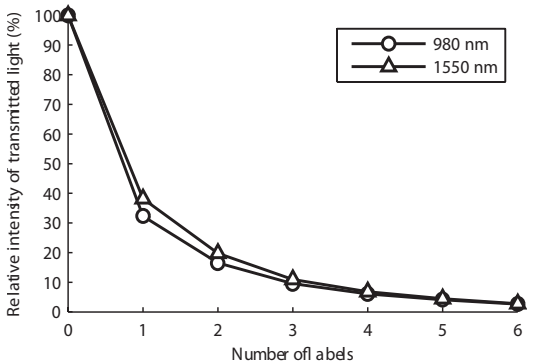

Fig. 6 Intensity of transmitted light through increasing number of labels for 980 and 1550 nm. This is reported as the light intensity transmitted for each wavelength normalized against the intensity recorded with no labels (=100%).

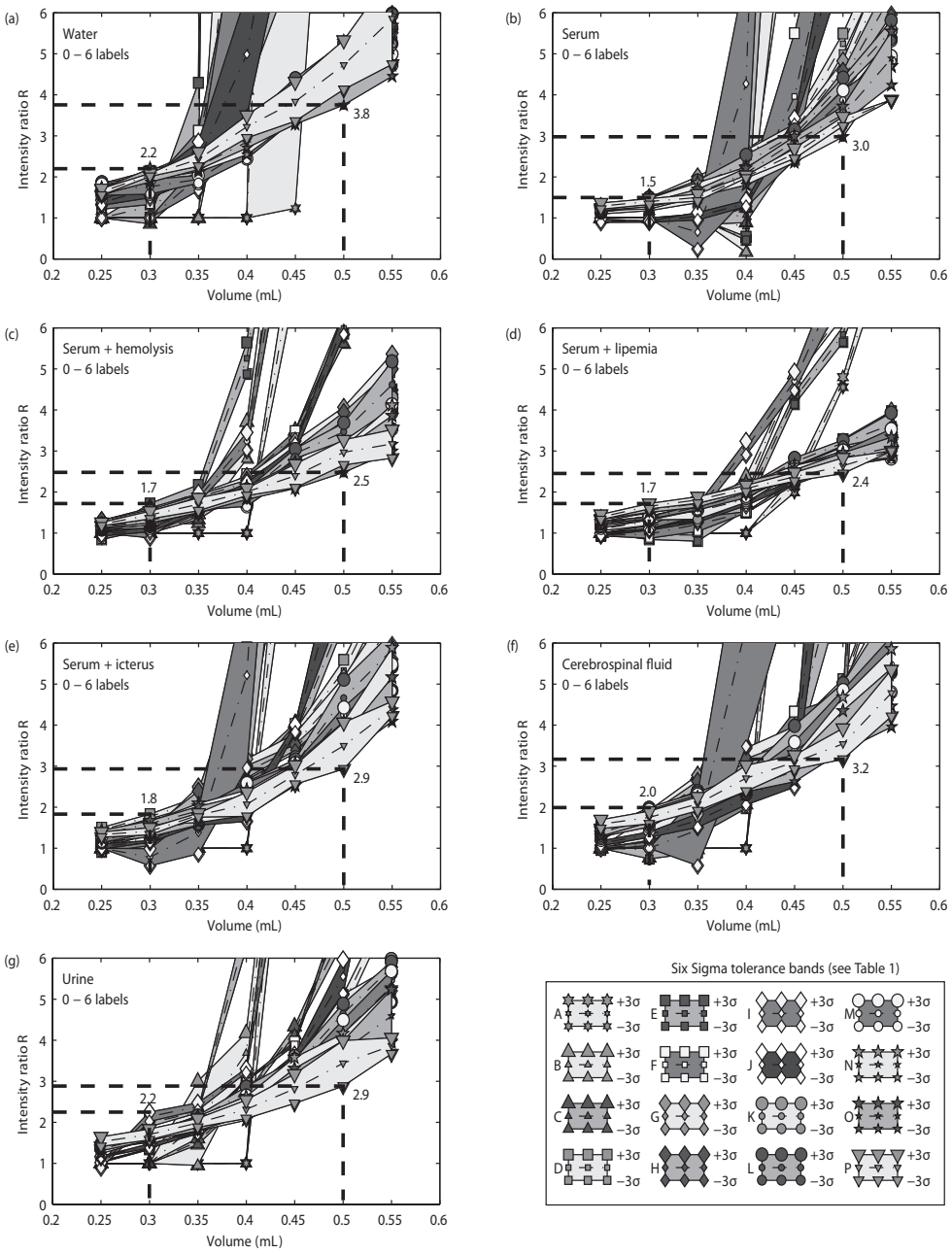

Fig. 7 Six Sigma tolerance bands for detecting the volume of medical samples at 0.4±0.1 mL for (a) water, (b) serum, (c) serum+hemolysis, (d) serum+lipemia, (e) serum+icterus, (f) cerebrospinal fluid, and (g) urine.

Table 1 The 16 possible combinations of 0–3 labels attached to a test tube.

Test ID	A	B	C	D	E	F	G	H	I	J	K	L	M	N	O	P
Facing laser diode	0	0	1	1	0	2	1	2	0	3	2	1	3	2	3	3
Facing detector	0	1	0	1	2	0	2	1	3	0	2	3	1	3	2	3
Total number of labels	0	1	1	2	2	2	3	3	3	3	4	4	4	5	5	6

absorption characteristics of the tube materials, labels, and also that of the samples to be tested. Choosing a threshold value that is between the intensity ratios of air and liquid provides a simple and reliable means of detecting the presence of a liquid and yields enough resolution to measure the volume level within the required tolerances,[12]

$$R_{\text{liquid}} > R_{\text{th}} > R_{\text{air}}. \quad (2)$$

Therefore, if the computed intensity ratio R is greater than the threshold R_{th}, liquid is present. On the other hand, if R is smaller than R_{th}, then air is present.

The actual prototype of the volume detection device is shown in Fig. 5. The minimum and maximum volume levels are measured with two separate, but identical, optical systems. For improved resolution, each volume measurement unit contains an optical aperture with a width of 1.0 mm in front of the photodetector. Not shown in Fig. 5 is the cover of the unit, which shields the system from environmental interferences.

The measurement time for the system is primarily determined by the time the laser diodes require to reach a stable output, which in both cases is 0.24 s. Because the laser diodes are turned on sequentially, the delay time due to the diodes is $0.24 \times 2 = 0.48$ s per tube. The sampling time for the volume detection is 0.01 s for each wavelength, resulting in an overall measurement time per tube of 0.5 s.

5 System Testing

The most important step of this method is to obtain the R_{th}, which will be used by the system as the primary decision criteria. Because most of the light-absorption variability is linked to the thickness and/or position of the labels (Fig. 6), which may vary between 0 and 3, there are 16 possible label combinations. The details of these scenarios are listed in Table 1 and identify the number of labels as well as their exposure to either the detector or the laser diode.

For the scenarios listed in Table 1, each of the seven liquids were added to separate test tubes in 0.05 mL increments and the intensity ratio was recorded. Each experiment was repeated 40 times, resulting in 4480 unique measurements for each liquid, and the mean as well as the standard deviation values were calculated. Figure 7 shows the -3σ to $+3\sigma$ ranges of the measured intensity ratios for the minimum acceptable volume as ribbonlike tolerance bands for each of the label combinations and all relevant liquids. These ranges are significant because identifying a threshold value that is outside this six standard deviation range (6σ) will result in a system with a reliability of better than 99.73%. There are two limiting cases for identifying the threshold value. The lower limit of R_{th} is determined at the smallest allowable volume (0.3 mL) by the largest $+3\sigma$ values of all possible combinations, which in this case, is 2.2 for water [Fig. 7(a)] and urine [Fig. 7(g)]. This ensures, with 99.73% reliability, that air is identified as the medium. The upper limit of R_{th} is determined at the largest allowable volume (0.5 mL) by the smallest -3σ value of all combinations, which is 2.4 for lipemia [Fig. 7(d)]. This results in a 99.73% reliability of detecting a liquid. For the volume-detection prototype, the actual value for the threshold R_{th} was taken as the mean of the upper and lower limits and set to 2.3. Hence, for volume measurements with a tolerance of 0.4 ± 0.1 mL,

$$R_{\text{liquid}} > 2.3 > R_{\text{air}}. \quad (3)$$

Thus, the volume measurement is then reduced to computing the intensity ratio of the reference and the detection wavelength, and compared to the threshold value. For the lower volume, if the intensity ratio is >2.3, then the minimum volume requirement is satisfied. Otherwise, if the intensity ratio is <2.3, then not enough liquid is present in the tube.

The actual liquid-level tolerances for the individual liquids can be obtained by intersecting the 2.3 intensity ratio line with the six-sigma plots shown in Fig. 7. The results are given in Table 2 and show that the combined liquid-level tolerance with a 99.73% reliability ranges from 0.31 to 0.48 mL.

Table 2 Actual liquid level tolerances based on an intensity ratio $R_{\text{th}}=2.3$ for 99.73% reliability (six sigma).

Liquid	Six-sigma detection tolerance (mL)
Water	0.31–0.45
Serum	0.36–0.45
Serum+hemolysis	0.35–0.48
Serum+lipemia	0.37–0.47
Serum+icterus	0.34–0.44
Cerebrospinal fluid	0.32–0.43
Urine	0.31–0.43
All liquids combined	0.31–0.48

6 Conclusions

The optical volume detection system described in this paper is capable of detecting the liquid level of medical samples in test tubes, which have an unknown number of paper labels attached (which can vary between zero and six layers). Using laser diodes at 1550 and 980 nm wavelengths as the detection and reference light sources and computing the ratio of the intensity of the transmitted light, a robust system was developed that allows the verification of volume requirements of 0.4 ± 0.1 and 4.0 ± 0.1 mL with $>99.73\%$ reliability in only 0.5 s. The system has no moving parts. Instead, the sequential measurements are achieved by switching the laser diodes on and off. To avoid this, and to further reduce the measurement time, it is also possible to use motorized light shields in front of the laser diodes, which would allow the laser diodes to be powered on.

Acknowledgments

The authors would like to acknowledge the financial support of the project from ARUP Laboratories. Particular thanks go to Dr. Charles Hawker and Dr. William Roberts

for their expertise in testing medical samples as well as William Owen for providing and characterizing the medical samples used in this research.

References

1. A. Jaramillo-Nunez and M. Lucero-Alvarez, "Optical laser level," *Opt. Eng.* **45**(9), 093601 (2006).
2. K. E. Maatta and J. T. Kostamovaara, "High-accuracy liquid level meter based on pulsed time of flight principle," *Proc. SPIE* **3100**, 268–277 (1997).
3. C. P. Yakymyshyn and C. R. Pollock, "Differential absorption fiber-optic liquid level sensor," *J. Lightwave Technol.* **LT-5**, 941–946 (1987).
4. A. K. Ghosh, N. S. Bedi, and P. Paul, "Package design for low-cost optical liquid-level sensors," *Opt. Eng.* **39**, 1405–12 (2000).
5. W. Yuan and D. Li, "Measurement of liquid interface based on vision," *Proc. of 5th World Congress Intell. Control and Autom.*, IEEE, Hangzhou, China, pp. 3709–3713 (2004).
6. J. D. Mc Neal, Y. Liu, and M. S. Adzich, "Sample level detection system," *US Patent No. 6,770,883 B2* (2004).
7. N. R. Bachur Jr. and T. G. Foley Jr., "System and method for determining fill volume in a container," *U.S Patent Appl. No. 2006/0154327 A1* (2006).
8. I. Fine and L. Shvartsman, "Method of optical measurement for determining various parameters of the patient's blood," *U.S. Pat. 6,711,424 B1* (2004).
9. T. E. Cadell and J. Samsoondar, "Apparatus and method for rapid spectrophotometric pre-test screen of specimen for a blood analyzer," *U.S. Patent No. 6,195,158 B1* (2001).
10. S. P. Hendee, H. D. T. Jones, D. A. Birnkrant, R. D. Johnson, R. E. Abbink, and R. G. Messerschmidt, "Analyte determinations," *U.S. Patent Appl. No. 2004/0241736 A1* (2004).
11. E. Musayev and S. Karlik, "A novel liquid level detection method and its implementation," *Sens. Actuators, A* **109**, 21–24 (2003).
12. B. J. Corbin, "Design of optical scanning system to detect volume and interferences in blood specimen in test tubes," M.S. thesis Univ. of Utah (2007).

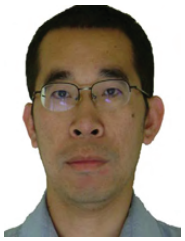

Xin Liu is a PhD candidate in the Department of Mechanical Engineering at the University of Utah, working in the Precision Design Laboratory (PDL) of Prof. E. Bamberg. He received his BS in 1997 and MS in 2003 in mechanical engineering from Jilin University of Technology, China. He worked three years as a design engineer at the Tianjin Research Institute of Construction Machinery, and two years as a staff engineer at the China Certification Center for Automotive Products. His research interests include optical measurement systems, mechatronics, and modern design methods.

Brendan J. Corbin is a mechanical engineer at Artann Laboratories in West Trenton, New Jersey, where he is developing a temperature profile spectrometer and a colonoscopy force monitor. He earned his MS in mechanical engineering in 2007 at the University of Utah and his BS in mechanical engineering at Syracuse University in 2005. At Syracuse University, he was awarded the George Farnell Senior Design Award by the ASME for his contributions. His research interests include optical instruments, rapid prototyping, and machine design.

Stacy J. Morris Bamberg is currently an assistant professor in mechanical engineering at the University of Utah in Salt Lake City, Utah. She heads the BioInstrumentation Lab, which focuses on developing minimally obtrusive, multimeasurement sensors and instrumentation, methods of extraclinical assessment, and devices for rehabilitation. Prof. Bamberg received her BS and MS in mechanical engineering from the Massachusetts Institute of Technology, Cambridge, Massachusetts, in 1996 and 1999, respectively. She did her doctoral research in the MIT Media Lab and received her DSc in medical engineering from the Harvard/MIT Division of Health Sciences and Technology, Cambridge, Massachusetts, in 2004. Other research areas of interest include aging, gait analysis, and use of inertial sensors for robotic navigation and orientation.

William R. Provancher has earned his BS in mechanical engineering and his MS in materials science and engineering, both from the University of Michigan, his PhD, from the Department of Mechanical Engineering at Stanford University, was in the area of haptics, tactile sensing, and feedback. His postdoctoral research involved investigating and designing bioinspired climbing robots, focusing on creating foot designs for climbing vertical surfaces with compliantly supported spines. He is currently an assistant professor in the Department of Mechanical Engineering at the University of Utah. Prof. Provancher teaches courses in the areas of mechanical design and mechatronics. His active areas of research include haptics, tactile sensing and feedback, and the design of novel climbing robots.

Eberhard Bamberg is currently an assistant professor in the Department of Mechanical Engineering at the University of Utah and the director of the Precision Design Laboratory. He received his MSc from Brunel University, Uxbridge, United Kingdom, in 1993, and his Dipl-Ing from the University of Stuttgart, Stuttgart Germany, in 1996 in mechanical engineering. He earned his PhD from the Massachusetts Institute of Technology in 2000 in the area of precision design. His postdoctoral research at MIT involved the development of a technology-assisted curriculum for courses in mechanical engineering. Prof. Bamberg teaches courses in the area of design and manufacturing, and his research interests include precision engineering, novel micro- and mesolevel manufacturing technologies, nontraditional machining techniques for semiconductors, and optical instrumentation.

CHAPTER 4

VARIABLE VOLUME DETECTION SYSTEM

After the development of the Max/Min Volume Detection System, a Variable Volume Detection System was proposed and prototyped.

Unlike the Max/Min Volume Detection System, which is limited to determining the liquid condition at two fixed positions, the Variable Volume Detection System can detect the position of the liquid surface by scanning the entire height of test tubes. Combining the location of the liquid/air interface with geometric information of the test tube acquired through a machine vision system, allows the volume of the liquid sample in test tubes to be calculated.

4.1 Structure of variable volume detection system

As shown in Fig. 4-1, the Variable Volume Detection System consists of two main parts, the laser sources and the detectors. Laser diodes (LD) with two different wavelengths are chosen as light sources. The 1550 nm wavelength LD is referred as the detection laser source, while the 980 nm wavelength LD acts as the reference laser source. The distance between the two laser sources is determined by the closest possible arrangement of the two detectors and is set to 32 mm.

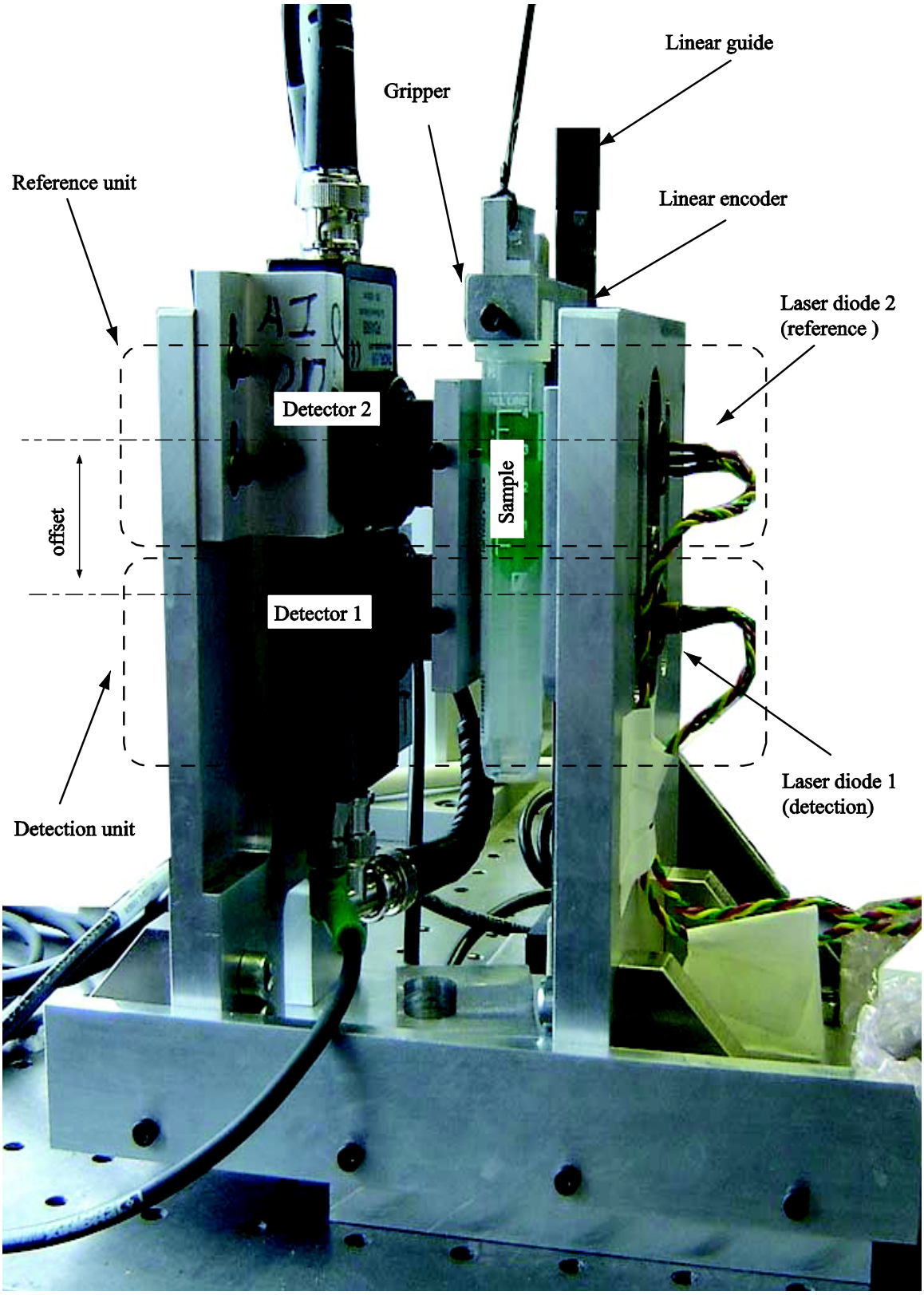

Fig. 4-1 Prototype of the Variable Volume Detection System. It consists of two laser diodes and two optical detectors.

The detectors are mounted at the opposite side of the laser sources relative to the test sample. Their optical axes are coaxial with those of the laser sources, and orthogonal with the center line of the test tube.

Each laser source has an optical output of up to 100 mW. To guarantee the reliability of the detection system, two driver boards were used to power the laser sources. The adjustable constant current of the driver boards based on feedback from the laser diode lead to a constant power output of the laser sources.

As shown in Fig. 4-2, the measurement principle of the system is based on lifting the test tube vertically past the optical system while simultaneously recording the position of the tube as well as the power of the transmitted laser lights. This is are achieved with a National Instruments multifunction data acquisition module (NI USB-6211), which converts the analog output signal of the optical detectors to a digital signal with 16 bit resolution. The data acquisition system also records the tube position, which is derived from a linear encoder that is mounted to the side of the gripper. The position is read as a series of square waves (quadrature counts). The max sampling speed is 250 kS/s.

4.2 Principle and process of the detection

Similar to the Max/Min Volume Detection System, the Variable Volume Detection System finds the level of the liquid surface by comparing the ratio of the transmitted powers at different heights. The process of the detection is shown as a flowchart in Fig. 4-3.

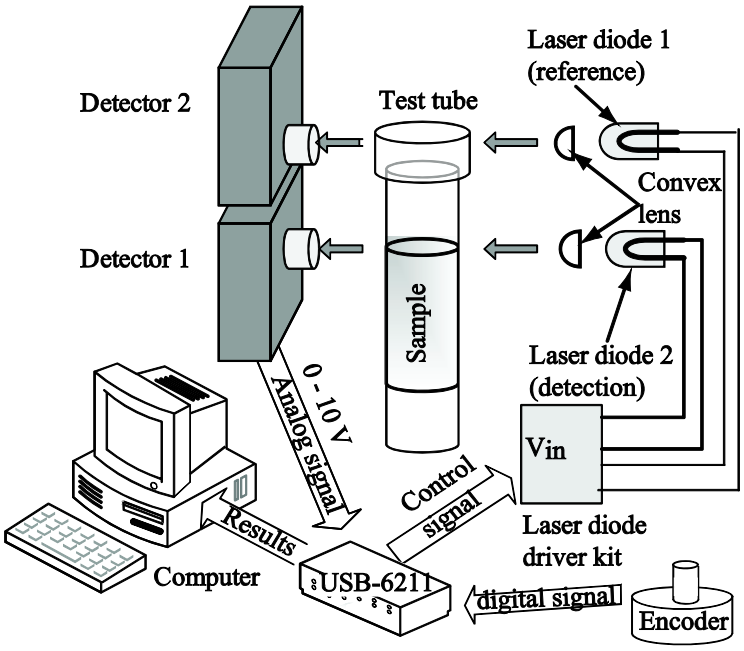

Fig. 4-2 A National Instruments multifunction data acquisition module (NI USB-6211) is used to acquire the position of the test tube and transmitted light power at this position.

After the test tube is placed at the initial position, a robotic gripper will engage and lift it up past the optics. The position of the test tube is recorded by a linear encoder. The lift up speed will be 40 mm/s. This allows the entire height of the tube to be scanned quickly (2 s for a standard 96.8 mm high tube). The sampling frequency is set to 1000 Hz that yields a spatial resolution 0.05 mm. When the starting position of the test tube is reached, the powers of the transmitted light of the two light sources are measured by the detectors continuously. The powers together with the tube position are sent to a computer and stored to a file. When the gripper reaches the end of the stroke, the measurement process is stopped. The test tube is sent back to its initial position by the robotic gripper.

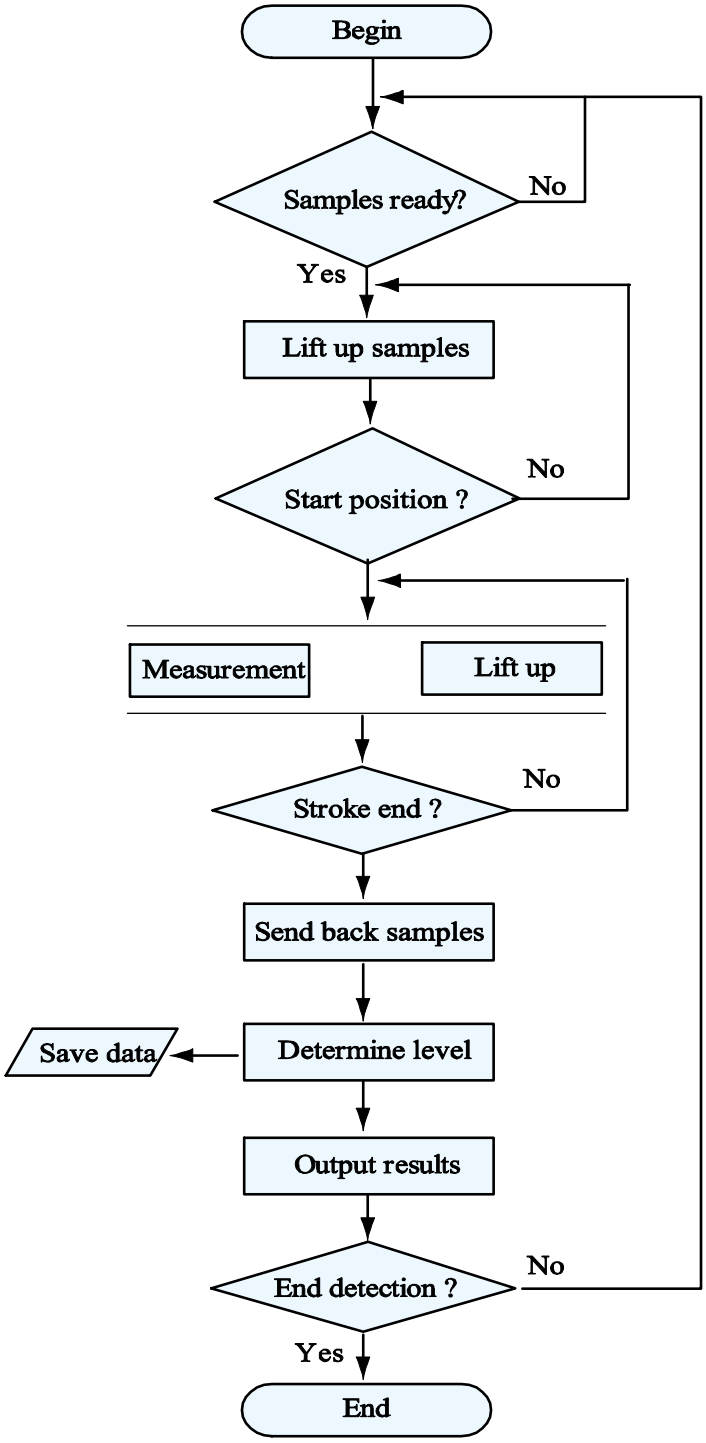

Fig. 4-3 Flowchart of the detection process.

The control software programmed in LabVIEW[1] shifts the position of the detection laser power back by 32 mm in order to compensate for the offset between the reference and detection systems.

The power ratio between the detection source and reference source is calculated. The first position where the ratio exceeds the threshold value is acquired. The height of the liquid surface in this test tube will be computed by subtracting the position value from the distance between the center line of the detection laser source and the bottom of the test tube at the initial position. It can be calculated as:

$$H_{\text{liquid}} = H_{\text{beam}} - T_{\text{tube}} \tag{4.1}$$

where H_{liquid} is the actual liquid level in the test tube, H_{beam} is the height of the center line of the detection laser diode to the reference bottom, and T_{tube} is the travel of the test tube before the surface of the liquid is detected.

The position of the liquid bottom surface is determined similarly, and the length of the liquid plug in the test tube can be calculated by subtracting the bottom position from the position of the top surface.

4.3 Experimental verification

Experiments were conducted to verify the principle and to establish the measurement uncertainty of the Variable Volume Detection System.

[1] LabVIEW is a graphical programming environment by National Instruments

4.3.1 Effect of slits and the shield box on background noise

To increase the accuracy of measurement, slits are mounted in front of the detectors and the laser sources. In order to eliminate environmental interferences, a shield box covers the system and blocks the outside light and electromagnetic waves.

The effects of slits and shield box are verified experimentally. The setup of testing is listed in Table 4-1. The detectors will be totally blocked during testing under situation *A* and *B*. This experiment measures the zero shifts of detectors without light input. *C* and *D* measures the environmental interferences with and without the shield box, while *E* and *F* test the effect of the slits.

The voltages measured by detectors with 3σ distribution are plotted in Fig. 4-4. The shield box plays the most important role in eliminating interferences from the environment. The slits in front of the detectors also decrease the noise noticeably.

4.3.2 Effect of slits to measurement results

Another experiment is conducted to verify the effect of slits on the measurement results.

Table 4-1 The combinations of testing setup

Test ID	*A*	*B*	*C*	*D*	*E*	*F*
Totally blocked	X	X				
With slit in front					X	X
With shield box		X		X		X

Notes: X means the system is tested under this specific condition.

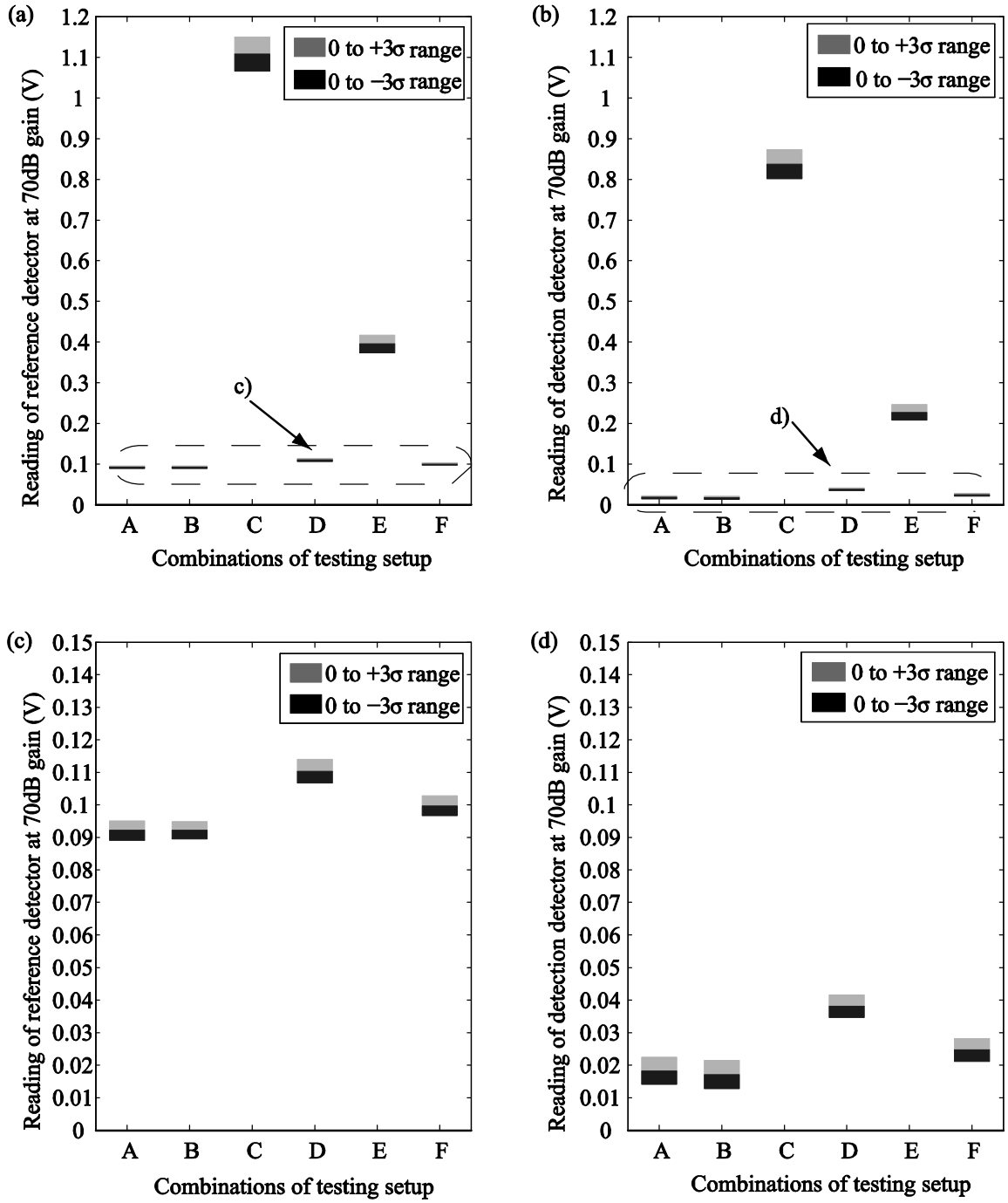

Fig. 4-4 The measurement results of reference and detection detectors at 70 dB amplification under different setup, with a level of confidence of 99.73% (a) The reference detector, (b) The detection, (c) and (d) The zoom area of (a) and (b), respectively.

Sealed standard testing tubes filled with water were used as samples in the experiments. The test tubes were attached with varying numbers of labels to their outside, according to Table 4-2. Before every test, a vertical gage was used to measure the height of the liquid surface center.

Every tube was scanned from top to bottom, and the power of the transmitted light at 980 and 1550 nm was recorded. Next, the transmitted powers of the two wavelengths were shifted to the same positions. The power ratio between the detection source and reference source was calculated using Eq. (4.1). The first five continuous positions where the ratios exceed the threshold value are acquired. The first position was considered as the position of the interface between air and liquid. The height of the liquid surface in this test tube will be computed by Eq. (4.1).

Comparing the detection value from 20 measurements with the actual height allows the average values and standard deviations to be computed. Based on the six sigma ranges shown in Fig. 4-5, the detection system with slits in front of detectors can detect the water in a standard test tube with an uncertainty of measurement of less than 0.4 mm with a level of confidence of 99.73%. Meanwhile, the detection system without slits in front of the detectors can detect the height with an uncertainty of measurement of less than 0.75 mm with a level of confidence of 99.73%.

Table 4-2 The nine possible combinations of 0–2 labels attached to a test tube.

Test ID	A	B	C	D	E	F	G	H	I
Facing laser diode	0	0	1	1	0	2	1	2	2
Facing detector	0	1	0	1	2	0	2	1	2
Total number of labels	0	1	1	2	2	2	3	3	4

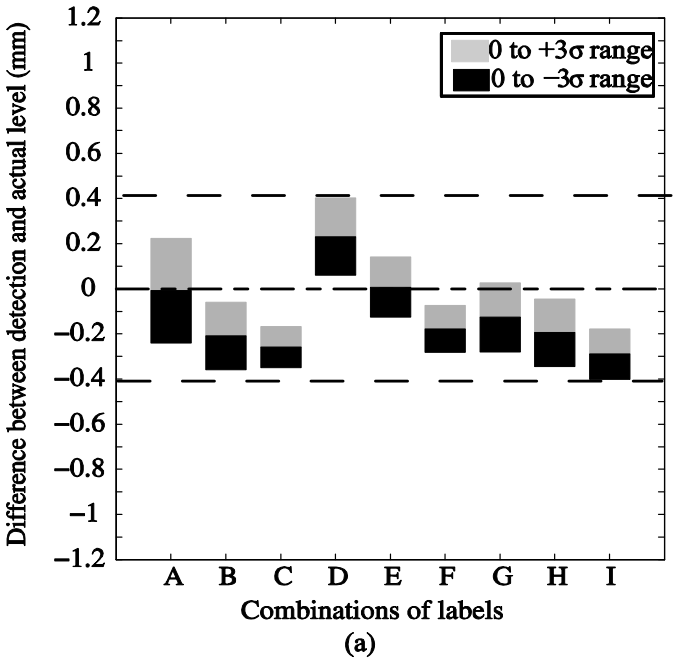

(a)

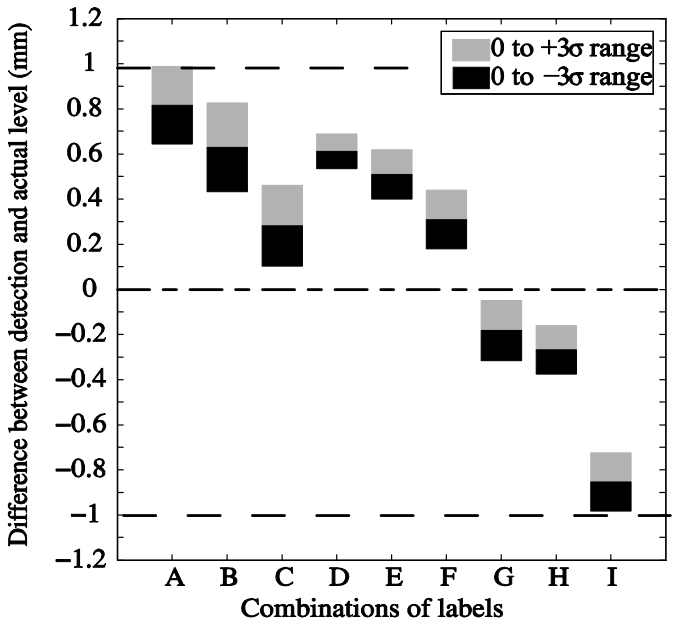

(b)

Fig. 4-5 The measurement results with a level of confidence of 99.73%. 1 mm in level correspond to 1.33 mL in volume for standard test tubes with an inner diameter of 13 mm (a) The system with slits in front of detectors. (b) The system without slits in front of detectors.

Based on the results, the slits have shown to significantly improve the measurement results.

4.4 Future work

To apply the Variable Volume Detection System to an industrial environment, a microcontroller based data acquisition and control system will replace the NI USB-6211 DAQ module. The analog to digital convertor (ADC) of the microcontroller will measure the power of the transmitted laser during the detection process. Digital input and outputs will record the encoder position and control the power supply of the laser diode driver boards. The measurement results will be sent to a host computer. The computer determines the level and volume of the liquid by analyzing the data acquired.

CHAPTER 5

INCREASING THE ACCURACY OF LEVEL-BASED VOLUME DETECTION OF MEDICAL LIQUIDS IN TEST TUBES BY INCLUDING THE OPTICAL EFFECT OF THE MENISCUS

Liu, X., Bamberg, S. J. M. and Bamberg, E. (2011). "Increasing the accuracy of level-based volume detection of medical liquids in test tubes by including the optical effect of the meniscus." *Measurement*, 44(4), 750-761

Measurement 44 (2011) 750–761

Contents lists available at ScienceDirect

Measurement

journal homepage: www.elsevier.com/locate/measurement

Increasing the accuracy of level-based volume detection of medical liquids in test tubes by including the optical effect of the meniscus

X. Liu, S.J.M. Bamberg, E. Bamberg *

Department of Mechanical Engineering, University of Utah, Salt Lake City, UT 84112, USA

ARTICLE INFO

Article history:
Received 6 August 2010
Received in revised form 2 December 2010
Accepted 7 January 2011
Available online 13 January 2011

Keywords:
Volume measurement
Optics
Optoelectronics
Meniscus model

ABSTRACT

A novel system for liquid volume detection is reported in this paper. The system uses two lasers with different wavelengths to scan the entire height of tubes. By detecting the shape and position of the meniscus that is formed at the liquid-air interface, the volume of liquid in a tube of known geometry can be determined. To increase the accuracy of this level-based volume detection, the shape of the meniscus must be considered. The optical effect of the meniscus in such a system was modeled and its effect on the volume detection simulated. A laboratory prototype was built and the biggest difference between the measured power of the transmitted light through the meniscus and the simulated data was less than 8%.

1. Introduction

Measuring volume in medical samples without removing the cap of the tube is an important first step in highly automated laboratories. Optical systems that are based on detecting the liquid level through the side of the test tube have been shown to work well as long as the test tubes are sufficiently transparent. Systems that incorporate this method include the edge detection method by Yuan and Li, based on a computer vision system [1]. The method invented by McNeal et al. moved the sample container past a fixed optical system that measured the power of the transmitted light. The liquid level in this system was recorded in response to a change in power as a result of differences in absorption between a liquid and air [2]. Level detection based on measuring the power of transmitted light was also employed in the system from Bachur and Foley. Here, in order to achieve a more robust system that could compensate for additional factors that reduce the light power, the transmitted light power through the sample was compared with the power of light transmitted through a reference sample [3]. Recently, Liu et al. [4] developed an optical system with the ability to distinguish between a liquid and air through an unknown number of labels attached to the outside of the tube. The system performed this measurement at two fixed positions, namely the minimum required lower level and the maximum allowable upper level with an uncertainty of measurement of 0.1 mL at a level of confidence of 99.73%.

While all of the above listed systems detected the liquid level from the side, none of the systems considered the shape of the liquid level. In general, the level of a liquid inside a container is not flat but forms a meniscus due to surface tension forces. The curvature of the meniscus, given that liquids typically have a much greater refractive index than air, will affect the amount of light transmitted. Furthermore, when using the level to determine the volume of liquid, the volume of liquid contained in the meniscus itself also plays an important role for measurement accuracy.

Numerical modeling of the meniscus has been performed by a number of researchers. Roura [5] used an energy method to obtain the relationship between the contact angle and surface tensions and showed that Young's equation can be extended to a thick capillary tube. The contact angle depended on the surface between the

* Corresponding author.
E-mail address: bamberg@alum.mit.edu (E. Bamberg).

0263-2241/$ - see front matter © 2011 Elsevier Ltd. All rights reserved.
doi:10.1016/j.measurement.2011.01.001

liquid and solid, liquid and vapor (air), and vapor/air and solid. Lee and Lee [6] evaluated the meniscus shape of the liquid in capillary tubes and found good agreement with previous work.

Longrigg [7] utilized the optical effect of the meniscus to develop a technique that utilized the reflection or refraction effect of a laser at the surface of a meniscus to measure the surface tension of the liquid. Dong et al. [8] measured the curved liquid surface by analyzing the reflective pattern of a tuning laser that illuminated the liquid surface in the vertical direction. The reflected light was captured with a CCD sensor and by measuring the diameter of the dark area, the boundary light path was obtained. Xu et al. [9] developed a holographic system based on interference fringes from two incident lasers with a small angle in between to measure the profile of liquid droplets. The system required the droplets to be placed on a flat substrate with a similar refractive index and allowed the wetting characteristics, the contact angle and the solid liquid surface tension to be determined. Ondris et al. [10] utilized the optical effect of the meniscus to measure the level of a liquid surface. This method used a CCD line image sensor to capture the power change in the vertical direction. The measurement range and accuracy depended on the size and quantity of the CCD sensors and light source. The light source system needed to emit rays that are parallel to the plane that passes through the center line of the tube and sensor. Also, the light had to be orthogonal to the tube center line.

In this paper, the effect of the meniscus on the measurement accuracy of level-based volume detection methods is presented. The technique described is part of a novel volume detection system that scans the length of a test tube with infrared wavelengths of two laser beams to detect the liquid level. The volume is then calculated based on the geometry of the test tube, the position of the liquid–air interface, and the volume contained in the meniscus.

2. Principle of detection

A critical element of the volume measurement described in this paper is the detection of the position of the interface that is formed between the liquid and air. The basis of the method is the fact that liquids absorb more light than air, which yields a difference between the powers of transmitted light through the liquid when compared to air. As an optical system that is based on transmitted light, optical effects such as reflection, scattering, diffraction, and absorption all contribute to the attenuation of the transmitted light. Therefore, in order to achieve a system that is insensitive to external effects such as labels attached to the tube, and ink that is printed on the labels, the system uses two laser beams as described by Liu et al. [4] with wavelengths 980 nm (reference wavelength) and 1550 nm (detection wavelength). This provides two independent sets of data of transmitted light versus position and taking the ratio between the detection and reference data sets allows the effects of attenuation that is not related to absorption by either air or liquid to be compensated. The main components of the system are shown in Fig. 1 and consist of the detection and reference measurement units, which are located at fixed positions, as well as an actuation system that moves the test tube vertically past the measurement units to create the scanning motion. The detection measurement unit consists of a laser diode with a wavelength of 1550 nm and a photodetector that is located on the same optical axis on the other side of the test tube. The reference unit uses a 980 nm laser diode but is otherwise identical to the detection unit. The distance between the optical axes of both measurements units is well quantified and is used as an offset to overlay the two separate measurements.

During such a scan, the laser light will encounter three distinct areas: air, liquid, and the meniscus that is formed at the air–liquid interface as illustrated in Fig. 2. Thus, the power of the transmitted light will be reduced by three separate effects: reflection at the tube surface, absorption by the liquid and tube, and refraction from the curved surface of the meniscus.

The height h_M of the meniscus in medical samples shown in Fig. 2c is not a constant but depends on the type of sample. For a standard test tube with an inner diameter of 13 mm and nominal volume of 5.0 mL, the meniscus height for various medical samples was measured to range between 1.0 and 2.8 mm. The change in the amount of the transmitted light caused by its optical effect provides the information required to determine its position and height. By determining the height and position of the meniscus in the tube, the accurate volume of liquid can be calculated. The total volume in the test tube can be computed as:

$$V_{\text{total}} = \pi D_{\text{tube}}^2 h_b/4 + V_M \tag{1}$$

where V_{total} is the actual liquid volume in the tube, D_{tube} is the inner diameter of the test tube, h_b is the position of the bottom of the meniscus, and V_M is the volume contained in the meniscus.

3. Meniscus modeling and simulation

To study the effect of the meniscus on the measurement accuracy, a numerical model is set up to simulate the detection process. First, the surface shape of the meniscus is modeled at specific conditions. The meniscus model is then implemented in a simulation that predicts the path and the change of power of the transmitted light that passes through the sample at different levels.

3.1. Profile of meniscus

The volume of the liquid that is raised by the surface tension at the air-liquid interface consists of a cylinder and an upper meniscus. The cylindrical part can simply be expressed as a cylinder with a diameter that is equal to the inner diameter of the tube. The meniscus part will be expressed by its profile, which is affected by the surface tension of the liquid, the dimensions of the tube, and the properties of the solid–air–liquid system where it is located. Considering the rotational symmetry of the meniscus, a cylindrical coordinate system (r,z) as depicted in Fig. 3 is used for the model.

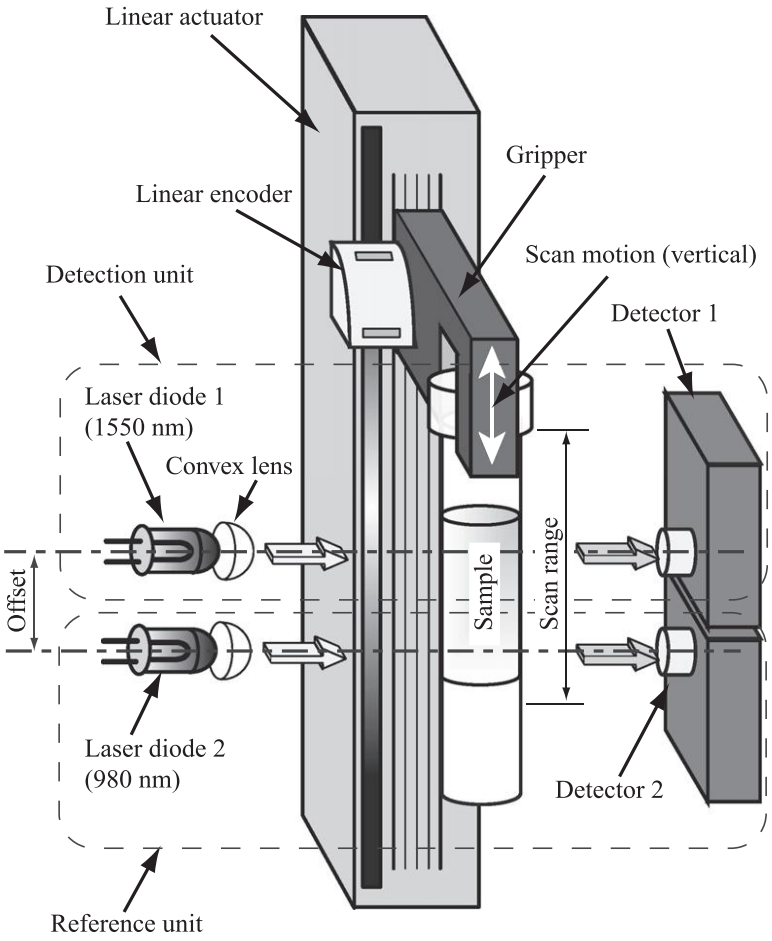

Fig. 1. The position of the air-liquid interface is detected optically by scanning the length of the tube with two laser beams while recording the power of the transmitted light through the sample as a function of position with two photo detectors.

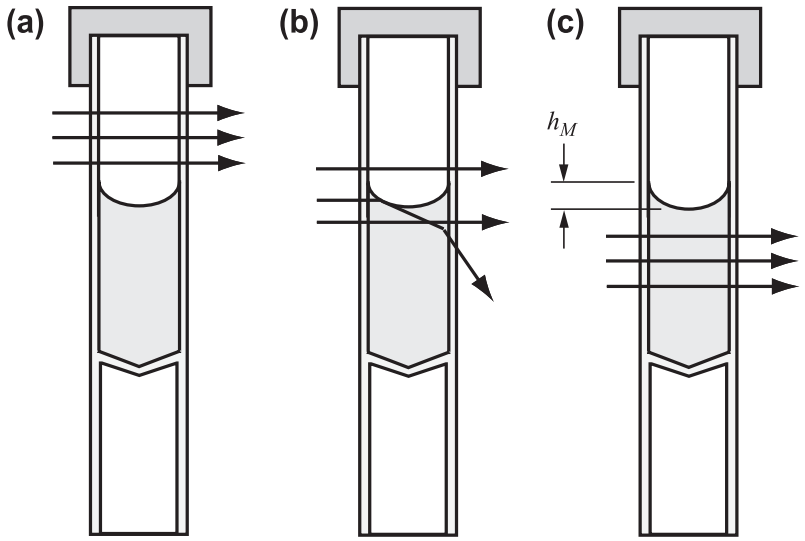

Fig. 2. The transmitted light may pass through (a) air, (b) the meniscus of the air-liquid interface or (c) through the liquid.

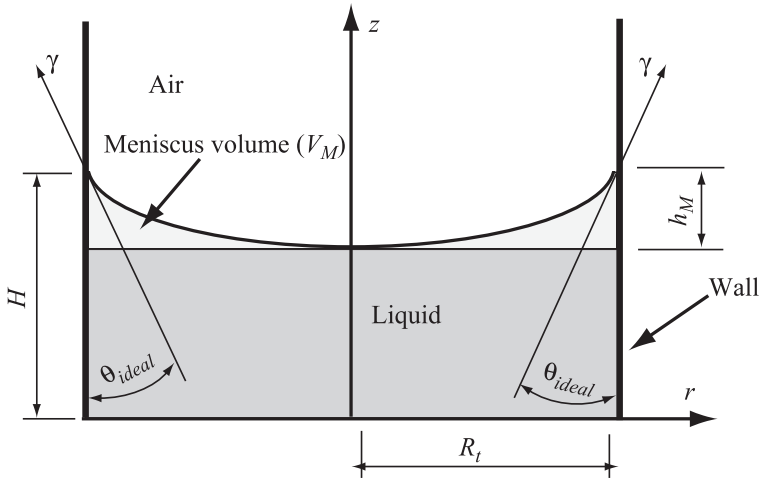

Fig. 3. The solid–liquid–air system consists of the tube wall, liquid, and air. The *z*-axis is the center line of the liquid cylinder and *r* is its radius. The origin is located at the bottom surface of the liquid that is raised by the surface tension force.

θ is the contact angle, which is constructed by the wall and the tangent line of the meniscus surface. The volume of the liquid that is raised by the surface tension force is determined by the balance of force due to the surface tension, the weight of the liquid, the viscosity force on the inner tube surface, and the inertia force. During volume measurements, the liquid remains stationary. Hence, the viscosity and inertia forces do not need to be considered. The general form of the meniscus volume can be simplified to [5,6]:

$$V = (2\pi R_t \gamma \cos\theta)/(\rho g) \tag{2}$$

where R_t is the inner tube radius, γ is the surface tension, θ is the contact angle, V is the volume raised by the surface tension, ρ is the density of the liquid, and g is the gravitational acceleration. The volume of the raised liquid can be found by integrating its profile $H(r)$ along the radius of the liquid:

$$V = \int_0^{R_t} H(r) 2\pi r dr \tag{3}$$

The contact angle of the meniscus surface at different radii can be expressed as the derivative of the profile at this point [11].

$$\frac{dH(r)}{dr} = \cot[\theta(r)] \tag{4}$$

At the position near the wall, the contact angle θ will be determined by the property of the solid–liquid–air interface. When sufficient energy is put into the system to overcome the energy barriers, the advance and recession angles will converge to a common value, referred to as the ideal angle θ_{ideal} [12,13].

$$\left.\frac{dH(r)}{dr}\right|_{r=R_t} = \cot(\theta_{ideal}) \tag{5}$$

At the center of the meniscus, the liquid surface will be horizontal, resulting in a contact angle of 90°.

$$\left.\frac{dH(r)}{dr}\right|_{r=0} = 0 \tag{6}$$

The height of the meniscus can be calculated from the difference between the top and bottom edges of the meniscus as:

$$h = H(R_t) - H(0) \tag{7}$$

The values of surface tension for medical samples can be taken from the literature and the height of the meniscus can be obtained experimentally. For water at room temperature, the surface tension is 0.07275 N/m [14]. The shape of the meniscus can then be determined by numerically solving the differential equation (Eq. (4)) using the boundary conditions (Eqs. (5) and (6)).

3.2. Numerical model of the meniscus shape

The numerical model is based on rotational symmetry, since the raised liquid is symmetric about the tube center axis. The volume can then be divided into multiple thin rings with wall thickness δ as shown in Fig. 4. For the case where R is less than the tube radius, Eq. (1) can still be applied by changing θ to the contact angle at this position [15].

The wall thickness of the ring is computed as the difference between the outside and inner ring radius $\delta = R_i - R_{i+1}$. The volume of every ring is determined by the thickness δ, initial height H_i and initial contact angle θ_i at its outer edge.

$$V_i = \int_{R_{i+1}}^{R_i} 2\pi r[H_i - \cot\theta_i(r - R_{i+1})]dr \tag{8}$$

The volume of liquid raised by surface tension in the tube is then found as the sum of the volume of all rings.

$$V = \sum V_i \tag{9}$$

The height of the liquid profile can then be calculated from Eq. (7). Fig. 5 plots the meniscus volume as a function of

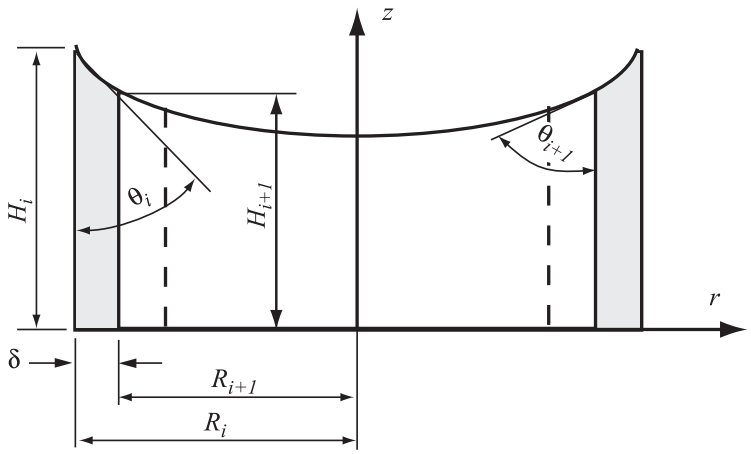

Fig. 4. The liquid raised by the surface tension can be divided into multiple thin rings with wall thickness δ. The volume of each ring is determined by the wall thickness δ, initial height H_i and the initial contact angle θ_i.

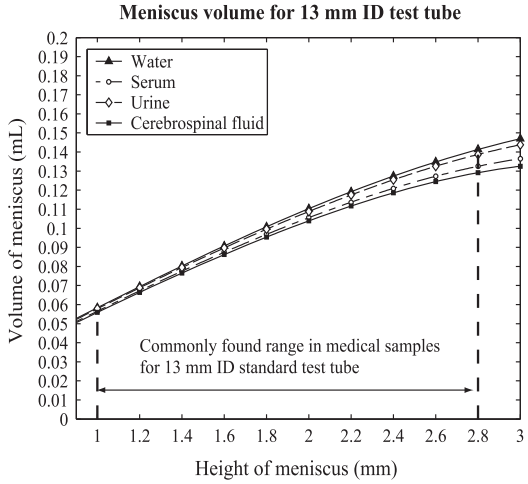

Fig. 5. The liquid volume contained in the meniscus can be calculated as a function of the meniscus height, the surface tension, and density of the liquid.

meniscus height for various medical samples. The surface tension and density properties were taken from the literature and are given in Table 1.

The meniscus volume V_m as a function of the meniscus height h_M can be obtained by fitting a polynomial equation to the discrete data points from the numeric integration of Eq. (9). For a tube with an inner diameter of 13 mm that is filled with water, a 5th order polynomial was chosen (Eq. (10)) and yields a coefficient of determination of $R^2 = 1$ (based on 7 significant digits).

$$V_M = -3.2162 \times 10^{-5} h_M^5 + 9.8034 \times 10^{-5} h_M^4 - 1.2233 \times 10^{-3} h_M^3 + 2.2006 \times 10^{-4} h_M^2 + 5.9299 \times 10^{-2} h_M + 2.1018 \times 10^{-5} \quad (10)$$

Table 1
Liquid properties.

Liquid	Density (g/cm^3)	Surface tension (N/m)
Water	1.0	0.07275 (20 °C) [24]
Serum	1.0239–1.025 [25,26]	0.05872 (20 °C) [27]
Urine	1.022	0.0691 [28]
Cerebrospinal fluid	1.00 [29]	0.046–0.060 [30]

3.3. Modeling the light power attenuation

Using the shape of the liquid in the tube, its effect on the power of the transmitted light can be computed by analyzing the light propagation through the sample. A Monte Carlo and ray tracing simulation method is used to solve the model. The collimated laser beam emitted from the source is modeled as a finite number of parallel rays. The power distribution of the light in a cross section can be expressed by the density of the rays in this range, which then forms the input domain of the model.

The light transport model is set up as depicted in Fig. 6. The sample is placed between the light source and the photo detector. By varying the position of the light source and detector along the height of the tube, the power measured by the detector will vary. The coordinate system of the model is located at the bottom center of the meniscus with the z-axis pointing upwards along the axis of symmetry of the tube. The x-axis is pointing in the direction from the light source to the detector and the y-axis is along the width of the beam's cross section. The path and power of every ray is determined individually and then added together to compute the effect of the sample on the transmitted light.

According to Snell's law, when light travels from one medium to another, the direction of the light path will change at the interface between the two media if the incident angle is not perpendicular and if the two media have a different refractive index [16]. The critical angle θ_c of the two media can be determined by their refractive indices n_1 and n_2 as $\theta_c = \sin^{-1}(n_2/n_1)$. If the incident angle θ_1 is less than the critical angle θ_c, refraction occurs and the light

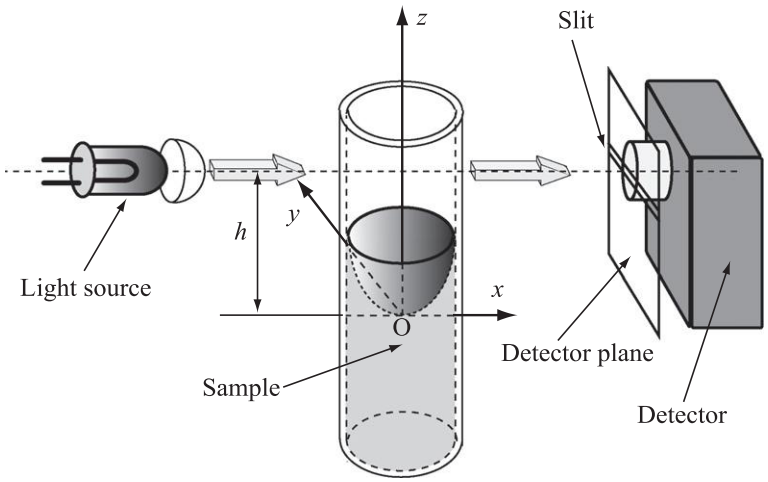

Fig. 6. The light transport model is based on a light source whose beam is separated into a finite number of parallel rays that are transmitted through the sample and received by a photo detector.

will pass through the interface and change its direction according to $n_1 \sin\theta_1 = n_2 \sin\theta_2$. When the incidence angle θ_1 is greater than the critical angle θ_c, total reflection will occur at the interface and the emergence angle will be the same as the incident angle, hence $\theta_1 = \theta_2$.

If the light travels through a homogenous medium, its power will decrease due to the absorption of the medium. The drop in power depends on the path length of the medium as well as the absorption coefficient of the material. Considering the detector spectral sensitivity, the power I_f of each ray at the exit of the optical path is given as

$$I_f = I_i D \exp(-\alpha L) \tag{11}$$

Here, α is the absorption coefficient of the material, L is the optical path length through the material, D is the detector spectral sensitivity, and I_i is the initial power. In the case of a scanning measurement system where the light beam is traveling from air through the meniscus into the liquid, the power of the transmitted light will be affected by both absorption as well as the deviation of the light path.

If a ray is located in the center plane and higher than the highest point of the meniscus (Fig. 2a), the ray will only travel in air and the tube wall in order to reach the detector. In this case, the power loss is due to absorption of light by the tube wall and scattering and reflection at the air-wall interfaces. If a ray is located in the center plane below the lowest point of the meniscus (Fig. 2c), the light will reach the receiver directly after passing through both tube walls as well as the liquid. For beams that are not located in the center plane, the tube's curvature drastically affects the incident angle, causing significant deviations of the light path as the beams enter the tube wall.

The drop in power, due to reflection at the interface depends on the refractive index of the media and the incident angle of the light [17]. The transmittance of light power can be expressed as

$$T = 1 - [(n_1 \cos\theta_1 - n_2 \cos\theta_2)/(n_1 \cos\theta_1 + n_2 \cos\theta_2)]^2 - [(n_1 \cos\theta_2 - n_2 \cos\theta_2)/(n_1 \cos\theta_2 + n_2 \cos\theta_1)]^2 \tag{12}$$

Here, n_1 and n_2 are the refractive indices of two materials and θ_1 and θ_2 are the incident angle and emergence angle of the light at the interface of two media.

In this model, a total of 3801 input rays simulate the laser beam of the light source at each position. The input rays have 100% of power individually and the total power of the input is the sum of all ray powers. The model traces each ray to determine if it reaches the detector, and also computes its power as a function of absorption along its optical path length through the liquid. Because the transmittance depends on the incident angle, every ray is calculated individually. The power value measured by the detector I_D is then obtained by adding the powers of all rays that reach the detector.

$$I_D = \sum_{i=1}^{m} \left[\prod_{j=1}^{n} T_j \cdot \prod_{k=1}^{l} \exp(-\alpha_k L_k) \cdot I_i \right] \tag{13}$$

where I_i is the initial power of each ray reaching the detector, T_j is the transmittance of a ray at each interface, and α_k and L_k are the absorption coefficient and length of every section of the optical path, respectively.

3.4. Optical parameter determination

The light sources are core components of the detection system. Considering the possibility that the test tube is opaque to visible light (e.g. label attached to outside of the tube), infrared wavelengths are chosen. As described by Liu et al. [4], 980 and 1550 nm, which have very different absorption coefficients in liquid but very similar absorption coefficients in the test tube (polypropylene) and labels (polyurethane), have shown to be the most suitable wavelengths to distinguish liquids from air. Meanwhile, the long lifetime (>1.1 million hours) and spectrum and power stability of laser diodes also guarantee the long term accuracy of the detection system [18,19].

To simulate the above model, the most important parameters are the optical properties of the liquid and

the tube, in particular the absorption coefficients and the refractive indices. The optical properties of water as a function of wavelength and temperature are well documented in the literature [20,21]. For a wavelength of 980 nm at 20 °C, the refractive index of water is given as 1.327 and the absorption coefficient is 0.46 cm^{-1}, while at 1550 nm, the literature shows 1.319 and 11.92 cm^{-1}, respectively.

The tube is made of polypropylene, whose refractive index is given by Shabana [22] as 1.52. The absorption coefficient was determined experimentally by placing a section of the tube material between a halogen light source and an optical spectrum analyzer (AQ6315E) as shown in Fig. 7. The light was focused and collimated using a set of lenses at the beam entry side as well as the beam exit side. When the incident light is normal to the interface, the transmission coefficient can be calculated as $T = 4n_1n_2/(n_1 + n_2)$ [17]. When the refractive index of air $n_1 = 1$ and the refractive index of the test tube $n_2 = 1.52$, the transmission coefficient is 96%. If the absorption is zero and ignoring the effects of secondary reflections at internal interfaces, the power of the transmitted light I_T can be determined as $I_T = I_I T^2$, where I_I is the power of the incident light. This allows the absorption coefficient of the test tube wall α to be calculated based on the thickness of the tube material as well as measurements by the spectrum analyzer though air (no tube material inserted) and identical measurements with the tube material inserted [23].

$$\alpha = -\ln\left[I_{T,\text{tube}}/(I_{T,\text{air}}T^2)\right]/L \tag{14}$$

Here, $I_{T,\text{tube}}$ and $I_{T,\text{air}}$ are the power of the transmitted light through the tube and air, respectively and L is the thickness of the tube material.

Based on 30 measurements with a resolution of 1 nm, the absorption coefficient for polypropylene was found to be 0.6 cm^{-1} and 0.48 cm^{-1} for 980 nm and 1550 nm, respectively.

3.5. Effect of printed labels

Actual medical samples, when they are tested in a laboratory, are contained in test tubes that are covered with labels that typically include bar codes and other forms of writing. During scanning, the beams may or may not encounter the label, and if a label is encountered, the beam may encounter both written and unwritten areas. To verify the robustness of the system in the presence of such variations, the effect of print on the label on the transmitted light was investigated.

A typical label as shown in Fig. 8 was mounted between the light source and the spectrum analyzer. Two areas with and without print were tested individually. The printed area was chosen from a barcode region, where the ink masks more than 40% of the total area.

Using the setup illustrated in Fig. 7, the power of the transmitted light was measured for both areas and the ratio between printed and unprinted areas is plotted in Fig. 9. As can be seen from Fig. 9, the print area absorbs much more power than the white area in the visible light range (400–800 nm). In the infrared range (>800 nm), however, the absorption rate is very similar, yielding a ratio of basically 100%. This is a clear indication that the 980 nm and 1550 nm light sources used in the system are not affected by the presence of ink.

3.6. Simulation

A program was coded to simulate the shape of the meniscus at specific conditions. With 0.1 mm resolution, the input light scans the sample at different height levels from 1.6 mm below the lowest point of the meniscus to 2.5 mm above its highest point. The cross section of the input light, in order to simulate the actual lighting condition, is set to a width of 10 mm and a height of 1 mm. The height of the meniscus is set to 1.6 mm, which is a value that was

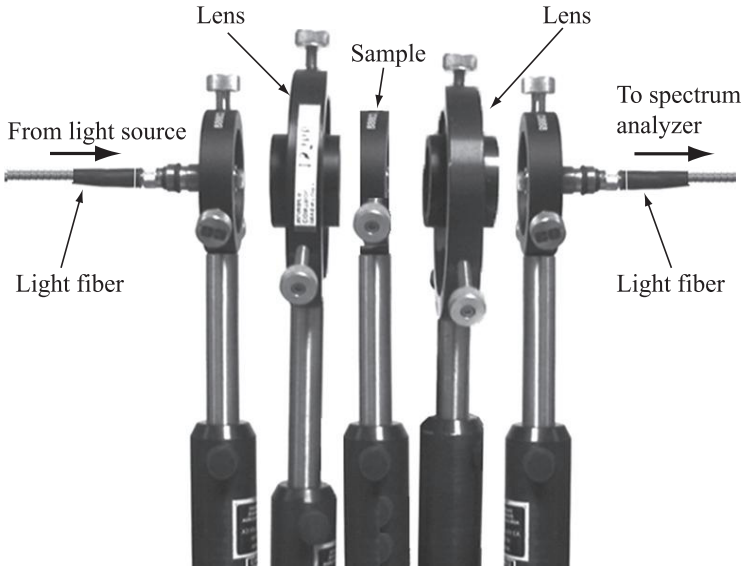

Fig. 7. Experiment setup to measure the absorption coefficient of test tube wall.

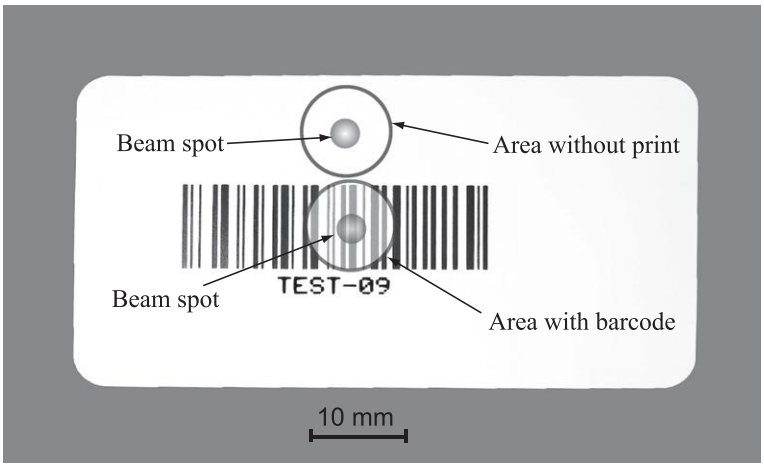

Fig. 8. Label sample used to measure the optical effect of print.

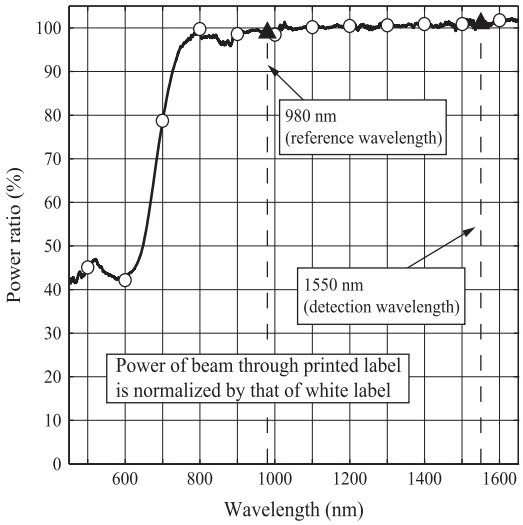

Fig. 9. The power ratio between beams through printed label and unprinted label areas.

measured during the verification experiments of the sample. The lens diameter in front of the photodetector is 9 mm.

First, the differential equations of the meniscus are solved numerically to obtain the shape of the liquid body. This data is saved to a file and included into the Monte Carlo simulation. For the simulation, the input domain of the model is the cross section of the incident beam, which was subdivided into a group of discrete rays that appear in this domain with the same probability as depicted in Fig. 10.

Next, the program calculates the path and power of every ray individually. If the intersection point of the exit light and the detector plane is within the rectangular sensor area, the power of this ray is regarded as be measured by detector. The total power received by the detector is found by summing the powers of all rays that are located within the sensor area. Changing the incident beam position and computing the output power at every position, the power change during the scanning process can be acquired, which allows the detection process to be simulated.

3.7. Comparison of experimental and predicted results

Fig. 11 compares the result of the simulation with measurements obtained experimentally. Also shown is the power ratio R, which is used as the primary measure to detect liquids in labeled test tubes [4]:

$$R = \frac{P_{\mathrm{REF}}}{P_{\mathrm{DET}}} = \frac{P_{980\ \mathrm{nm}}}{P_{1550\ \mathrm{nm}}} \tag{15}$$

As can be seen in Fig. 11, the experimental results are in close agreement with the simulations. In Fig. 11a, when the incident light is below the bottom of the meniscus, the power attenuation is primarily the result of absorption by the liquid. Since the absorption coefficient at the reference wavelength is small, the drop in power is small. When the light is above the meniscus, it propagates through air and the tube wall, thus the power is only attenuated by the tube. When the detection light enters the sample at the meniscus, a portion of the light will be deviated away from the detector, causing a significant drop in light power.

In Fig. 11b, when the light is below the bottom of the meniscus, the light is almost completely absorbed, owing to the large absorption coefficient at the absorption wavelength of 1550 nm. Along the meniscus, the light power increases gradually until the incident beam is above the highest point of the meniscus. The power ratio of the two wavelengths is shown in Fig. 11c. This is the primary measure for the detection of liquids in labeled test tubes. When the light is below the meniscus, the ratio reaches the maximum value. It decreases to 1 once the full height of the beam has entered the meniscus.

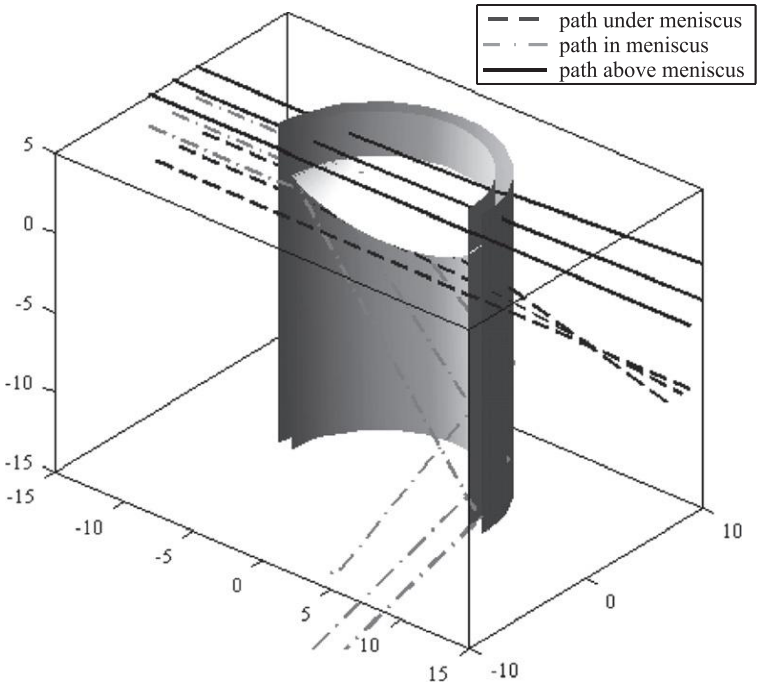

Fig. 10. The incident light is divided into a group of rays that propagate through air, the meniscus, and the liquid.

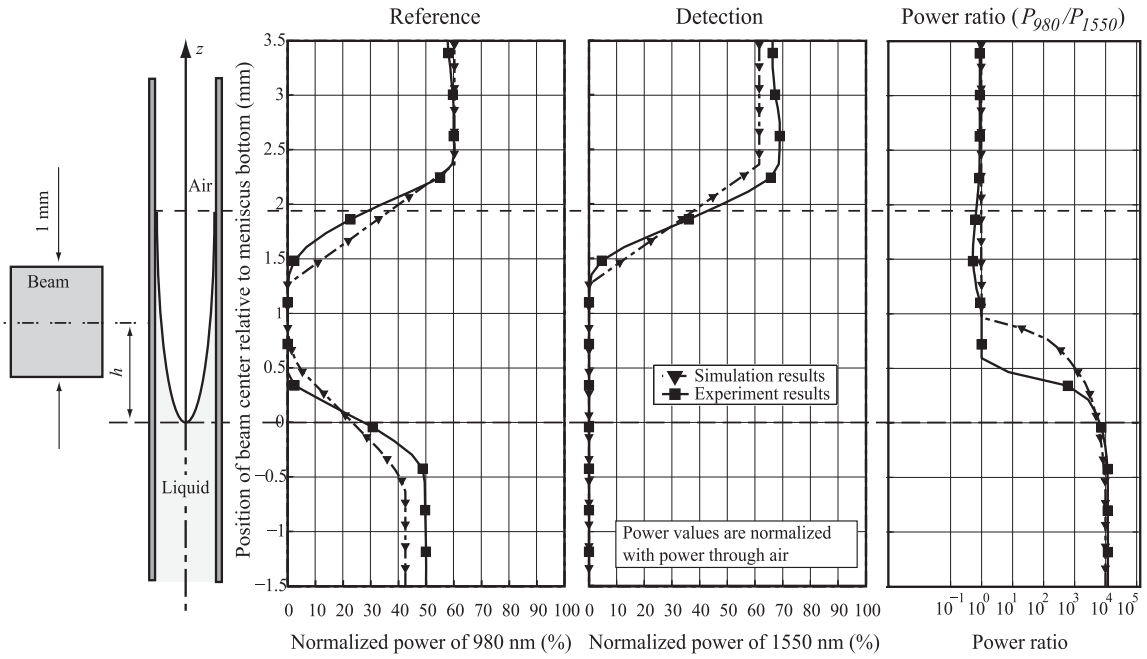

Fig. 11. The normalized power of the transmitted light at (a) the reference wavelength of 980 nm and (b) at the detection wavelength of 1550 nm. Also shown is (c) the ratio of the reference and detection wavelength powers [4].

4. Prototype and system verification

A functional prototype as shown in Fig. 12 was built to verify this detection method. For simplicity, the prototype used a beam splitter as described by Liu et al. [4] to combine the detection and reference wavelengths into a single optical path, thereby eliminating the need for a second photodetector. The sample was fixed on a moveable stage and placed between the sensor and laser diode with a clearance of 2–3 mm. Slits with 1 mm height were

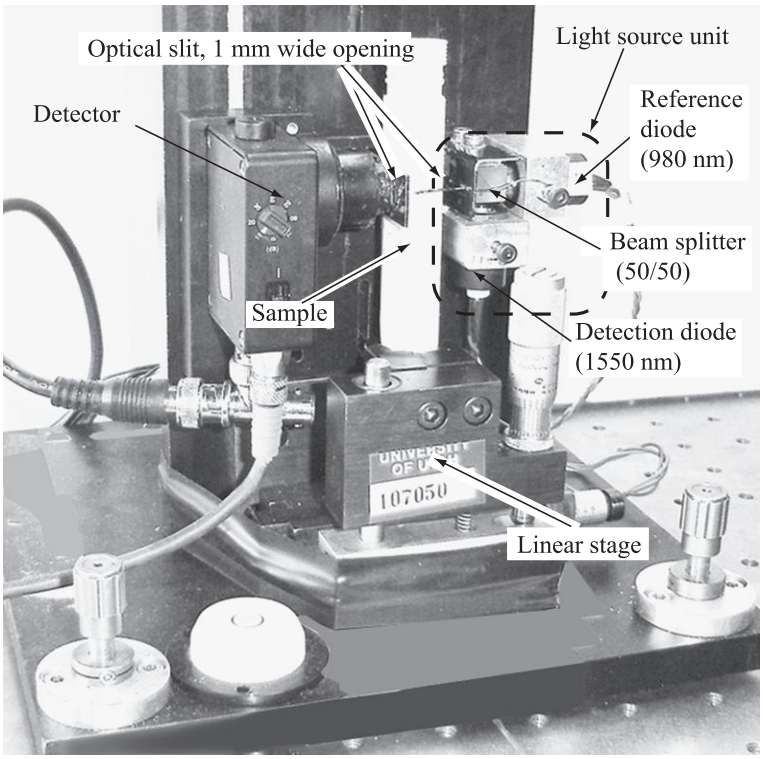

Fig. 12. Functional prototype of volume detection system.

mounted in front of the beam splitter and detector. Not shown in Fig. 12 is the light proof cover of the unit that shields the system from environmental interferences.

For the verification, water was used instead of medical samples. This is based on Liu et al. [4], who have shown that water is a suitable substitute for volume detection experiments. Using a calibrated pipette, well-quantified amounts of water were filled in sealed, standard testing tubes with varying numbers of labels attached to the outside, according to Table 2. The samples were allowed to rest at room temperature for two hours to ensure that a static state was reached. Before every test, a vertical gage was used to measure the height of the meniscus by detecting the heights of the edge and bottom center of the meniscus. For the 13 mm standard tubes, the average meniscus height was measured as 1.6 mm.

For every label combination, the tube was scanned from top to bottom with 0.127 mm (0.005 in) resolution and the power of the transmitted light at 980 and 1550 nm were recorded. Next, the power ratio of the two wavelengths was calculated using Eq. (15). Before and after every test, the power of the two wavelengths was verified by measuring the light power without a sample. Owing to the long term stability of laser diodes, no variations in power output were measured.

As shown in Fig. 13, the position of the top edge of the meniscus can be identified using the intersection of two linear fits to the power curve of the detection wavelength. Using the least squares method, the first line (*curve fit 1*) is fit to the power curve using data points with power values of greater than 98%. This line is intersected with *curve fit 2*, which is a line-fit for data points whose power values range from 10 to 90%. The intersection point of the two lines marks the position where the lower end of the beam enters the top edge of the meniscus.

A similar method is used to determine the position of the bottom edge. First, for position values below the intersection point of *curve fit 1* and *curve fit 2*, the maximum power values for the reference curve are identified and a line is fit using the least square method (*curve fit 3*). Next, a line is fit for power values that range from 10 to 70% (*curve fit 4*). The intersection point of *curve fit 3* and *curve fit 4* marks the position where the reference beam has completely exited the meniscus and is now entirely propagating through the liquid.

The meniscus height is computed by subtracting the position of the top edge from the position of the bottom edge. This yields a meniscus height of 1.7 mm, which is 0.1 mm more than the actual meniscus height. Comparing the detection value from 50 measurements with the actual volume allows the average values and standard deviations

Table 2
The nine possible combinations of 0–2 labels attached to a test tube.

Test ID	A	B	C	D	E	F	G	H	I
Facing laser diode	0	0	1	1	0	2	1	2	2
Facing detector	0	1	0	1	2	0	2	1	2
Total number of labels	0	1	1	2	2	2	3	3	4

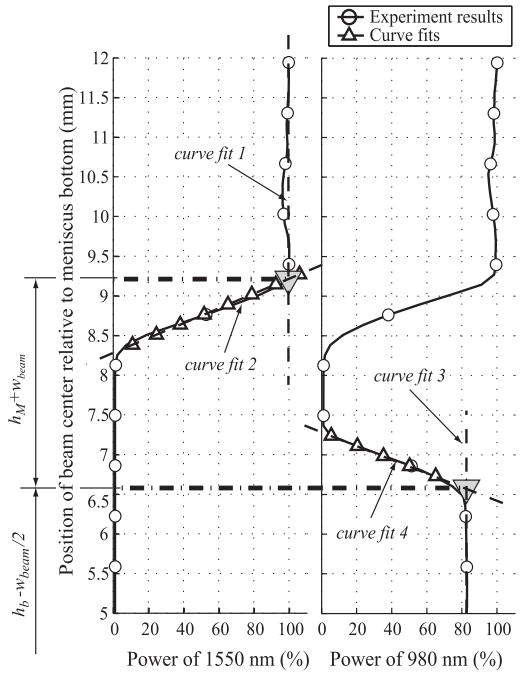

Fig. 13. The shape and position of the meniscus in tube can be detected by finding the intersection points of the fitting lines. In this figure, h_b is the height of meniscus bottom, h_M is the height of meniscus, and w_{beam} is the height of the beam.

to be computed. Based on the 6 sigma ranges shown in Fig. 14, the uncertainty of measurement at the 99.73% level of confidence (6σ) is 0.04 mL, which is about 1.6% of the average liquid volume of 2.5 mL.

Based on the linear resolution of 0.127 mm, only five data points could be used for the curve fit. The actual volume detection system to be installed at ARUP Laboratories will utilize a resolution of 0.05 mm, which will allow the uncertainty of measurement to be reduced further.

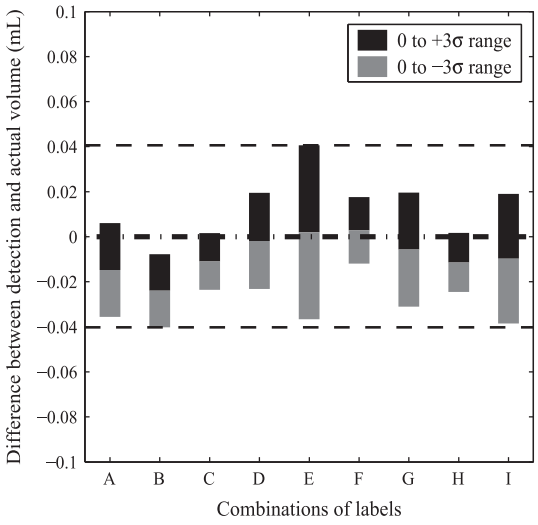

Fig. 14. The detection method, which considers the meniscus shape and position to calculate the volume, can detect the water in a standard test tube with an inner diameter of 13 mm with an uncertainty of measurement of less than 0.04 mL with a level of confidence of 99.73%.

5. Conclusions

When using an optical method to determine the volume of a liquid in tubes based on the liquid level, the meniscus that forms at the liquid-air interface can play an important role that leads to deviations of the measurement results from the actual value. To increase the measurement accuracy in small diameter tubes, the volume of the meniscus must be taken into account. This can be achieved by identifying the height and position of the meniscus through curve fits to the power curves of both the reference as well as the detection wavelength. This allows the volume of the liquid in the tube to be computed by summing the volume of the meniscus and the volume of the liquid below the bottom of meniscus.

The scanning process of this optical volume detection process was modeled and simulated. The simulation results are in close agreement with the experimental results. Based on a series of experiments with test tubes that had 0 to 2 layers of labels attached to the outside, the uncertainty of measurement at the 99.73% level of confidence was found to be 0.04 mL, or 1.6% of 2.5 mL, which is the volume for a tube that is filled to 50% of its maximum capacity.

Acknowledgements

The authors would like to acknowledge the financial support of the project from the ARUP Institute for Clinical and Experimental Pathology®. Particular thanks go to Dr. Charles Hawker and Dr. William Roberts for their expertise in testing medical samples.

References

[1] W. Yuan, D. Li, Measurement of liquid interface based on vision, in: Proceedings of Fifth World Congress on Intelligent Control and Automation, June 15–19 2004, Hangzhou, China, 2004, pp. 3709–3713.
[2] J.D. McNeal, Y. Liu, M.S. Adzich, Sample level detection system, United States Patent # 6770,883 (2004).
[3] N.R. Bachur Jr., T.G. Foley Jr., System and method for determining fill volume in a container, United States Patent # 7604,985 (2009).
[4] X. Liu, B.J. Corbin, S.J. Morris Bamberg, W.R. Provancher, E. Bamberg, Optical system to detect volume of medical samples in labeled test tubes, Opt. Eng. 47 (9) (2008) 094402-1–094402-6.
[5] P. Roura, Contact angle in thick capillaries: a derivation based on energy balance, Eur. J. Phys. 28 (4) (2007) L27–L32.
[6] S.L. Lee, H.D. Lee, Evolution of liquid meniscus shape in a capillary tube, J. Fluid. Eng. 129 (8) (2007) 957–965.
[7] P. Longrigg, The use of laser light to measure surface tension of a liquid, in: Proceedings of the Medicine and Biology, Optical Techniques for Measurement and Control, Spectroscopy, Photochemistry and Scientific Measurement Symposium of ICALEO '85, 11–14 November 1985, 1986, pp. 83–88.
[8] J. Dong, R. Miao, J. Qi, Visualization of the curved liquid surface by means of the optical method, J. Appl. Phys. 100 (12) (2006) 124914-1–124914-5.
[9] Y. Xu, N. Zhang, W.J. Yang, C.M. Vest, Optical measurement of profile and contact angle of liquids on transparent substrates, Exp. Fluids 2 (3) (1984) 142–144.
[10] L. Ondris, M. Trnovec, M. Keppert, V. Rusina, J. Buzasi, An optoelectronic hydrolevelling system, Meas. Sci. Technol. 5 (10) (1994) 1287–1293.

[11] G. Bottomley, Meniscus shapes and capillarity effects in wide tubes, Aust. J. Chem. 25 (3) (1972) 519–521.
[12] E. Rame, On an approximate model for the shape of a liquid–air interface receding in a capillary tube, J. Fluid Mech. 342 (1997) 87–96.
[13] T.S. Meiron, A. Marmur, I.S. Saguy, Contact angle measurement on rough surfaces, J. Colloid Interface Sci. 274 (2) (2004) 637–644. 2004.
[14] N.B. Vargaftik, B.N. Volkov, L.D. Voljak, International tables of the surface tension of water, J. Phys. Chem. Ref. Data 12 (1983) 817–820.
[15] J.C. Biery, J.M. Oblak, Calculational method for determination of surface tensions from photographed menisci. Application to water and mercury, Ind. Eng. Chem. Fund. 5 (1) (1966) 121–128.
[16] D. Meschede, Optics light and lasers: the practical approach to modern aspects of photonics and laser physics, second ed., Wiley-VCH, Weinheim, 2007.
[17] K.K. Sharma, Optics: principles and applications, first ed., Academic Press, Amsterdam, 2006.
[18] S. Kobtsev, S. Kandrushin, A. Potekhin, New approach to long-term frequency stabilisation of radiation of single-frequency lasers, in: Proceedings of the SPIE, 6731, 2007, pp. 67312U-1–67312U-8.
[19] H.P. Meier, V. Graf, Research lab converts to diode-laser manufacturer, Laser Focus World 32 (10) (1996) 51–53.
[20] L. Kou, D. Labrie, P. Chylek, Refractive indices of water and ice in the 0.65 to 2.5 micrometer spectral range, Appl. Optics 32 (19) (1993) 3531–3540.
[21] G.M. Hale, M.R. Querry, Optical constants of water in the 200 nm to 200 μm wavelength region, Appl. Optics 12 (3) (1973) 555–563.
[22] H.M. Shabana, Determination of film thickness and refractive index by interferometry, Polym. Test. 23 (6) (2004) 695–702.
[23] C.W. Robertson, D. Williams, Lambert absorption coefficients of water in the infrared, J. Opt. Soc. Am. 61 (10) (1971) 1316–1320.
[24] N.B. Vargaftik, B.N. Volkov, L.D. Voljak, International tables of the surface tension of water, J. Phys. Chem. Ref. Data 12 (1983) 817–820. Copyright 1984, IEE.
[25] N.A. Mody, M.R. King, Influence of Brownian motion on blood platelet flow behavior and adhesive dynamics near a planar wall, Langmuir 23 (11) (2007) 6321–6328.
[26] R. Rhoades, D. Bell, Medical physiology: principles for clinical medicine, Lippincott Williams & Wilkins, 2008.
[27] J. Rosina, E. Kvasnak, D. Suta, H. Kolarova, J. Malek, L. Krajci, Temperature dependence of blood surface tension, Physiol. Res. 56 (2007) S93–S98.
[28] W. Donnan, F. Donnan, The surface tension of urine in health and disease: with special reference to icterus, Br. Med. J. 2 (2347) (1905) 1636.
[29] A.C.P. Lui, T.Z. Polis, N.J. Cicutti, Densities of cerebrospinal fluid and spinal anaesthetic solutions in surgical patients at body temperature, Can. J. Anaesthesia–J. Can. D Anesthesie 45 (4) (1998) 297–303.
[30] H.L. Brydon, R. Hayward, W. Harkness, R. Bayston, Physical-properties of cerebrospinal-fluid of relevance to shunt function. 2. The effect of protein upon CSF surface-tension and contact-angle, Br. J. Neurosurg. 9 (5) (1995) 645–651.

CHAPTER 6

MACHINE VISION FOR TUBE TYPE DETECTION

6.1 Introduction

In this chapter, a machine vision system is introduced, which can identify the type of test tube through geometric recognition based on the tube outline.

When detecting the liquid volume in a test tube, two important parameters are involved. One is the relative position of the liquid top surface to the bottom of the liquid. Another one is the geometric size of the container, which is expressed by its inner diameter. If the level of the liquid is acquired, the volume of the liquid can be simply determined by multiplying the cross section area and the height of the liquid. Alternatively, it can simply be retrieved from a database based on the liquid surface position and the type of the test tube.

While the position and height of the liquid interface can be acquired by the volume detection system presented in Chapter 4, the inner diameter of the test tube cannot easily be measured directly. Thus an indirect method based on the dimensions of the tube outline is proposed. The system uses a machine vision to measure the outside geometric characters of test tubes, and identify their types. After recognizing the type of test tubes, a program will retrieve the inner diameter from a data file, and calculate the liquid volume by the positions and heights of their interfaces.

6.1.1 Objectives and requirements

Because the samples come from all around the country, the liquid is contained in different kinds of test tubes used in biomedical labs. After obtaining the level of the liquid in a tube, the liquid volume can be calculated by the height and position of the liquid interface and the geometry of container. In this process, one of the most important steps is to acquire the inner diameter of the test tube, which cannot be acquired by direct measurement because of the potential biohazard of samples. Since only limited types of test tubes appear in the lab, each with their own inner and outside dimensions, the tube type can be identified by its outside geometric properties. Then the inner dimension can be determined based on the type of the test tube and previous measurement results. Considering the identification speed and geometric properties of the test tube, a non contact method utilizing machine vision will be used in this system. It can identify the geometric character as well as measure the dimension. Then the type of the test tube is determined based on the measurement results with reasonable robustness. Some specific conditions, such as different thickness of labels are also taken into account. The errors leading to deviations from the actual size are compensated.

6.1.1.1 Error source of identification

Before setting the requirements of the system, the sources leading to incorrect identification should be analyzed. The first source is the thickness of labels. To help technicians identify the sample, labels are attached to the outside of the test tube. Every layer of label has a thickness of about 0.1 mm. Normally the test tube is covered by 1-6 layers of labels that lead to a change in diameter that can range from 0.1 to 0.6 mm.

The second source for incorrect identification comes from the tightness of caps on test tubes. When the cap is not screwed or pushed tightly on the tube, the length of the test tube is a longer than usual. The length change ranges from 0 to 1 mm depending on the test tube.

The third source is colors of caps or test tubes. Researchers use colored caps to represent different conditions or liquids of samples. Sometimes brown test tubes are used to shield the sample from light. Among the samples collected at ARUP, tubes with seven colors were found, some even having two colors (white and brown). When pictures are captured, the colors of the samples will lead to different image qualities.

The fourth source is linked to prints on the labels, which may lead to a mistake when distinguishing the object from the background. The words and barcodes are printed on labels with black ink. They may be considered as part of the background if they appear near the edges of the tube image.

The fifth and final error source is the environmental interference. This system will run on an inspection line in a complex electromagnetic environment in the lab. For example, the illumination condition may change following the outside environment. If a test tube were illuminated at a different level or by colored lights, the final identification result will be influenced.

6.1.1.2 Requirements for the identification system

Considering all of the above mentioned error sources, several requirements must be met in order to acquire a trustable result by an identification system.

1. The system must be able to recognize a test tube by its outside profile and be able to handle the measurement uncertainties that arrive from having labels attached to the outside.
2. The system must be to identify a test tube correctly even if the color is not uniform. For example, the cap of the tube has a different color, or labels just cover part of the test tube.
3. The cap of the test tube must not be removed during the identification process to avoid the potential biohazard from the sample.
4. The test results must be independent of the outside environment. The environmental interferences will not affect the final results.

In sum, this project requires that the machine vision system can identify the type of test tubes under real conditions as they are experienced in a laboratory and with reasonable robustness.

6.1.2 Review of previous work

Machine vision is a new technology rising along with the progress of computer and optical-electronic technology. It normally includes the electronics, mechanical engineering, software and optical fields, etc. It has been applied in many areas, such as automotive industry (Kochan 2002), agricultural (Jimenez *et al*. 1999), food processing industry (Habets 2002), and construction engineering (Chu *et al.* 2009), etc. In these applications, the process of machine vision can be divided into several subsections such as image acquirement, object features extraction, object recognition, and result determination. Recently, the research of machine vision mostly focuses on the fields of

graph processing, such as edge-finding, pixel analysis, segmentation and object recognition.

The edge detection is one of the most fundamental technologies in graph pretreatment after the image acquisition. It plays an important role in image processing. Many methods, such as Sobel, Prewitt and Canny detector have been developed to find the edge of objects in an image (Canny 1986; Deriche 1988; Fathy *et al*. 1994; He *et al*. 2008; Hou and Wei 2002; Lindeberg 1998; Manjunath and Chellappa 1991; Mehrotra and Shiming 1996). They are normally divided into two groups, the gradient-based and morphological-based edge detection operators. Gradient-based edge detection is a straightforward method to identify points on an edge by searching the gradient change position in an image. The morphological-based operators, however, are more effective during most image processing applications.

To acquire accurate results, most of image analysis systems need to distinguish the object from the background of an image. The most common methods for object segmentation and feature extraction are based on the edge detection. (Brejl and Sonka 1998; Silva *et al*. 2001; Strzecha *et al*. 2007)

After the features of objects are acquired, the category of objects can be recognized. This normally is performed by comparing features with attributes of objects in an object library stored on a computer (Flemmer and Bakker 2009). The artificial neural network is one of the most powerful tools for the image recognition (Bir *et al*. 1999; Dainty *et al*. 1999; Georgieva and Jordanov 2009; Khabou *et al*. 1999). Machine vision systems can recognize the categories of moving objects, as well as that of static

objects (Strehl and Aggarwal 1999). In some applications, the object position can be located in a digital image with a rapid operation (Carbonetto *et al*. 2008; Davies 2008).

The above processes involve several kinds of mathematical methods (Joo and Haralick 1989), including matrix operations or optimization routines. Other than using the traditional digital computing, optical processing is another powerful method under some given conditions. It has been applied in the areas of data acquisition, feature extraction, and pattern recognition. It has the advantage of processing large amounts of data with higher speed. It is showing as a promising research area (Strand 1988).

With the wide usage of machine vision technology in every field, a number of new developments have appeared. One of these improvements is the invisible band image capture and analysis. It has been applied in many actual situations with increasing frequency (Dainty *et al.* 1999; Jimenez *et al*. 1999). The infrared wavelength band is the most widely used band, which can acquire much better results compared to the visible wavelength during image capture. Another improvement is the development of computer hardware and algorithms used in image processing. They can improve the efficiency of image processing noticeably (Cypher and Sanz 1989; Dainty *et al*. 1999; Khabou *et al*. 1999).

6.1.3 Preview of this chapter

In this chapter, the current work and the literature about machine vision are reviewed. A machine vision system that can identify the type of test tubes is introduced and its principle is presented. Furthermore, the general process of identification is listed. Also, the prototype of this system is set up and a determination regulation is defined.

Verification of the system is achieved through a series of experiments. Finally, conclusions and future work are presented at the end of this chapter.

6.2 Principle of machine vision system

Normally, the machine vision method consists of several sequential processes. These are image acquirement, image operation, and image analysis, which involve windows method, noise suppression, filter choice, edge detection, and character detection, etc.

The first step is image acquirement. An optical electronic system captures the static images of objects. In general, the image capturing system is composed of illumination sources, optical lens and sensors. The illumination system will emit light to light up the desired object. The light reflected by or transmitting through the object passes through the lens, and creates a real image on an image plane. An optical-electronic sensor is mounted on this plane, and transfers the light signal to electronic digital signal and constructs a data file of the image. Thus the object is represented by a digital image, which can be stored, treated and analyzed by a computer. In order to obtain high quality images, a carefully selected background needs to be installed. For simplification, the optical system and sensor are replaced by a digital camera, which captures the image of object, and sends it to the computer.

Next, an image pretreatment process is operated by a computer program to prepare the image for future determination. The image pretreatment includes noise suppression and image sharpening. Sometimes it also modifies the distortion caused by optical aberration and projection effect. After the operation, the image qualify will be improved, and the object contained will be more clear and more easily identifiable.

After the pretreatment, an analysis is conducted to obtain the information of the interested object. The information includes color, shape, dimension and position of the object. This is the general principle and process of machine vision.

In this project, some of the processes can be simplified to save time and effort. Here, the identification system will extract the characteristics of the test tubes from the image captured by a digital camera. Next, the characteristics are compared with the geometric data of all test tubes stored in a database. The degree of similarity between the image tubes and actual objects is used to determine the type of test tubes by a fuzzy logical determination process. Finally, the result will be sent to another computer for the further work.

6.3 Feature analysis

To distinguish the type of test tubes, it is important to find the difference between them. In this system, a digital camera will inspect test tubes from the outside using the visible spectrum range. The geometric shape and color of them are the obvious characters, and are easily detected. Thus, the detection of shape and geometric size of objects is an appropriate method to obtain the necessary data for the type identification.

Because only a limited number of test tubes types appeared in the Core lab, a feature data file of typical test tubes can be prepared prior to the real determination.

As shown in Fig. 6-1, the typical geometric proprieties of a test tube include the overall length including the cap, the cap diameter, the diameter of the test tube, and the shape of its bottom. All these features can be used to identify the type of a test tube. They can be measured and stored in a data file, and be used in the further determination process.

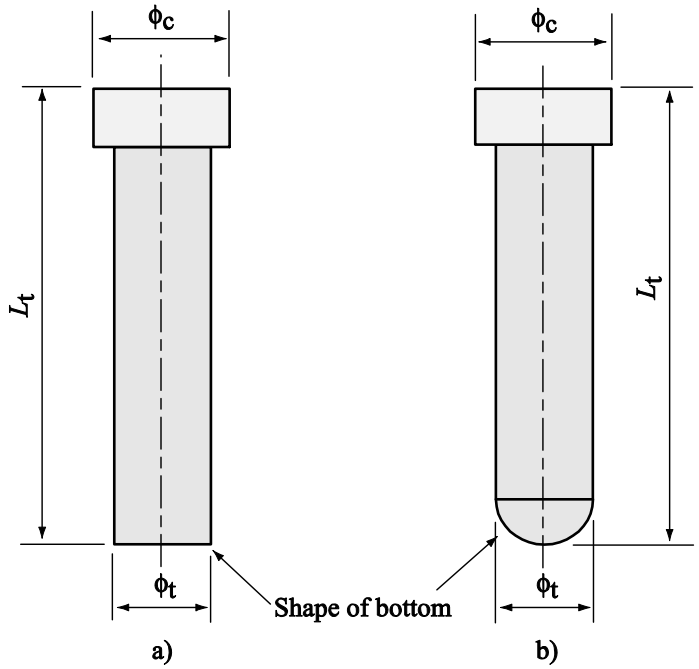

Fig. 6-1 The profile characters of the test tube. a) The bottom of the test tube is flat. b) The shape of bottom is a hemisphere.

To prepare the data file, ARUP provided fifteen test tubes that are commonly encountered in the Core Lab. The relevant geometry for each tube was obtained and recorded.

When measuring the diameter of tubes, the dimensions are acquired without attached labels at different positions along the length. Each type of test tube is measured 30 times and the maximum and minimum values for every measurement are recorded. Therefore, the diameter of a tube tested under actual condition can range from the minimum measurement value of the diameter up to maximum diameter plus the added thickness of up to 6 layers of labels.

The same principle is applied to the diameter of the cap as well as the length of the tube, which are stored with maximum and minimum measurement values. Table 6-1

presents the geometric and color characteristics of each type of test tubes and combination.

As shown above, the main characteristics differences of all types of tubes are the outside diameter of the test tubes, the length of the tubes with caps, the shape of their bottoms and the diameter of their caps. Detection of these details will give the machine vision system enough information to identify their types.

The color of caps is also listed in Table 6-1. It is important because some details of the shape may disappear after the image is transformed from the color to the gray scale. That may lead to incorrect measurement results of the image analysis process. In particular, if a cap is black, it may be indistinguishable from the background if it is black too. As a result, the analysis program will recognize the cap as part of the background and the computer will regard the diameter of the cap as zero instead of its real value.

Table 6-1 The features of the test tube

Type	Outside diameter of tube (mm)	Length of tube (mm)	Outside diameter of cap (mm)	Shape of bottom	Color of cap
1	12.15-12.7	81.8-82.1	11.8-12.41	Round	White
2	12.63-13.36	81.82-82.2	15.97-16.23	Round	Brown
3	12.63-13.36	81.82-82.2	15.97-16.23	Round	White
4	12.52-13.38	83.68-83.9	16.02-16.2	Flat	Purple
5	11.8-12.9	89.44-89.55	11.36-11.92	Round	Orange
6	15.23-16.04	87.31-87.51	15.35-16.8	Round	Yellow
7	15.1-15.4	91.2-91.5	18.08-18.5	Flat	Green
8	14.78-15.2	96.6-96.8	17.5-18.2	Flat	White
9	11.47-13.03	101.88-102.01	17.35-18.3	Round	Green
10	14.78-15.2	98.28-98.5	16.4-16.9	Flat	White
11	14.76-15.8	97.94-98.47	19.24-19.76	Flat	White
12	15.21-15.82	101.93-102.1	18.01-18.64	Flat	Yellow
13	12.31-13.02	107.68-107.91	11-15.09	Round	Green
14	12.37-12.95	108.95-109.28	12.69-13.33	Round	Yellow
15	15.96-16.51	107.72-108.01	15.81-17.06	Flat	Black

After all characteristic parameters of the test tube are acquired, the data is stored in a data file with a specific format. When a new type of test tube appears in the lab, the data file can be expanded by simply adding the relevant geometric data the new tube type.

After the data file containing the feature dimensions is built, the type detection of test tubes can be conducted. The feature dimensions of the detected object are measured during the image analysis and compared with the data stored in the feature dimension file. The type of inspected tube is identified by the degree of similarities.

6.4 Process of detection

In the Core lab, samples are carried by test tube holders moving on a track. Each test tube holder has attached its own barcode to identify the sample. After a sample is taken out from a storeroom, it will first pass through a barcode reader which reads the information and sends the result to a computer. When the sample arrives at the machine vision system, a robot will grip and lift it up from the test tube holder and place it at the image acquisition position, followed by the process of tube identification.

After the type of the test tube is identified, the inner geometric size of the test tube can be retrieved from a database. Based on the surface position and profile of the liquid in it, the computer can determine the liquid volume. The details of machine vision detection are listed as the following steps.

6.4.1 Image acquisition

After an inspected tube is placed at the detection position, a digital camera acquires the image. Typically, the image is in color and sized such that can capture the longest test tubes and the widest diameter of caps. Capturing pictures under repeatable

conditions will simplify the identification program by ignoring most influences from the environment. For this reason, images are acquired at the same position, viewing angle and background during every test. Sample illumination is also kept constant.

6.4.2 Preprocessing of image

A computer will receive the digital data of the image as an image file. It will process the image first before detecting the features of the test tube. The pretreatment includes reducing noise, and improving signal quality (Davies 2005).

In this project, to simplify the program and detection algorithm, the color image captured by the digital camera is converted to a gray scale image. The original digital image is expressed as a RGB image, which uses three primary color channels to specify the color of every pixel. The format of data received by the computer is a 640×480×3 matrix. The first two dimensions are the width and height of the image in pixels. The third dimension is the intensity of the three color channels. After the color conversion, the image will be expressed by intensity data of every pixel, which is now a simple 640×480 matrix.

Many conversion functions were developed to translate the RGB image into gray images. In this project, a simple equation 6.1is used to transfer the RGB image to grayscale (Bockstein 1986).

$$Y = 0.3R + 0.59G + 0.11B \tag{6.1}$$

where *R*, *G* and *B* are the intensity values of the three primary colors (red, green, and blue) for each pixel and *Y* is the brightness value of this pixel after the image is converted to a gray image.

6.4.3 Edge detection

After preprocessing of the image, the next step extracts the features of the object from the image. The simplest method is edge detection, which identifies the object in the image by finding the outside profile. In this project, a LabVIEW function using a gradient method detects the edge of the test tube profile. This method is explained in Fig. 6-2.

In Fig. 6-2, the lines *A* and *B* represent the outside edge of the test tube while lines *C* and *D* represent the outside wall of its cap and line *F* is the position of its bottom.

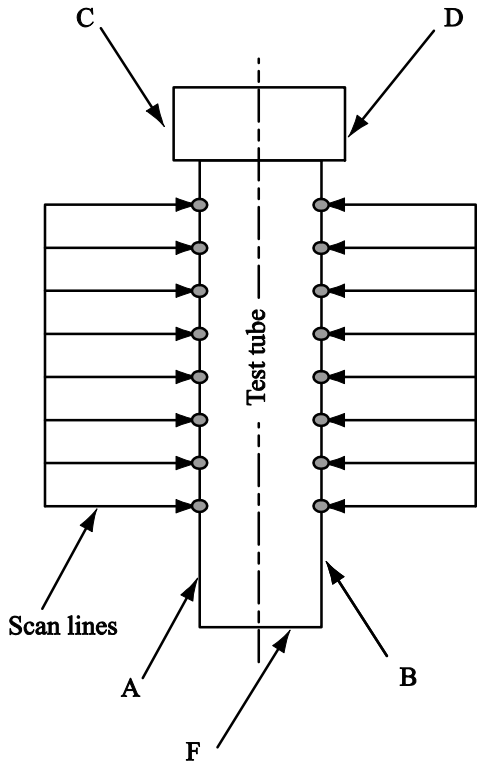

Fig. 6-2 The edge of tube wall detection by scanning in the vertical direction of the test tube.

To identify the edges of the test tube, the entire image is scanned by a series of parallel lines in the vertical and horizontal direction. The intensity values of each pixel of every line are recorded by a computer. The intensity change gradients are calculated. By comparing the intensity to a pre-set threshold, the points where the change in intensity is above the threshold are located. These points are considered as the points located on the edge of the profile. Next, the points are fitted to a straight line, which will represent in closed form the edge of the test tube (National Instruments 2008).

6.4.4 Dimension measurement and modification

After the profile edges of the test tubes are detected by the program, the system can obtain the coordination positions of the lines and/or circles by pixels and calculate the dimensions of the profile shown in the image. Due to the optical aberration and projection effect, these dimensions must be modified to acquire the actual dimension values of test tubes. Then, the results of measurement are sent to the next step for type identification.

Fig. 6-3 shows the image formation of the identification system. A sample is placed at its checked position and illuminated. The reflected light is refracted by a lens unit and forms a small and upside down real image on an image sensor. The sensor translates the image to a digital image signal, which describes the image by the value of every pixel. For convenience, we set a virtual plane called the measurement plane, where all measurements take place. It passes through the center line of the sample and is normal to the optical axis of the system. The plane of the sensor surface is called sensor plane or image plane.

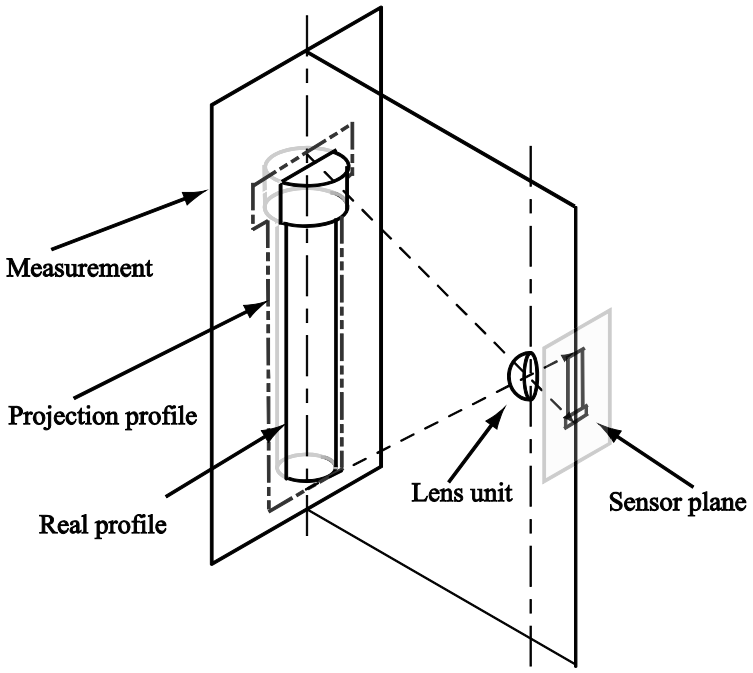

Fig. 6-3 The profile of object that is projected on a sensor plane.

On the sensor plane, the sizes and positions of a test tube image can be described by the number of pixels. When a detection system is set up, the conversion relationship between the pixel numbers of image and the sizes of samples is determined. The actual dimensions of samples projected on the measurement plane can be calculated by the Eq. (6.2).

$$L = N_p \cdot \lambda \tag{6.2}$$

where L is the actual dimension of a sample projected on the measurement plane. N_p is the pixels number of this dimension shown on image plane, andλ is the conversion ratio between these two values.

Because of the perspective distortion of the system, the image projected on the sensor is different from the original object in shape. As shown in Fig. 6-3, the profile image of an object on the sensor plane does not correspond to its actual size. Instead, it is actually an image based on the maximum outlines of a sample. These outlines are created by the interaction between the measurement plane and the tangential planes of the test tube and the center of lens. Using the outlines to measure the sizes of objects will lead to measurement results that are bigger than the actual object. So, when calculating the dimension of an object by machine vision, the distortion must be taken into account to obtain correct values.

The amount of distortion is based on the relative position between the camera and the detected samples, the focus length of the camera lens units, and the diameters of the test tubes. The further the object to be measured is located away from the optical axial of the camera, the bigger the distortion. The distortion also increases as the distance between the camera and object decreases. Moreover, larger objects also cause an increase in distortion of the image on the sensor plane.

Several modification equations and steps based on the above parameters are created to correct the image distortion, and help to obtain accuracy measurement results. The diameters of the test tubes and caps can be obtained from the distance between their outlines. As mentioned above, this measurement result will differ from the actual dimension, requiring the result to be modified.

As shown in Fig. 6-4a), ϕ_{img} is the diameter of the sample image formed on the sensor plane. It is the distance between two outside edges of the tube wall and expressed by the number of pixels. ϕ_m is the diameter of the sample projected on the measurement plane, whose value is calculated by multiplying the pixel value of ϕ_{img} on the sensor plane and conversion ratio. It is, however, bigger than the actual diameter of the test tube ϕ_t.

A simplification of their geometric relationship is illustrated in Fig. 6-4b) where CO is the distance between the lens plane and the centerline of the test tube, f_1. AO is the radius of the sample image, equal to $\phi_m/2$. BO represents the actual diameter of the test tube or cap$\phi_t/2$. Eq. (6.3) expresses the relationship between them.

$$BO = AO \cdot CO/\sqrt{AO^2 + CO^2} \tag{6.3}$$

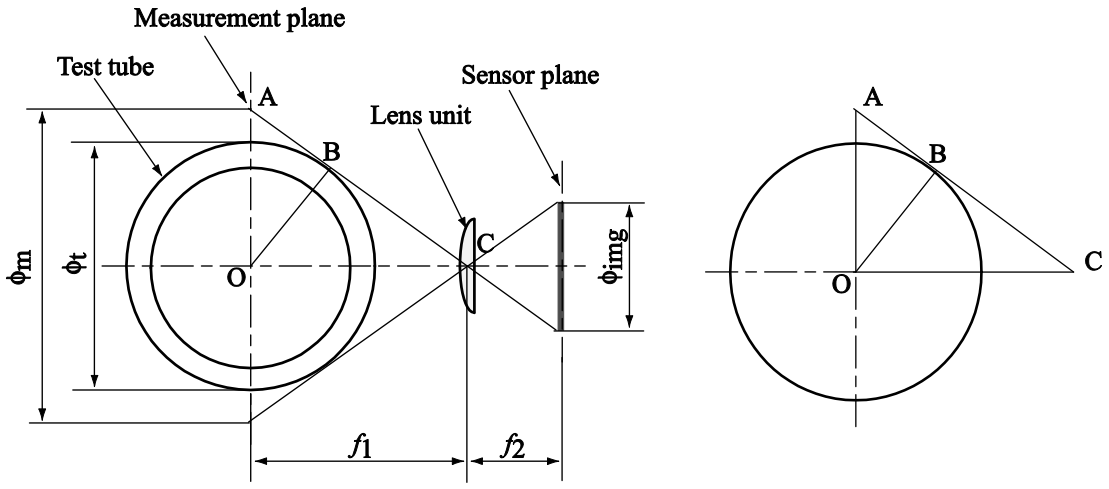

a) b)

Fig. 6-4 The measurement results of the diameter is bigger than that of the actual size. a) The amount of distortion depends on the diameter of the test tube and the distance between object and camera. b) The modification can be simplified to a simple geometry calculation.

Since f_1 is a fixed value after the system is set up, and ϕ_m can be detected by the product of the pixel number of ϕ_{img} and the conversion ratio, the actual diameter of the test tube or cap ϕ_t can be obtained by Eq. (6.4).

$$\phi_t = f_1\phi_m/\sqrt{(\phi_m/2)^2 + f_1^2} \tag{6.4}$$

After the actual diameter of the test tube ϕ_t is obtained, the length distortion of the test tube can be corrected in the next step.

While using edge detection to find the diameter of the test tube and cap projected on the sensor plane, the edge position of the bottom formed on the sensor plane is acquired too. To simplify the program used to measure the length of test tubes, when samples are placed at the testing position, the tops of caps are aligned with one side of the image. Thus, the bottom of a tube becomes a free end located on a specific position, which depends on its length. If the bottom position of the test tube can be inspected and determined in sensor, the length of the test tube is identifiable.

The height of the test tube will be detected by measuring the distance between the bottom of the test tube and the end edge of the image. It is explained as the pixel number too. After multiplied with the conversion ratio, the length of the test tube project on measurement plane is acquired.

As mentioned before, the length of a projected sample is bigger than the actual tube value. A correction must be conducted to modify this distortion. Two modifications and measurement methods are used to operate this correction based on the shape of bottoms.

Test tubes tend to have two different types of bottom shapes, which are either flat or a hemisphere. They lead to different distortions of the image when they are projected on the measurement plane. As shown in Fig. 6-5a), the sphere radius of the hemisphere bottom has the same value as the radius of the test tube. Because of the perspective, the length distortion of tubes with a hemisphere is less than that with a flat bottom, as shown in Fig. 6-5b). The actual length of the test tubes has a specific geometric relationship with the length of the tube projected on the measurement plane. It also is a function of the position of the lens unit, sensor and samples.

Fig. 6-6 shows the simplifications of their geometric relationship, which are used to correct the error for the hemisphere and the flat bottom, respectively.

Here, DO is the distance between the lens plane and the measurement place, f_1. AD is the distance between the tube image edge and the optical axis of system, L_{bm}.BD represents the actual distance between the bottom of the test tub and the optical axis, L_b. The relationship between them can be expressed by Eq. (6.5) for the test tube with a hemisphere bottom, while Eq. (6.6) for is used for samples with a flat bottom.

$$BD = AD - R_t \cdot \sqrt{DO^2 + AD^2}/DO + R_t \tag{6.5}$$

$$BD = AD - AD \cdot BC/DO \tag{6.6}$$

Since f_1 is a constant value after the system is set up, and L_{bm} can be detected by the product of the pixel number of L_{bimg} and the conversion ratio. The modification equation used to acquire an accuracy length of the test tube with hemisphere bottom can be expressed as Eq. (6.7). When working with a test tube with a flat bottom, the modification can be described by Eq. (6.8).

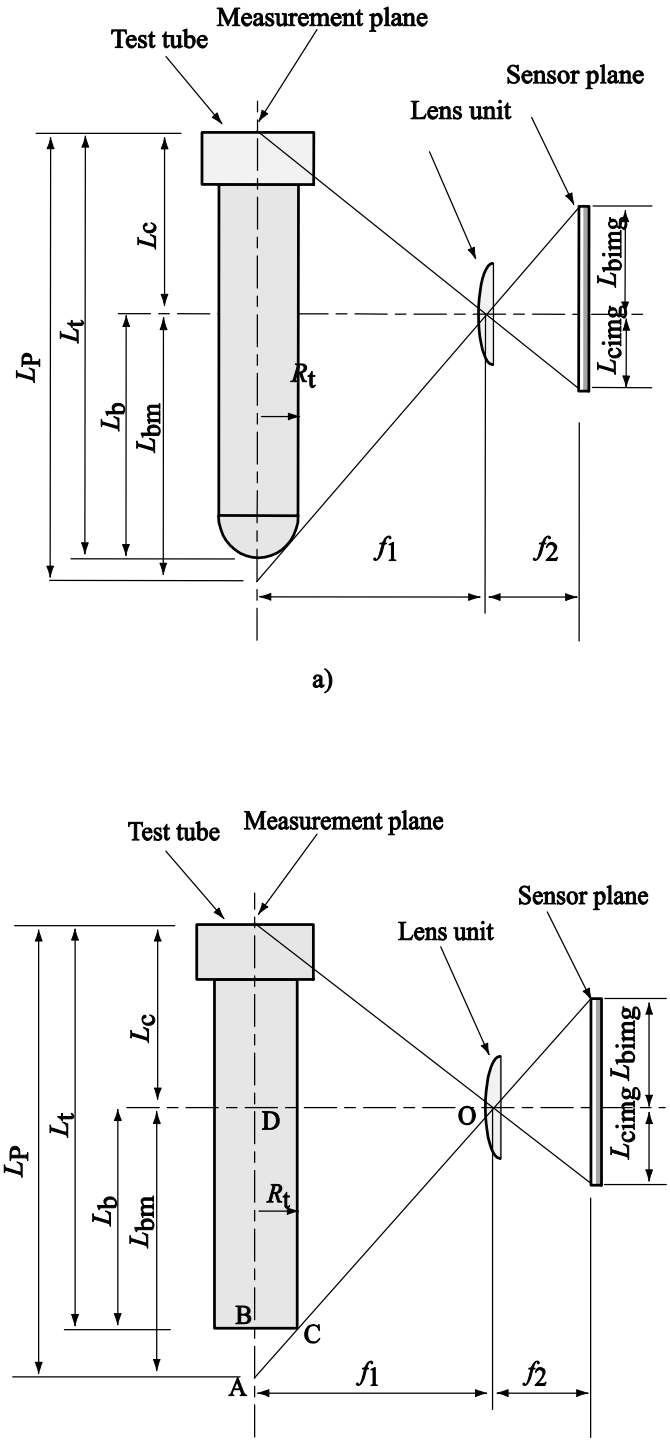

Fig. 6-5 The projection distortion of the length detection of the test tube. Because of the perspective effect, the length of the test tube detected is bigger than its actual size. a) The shape of bottom is a hemisphere. b) The bottom of the test tube is flat shape.

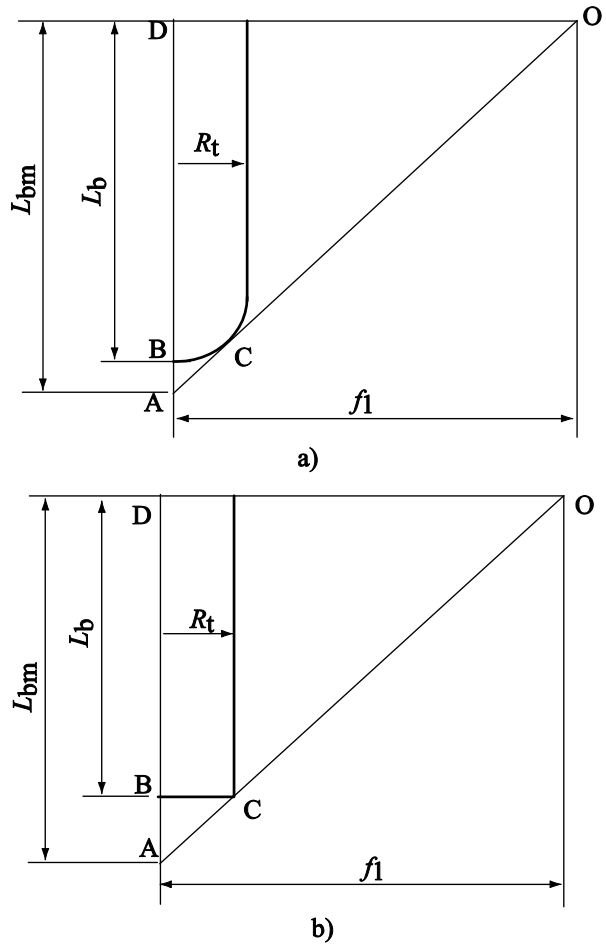

Fig. 6-6 The geometric relationship between the actual dimension and the sample image size of the test tubes. a) The shape of the bottom is a hemisphere. b) The bottom of the test tube is a flat shape.

$$L_b = L_{bm} - R_t \cdot \sqrt{f_1^2 + L_{bm}^2}/f_1 + R_t \tag{6.7}$$

$$L_b = L_{bm} - R_t \cdot L_{bm}/f_1 \tag{6.8}$$

Thus, the total length of the test tube can be measured by $L_t = L_b + L_c$. The error caused by the optical perspective is corrected by the modification equations. These results are the feature of the test tube used to identify the type of test tubes.

6.4.5 Determination and identification

Following the dimension measurement, type determination of test tubes is another important part in this process. In this part, a fuzzy logical decision strategy is used to identify the type of tube (Baldwin 1996; Harris 2006).

Before identifying the type of test tubes, the measurement and detection errors should be analyzed. When identifying a test tube, three kinds of errors or uncertainty sources appear, and need to be considered. The first error is the sample error, which comes from the actual dimension measurement uncertainty of test tubes. Another one is the causal errors of measurement caused by the environment or hardware changes. The last one is the system error that is caused by the detection method, or the image conversion (Caria 2000).

The sample error comes from the manufacturing errors of the test tubes, the number of labels attached to the test tubes, and the tightness of the caps. To facilitate low manufacturing cost, tubes are typically made by injection molding. This process cannot guarantee that all products have exactly the same dimensions without a measurement uncertainty. Furthermore, printed labels are attached the outside of the test tubes to identify the specimen including the type of liquid, the patients name and what test are to be performed. Because a test tube may be processed by several operators before it reaches the Core Lab, the number of label layers may vary from 0 to 6 layers. Thus, the thickness of the labels will lead to a variation of the sample diameter from 0 to 0.6 mm, considering each layer of label is about 0.1 mm thick. Taking these two conditions into consideration, the actual diameter of a test tube with labels is a range rather than a specific value. The possible minimum value of it is the minimum diameter of the test

tubes without labels. The maximum limitation is the sum of maximum diameter of the test tubes and the thickness of six layers labels, which is about 0.6 mm. Thus, if a measured value of the diameter is located within the range of a test tube, the type of tube must be considered a possible candidate. Tightening the caps to different levels has shown to result in variations between 0 to 1 mm. Therefore, any test tube having a length within this range will be seen as the same type of test tubes.

The sources of casual errors are the changes of environment or hardware during detection. For example, instability of the power supply may lead to an intensity change of the light sources, possibly resulting in blurred images. Another example is the distortion of the acquired image due to thermal expansion of the image sensor, which affects the pixel-based measurement method used.

The last error source is system error. It is attributable to the principle and setup of the system. For example, when an image is processed to increase contrast and reduce noise, different methods or parameters will result in images in which the object edges vary. The aberration caused by the lens unit also creates deformation of the shape in an image. And finally, the inaccuracy of the conversion ratio between pixel and dimension will lead to errors as well.

Because the casual and sample errors cannot be eliminated in the measurement process, the method to identifying the test tube must be able to tolerate them. To enhance the robustness of the identification system, the method using a single threshold to judge the type of test tube is replaced by a range threshold method. In this method, the similarity degrees of the samples and one type of test tubes is used to determine the type of test tubes. If the measurements results of a test tube are outside yet close of the

theoretical range of a type of tube, the dimension of this tube should be regarded as a potential match rather than disregarding it. On the other hand, if the measurement results are far from the dimension range of a type of tube, the system must recognize the tube as a mismatch.

Based on the above principle, a fuzzy logical determination is introduced in the system. Each measurement result is assigned a fuzzy number from 0 to 1 regarding the similarity degree between it and the characteristic value of a specific tube feature.

The characteristic data file of different test tubes is created based on manual measurement results before the detection. In the data file, the maximum and minimum manually measured values of each characteristic are used to indicate the dimension range of each tube feature. When the measurement value is located inside the range, the fuzzy number1 is assigned to this condition. Another range is set by relaxing the restrictions of the actual dimension range with a measurement uncertainty value on both sides of the actual range, referred to as the allowance range. When a measurement result is located inside the allowance range but outside of the actual dimension range, a fuzzy number, which is bigger than 0 and smaller than 1, is offered to this condition. The value depends on the deviation of measurement result from the actual dimension range. When a measurement result is located outside of the allowance range, the fuzzy number is assigned as 0. These two kinds of ranges are described by four values for each dimension in the data file. The shape function of the fuzzy set membership is specified as a trapezium, as shown in Fig. 6-7. Because the function is described by a series of linear equations, a specific measurement result can easily retrieve the fuzzy number.

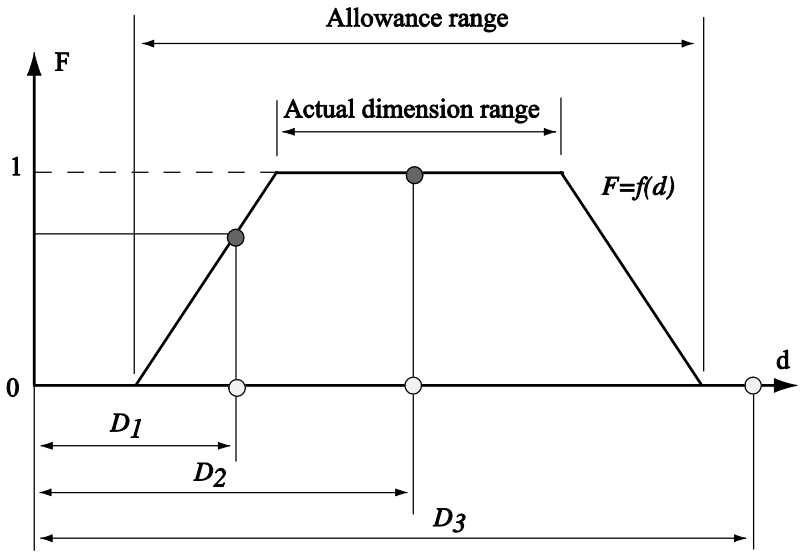

Fig. 6-7 The trapezium shape function to set the fuzzy number for measurement results.

The fuzzy number of a measurement value represents the degree of a match to a type of test tube. As shown in Fig. 6-7, when the value D_1 is located inside the allowance range but outside of the actual dimension range, its fuzzy number is given by the equation that describes the sloped line from 0 to 1. D_2, on the other hand, is located inside the actual dimension range, and therefore will have a fuzzy number of 1. If D_3 is a measurement value outside of the allowance range, its fuzzy number will be set to 0.

During the detection, several dimensions of tube features are measured. Each dimension result, such as the tube length, is evaluated against the relevant characteristic dimension of all possible types of test tubes. After evaluations, the measurement result is assigned a series of fuzzy values corresponding to the similarity degrees of all types of test tubes for a given feature. These values create a fuzzy set and its elements are arranged along with the sequence of test tubes stored in the data file. Then all sets of

different features are combined together in a fuzzy matrix. In it, each element represents one similarity degree of a specific feature between the detected sample and a corresponding type of test tubes. Each column of this matrix represents one given characteristic of all types of tubes. Each row of this matrix represents a specific type.

After assembling the matrix, a fuzzy logical determination is conducted to identify the type of test tube. The determination process includes several steps.

First, a weight vector is set by deciding the character importance to identification of test tubes. As mentioned previously, because the length and diameter of test tubes can be measured with better accuracy than the cap diameter, they are assigned a larger weight factor than the cap diameter.

Next, the weight vector is used to evaluate the fuzzy matrix. This step creates a set representing the similarity between the sample and different types of test tubes. The element value depends on the similarity degree of the feature. The more similar a feature appears, the bigger this value becomes, and vice versa. Finally searching the maximum element value in this set is the key factor that identifies the type of tube.

6.4.6 Results output

Prior to the tube identification process, samples will pass through a barcode reader. The barcode attached to the outside of the tube carrier will be read and sent to a computer. A program will combine the identification result and the sample information to a text file and send it out by a serial port using a specific format.

6.5 Hardware and software

6.5.1 Hardware setup

An identification system is designed as shown in Fig. 6-8.

It is composed of 6 parts, a camera and its support stage, a light source, a background, a robotic system, a shield box and a computer system.

A functional prototype is set up as shown in Fig. 6-9. It uses a stage to replace the robotic system to handle test tubes.

6.5.1.1 Camera and its support stage

The digital camera is the core of the hardware in a machine vision system. It integrates a lens unit and a sensor together. The resolution and degree of image aberration are its main characteristics. A camera with a higher resolution and well-designed lenses can obtain a higher quality image and better measurement results, but at increased cost. Here, a common webcam (Lianyingshuangshuang V1) is used as an image detector in the prototype of system. It can acquire a color image with max 640×480 pixels resolution. This camera is mounted on a support stage with 3 degrees of freedom (DOF). The stage can be rotated around the x- (roll), y- (pitch), and z-axis (yaw), allowing for easy camera alignment.

The image captured by this camera is rectangular in shape with a resolution of 640×480 pixels. To use the sensor of the digital camera most effectively, the image of the tube will be taken along the wide direction of the sensor and the diameter of the tube will be taken in its narrow direction. To ensure that the system can detect all of the samples encountered in the lab, the entire profile of the longest tube among the samples must fit inside the image while simultaneously maximizing the size of the object to obtain the largest possible pixel count for each feature.

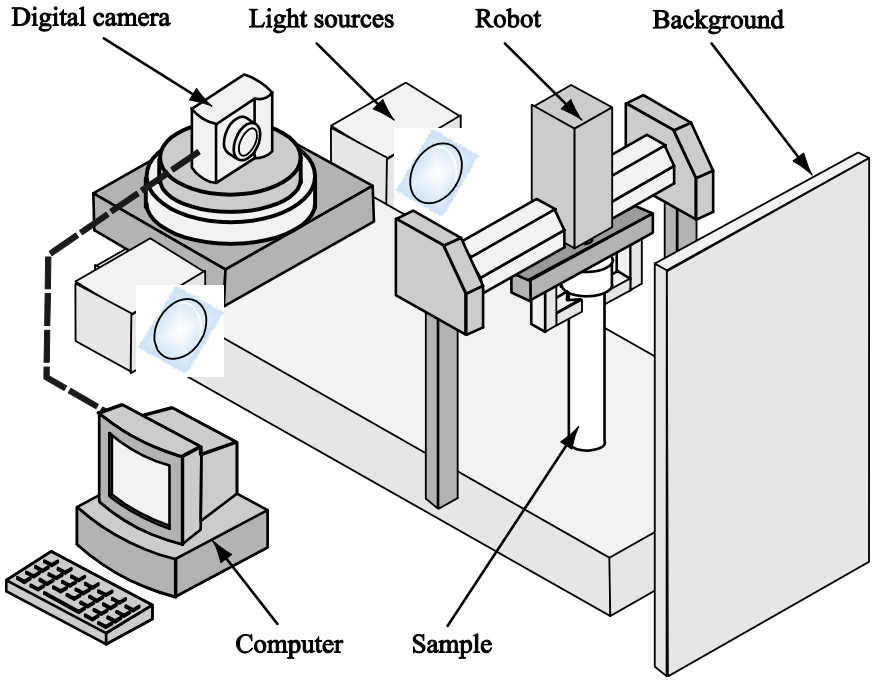

Fig. 6-8 Scheme of designed machine vision system. Not shown is a shield box used to shield outside interference.

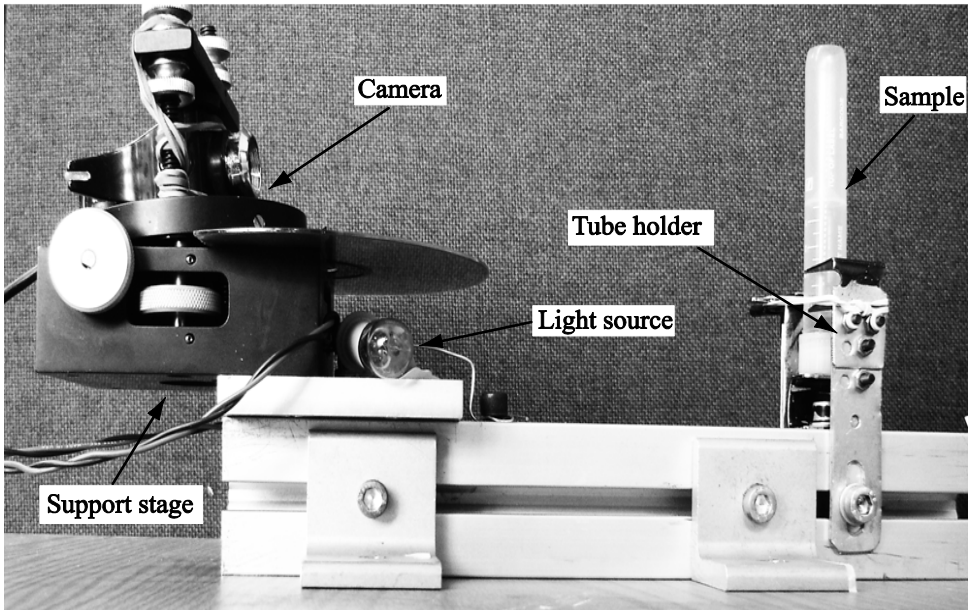

Fig. 6-9 Prototype of designed machine vision system.

6.5.1.2 Light source

The light source is another critical part of the machine vision system. A well designed and arranged light source can illuminate the object evenly, thereby avoiding image blurring and shades, which helps to increase the accuracy of the detection process.

The most efficient way to arrange the light source would be to make it coaxial with the camera. Since this is difficult to achieve, the prototype uses two light sources (GE 12V) that are mounted just left and right of the camera. This creates an illumination that is close to being coaxial while the overlap between the two illuminations eliminates shading of the background.

6.5.1.3 Background

To simplify the image processing, a black board is mounted behind the samples as a background. This helps the software to distinguish the sample efficiently. In order to decrease the effect of the shade that is created by the non-coaxial illumination, the background is mounted at a distance of at least 60 mm behind the sample and therefore far away from the image plane on which the camera is focused.

6.5.1.4 Robotic system

The test tube is held by a robotic gripper that carries it vertically to a specific position. After inspection, the gripper will return the tube to its carrier. The gripper is aligned such that the center axis of the tube is aligned with the optical axis of the camera. In the prototype, the robotic system is replaced by a tube holder with a V-shaped clamp.

6.5.1.5 Shield box

A shield box, not shown in Fig. 6-9, is used to prevent interferences from environmental light. Because this system will work in a lab, the outside environment is complex. Changes of other light sources will affect the quality of the image, which may affect the detection outcome. To avoid this interference, a box, with the inside painted black to avoid reflections, is mounted to cover the system.

6.5.1.6 Computer

A computer is used to perform the identification process using a LabVIEW program. First, it receives the acquired image from the digital camera. Next, it will process and analyze these images, and detect geometric proprieties of samples. By comparing the sizes and shapes of samples with the characters of standard samples, it will identify the types of test tubes. Finally, it will send out the inspection results to another computer.

6.5.2 Software and programming

All the detection process is controlled by a program running on a computer. This program is coded by LabVIEW and Matlab.

6.5.2.1 LabVIEW

LabVIEW is software developed by the National Instruments Corporation to imitate physical instruments. It can conduct complex operations such as sampling and displaying by assembling a graphical code. It also includes numerous tool boxes to

simply the programming. NI-Vision is one of these tool boxes to realize the functions of capturing and processing of images.

In this project, a LabVIEW program captures the image through a webcam, preprocesses the image, and identifies the profile of samples. Simultaneously, it shows the test tube and its profile on the computer screen with highlighted outlines.

LabVIEW also has a communication tool box that contains functions to read and write data through RS232 serial ports. In this program, these functions are used to send the results to the next step.

6.5.2.2 Matlab

While the graph program of LabVIEW is well suited to control the hardware and acquire data, its ability to analyze data and conduct cpu-intensive calculations is limited. Owing to powerful ability to handle matrix calculation very efficiently, Matlab is used to analyze the data and perform the identification functions in this project.

To integrate the Matlab functions, LabVIEW has two simple methods to run a Matlab program. The first method runs Matlab functions in Mathscript node. The second method calls the Matlab program as a function. Mathscript node works as a complier of Matlab. Most Matlab functions can run this way without having Matlab installed on the local computer.

The more complex Matlab functions, which cannot run in Mathscript node, can be called by the main LabVIEW program and executed in the background. Under this condition, Matlab must be installed on the local computer.

Because the Matlab functions used in this project are relatively simple, a Mathscript node is embedded in the program.

6.6 Experiment of machine vision

Several experiments were conducted to verify this system. The first tested the precision of the dimension measurements. The second tested all possible test tubes collected and verified the entire system.

6.6.1 Verifying measurement precision

This experiment was set up to test the dimension measurement function of the machine vision system. It tested the accuracy and measurement uncertainty range of the measurement. In this experiment, a standard test tube without labels was tested. The machine vision system measured the dimension of the test tube profile. The results were compared with the actual size of the test tube. The error and error source were analyzed.

6.6.1.1 Experiment set up

A standard test tube without labels was measured as the sample. The shape of the tube is not a perfect cylinder. Instead, the diameter near the top was measured as 15.2 mm while the diameter near the bottom measured 14.9 mm. The tube length measured 96.1 mm with the standard cap screwed on tightly. The average diameter of the cap is 17.8 mm. The test tube is translucent, and the color of the cap is white. A digital caliper (CD-6” CS, made by Mitutoyo Corp.) was used to measure the dimension of the test tube manually.

The function prototype shown in Fig. 6-9 measured the dimension by machine vision.

6.6.1.2 Experiment process

This experiment consists of two main parts. One is manual measurement of the test tube and cap dimensions. The second part is to detect the same parameters by the machine vision system.

During the first step of the experiment, the sizes of the test tube and its cap are measured 30 times respectively by a digital caliper (CD-6" CS, made by Mitutoyo Corp.). The mean value and 3 standard deviations of the dimension are calculated. Then the sample is measured by the machine vision system.

First, the test tube is placed on a support system, making sure that the top of its cap fully contacts the stage surface. After it was mounted at the correct position, light sources are turned on, and the shield box is closed. Then, the machine vision system conducts the detection. The digital camera captures the image of the test tube and sends it to a computer. The LabVIEW program detects the size and shape of the test tube.

Finally, the program saves the results of the detection to a file. The test tube is removed from the identification position and remounted to the tube holder. This randomizes the gripper position in order to obtain statistically relevant results. 40 tests are conducted in this experiment.

6.6.1.3 Results and analysis

The test results are collected and analyzed. Three main dimensions of the test tube are measured both by the machine vision system and a caliper. The measurement results of the length and diameter of the test tube, and the diameter of its cap, are averaged

respectively. Standard deviations and their 3 σ ranges are calculated. The distribution of the measurement results are plotted in Fig. 6-10.

Fig. 6-10a), c) and e) show the mean values and 6 σ ranges of results measured by the machine vision system and a digital caliper. The mean values measured by the two methods have a small difference. This is caused by the calculation error when translating the image pixels to an actual size. The machine vision system has a slightly bigger 6 standard deviation range than that measured by a digital caliper. It indicates that the machine vision system has very good repeatability close to that of a digital caliper.

To improve the accuracy of the identification, the data file of features is modified to match the actual measurement of machine vision. In Fig. 6-10b), d) and f), the data measured by the caliper is shifted by a small amount to yield overlap between the measured data of both methods. Thus, if one considers the average results measured by the caliper as actual values, the length measured by the machine vision system only has a ±0.3 mm standard deviation range. The test tube diameter measured by the system is located between the max value and min value of the actual size, with ±0.2 mm 6 σ ranges. The diameter of the cap has a bigger error range of about ±0.9 mm.

By analyzing the testing results of this experiment, two aspects of detection need to be taken into consideration. The first aspect involves the shift of the mean value. In Fig. 6-10 a), c), all average values of the machine vision results are less than the mean value of the manual measurements during this experiment. The second aspect is the bigger error range of the measurement results of the cap.

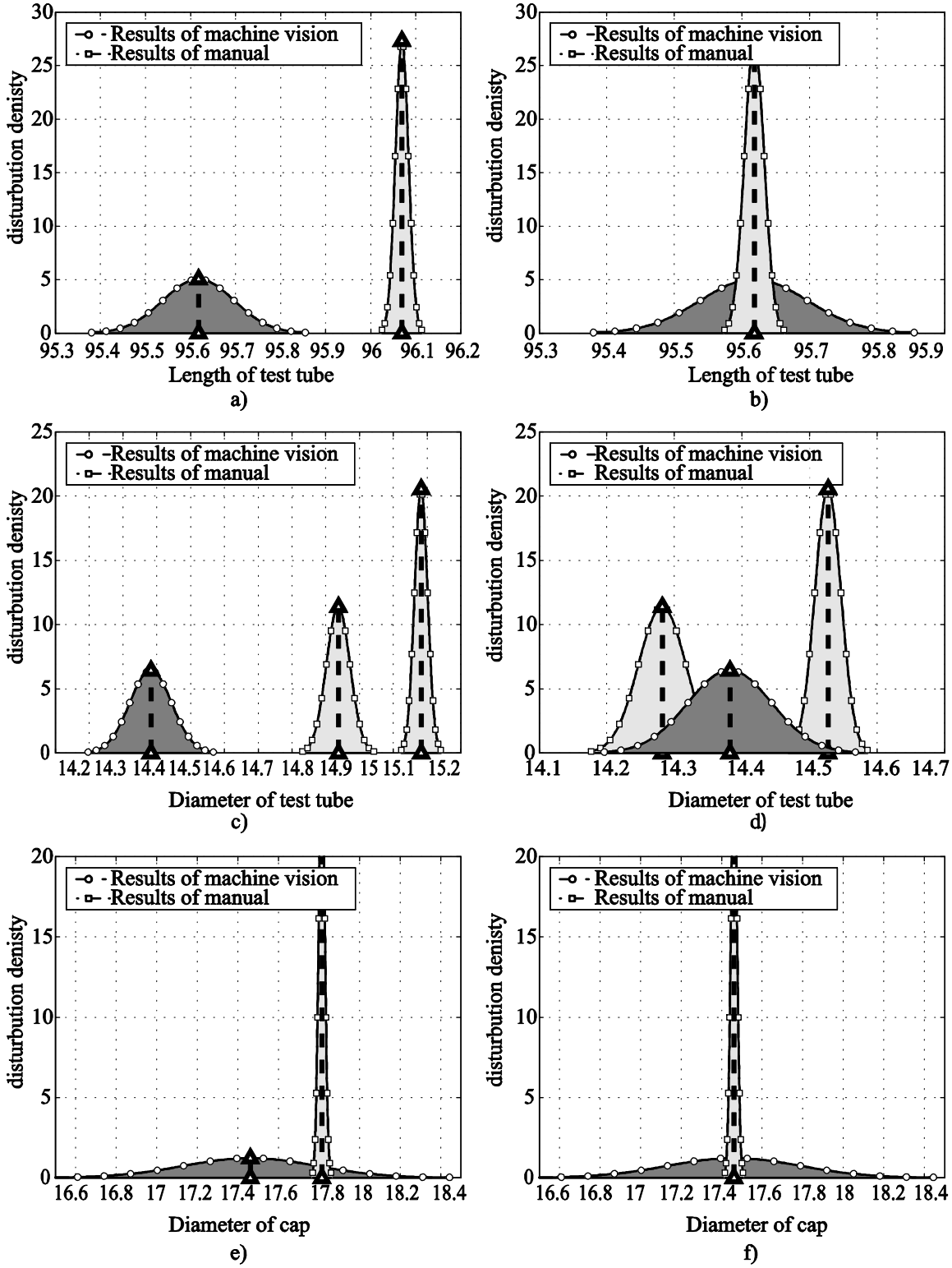

Fig. 6-10 The mean value and ±3 σ range of the test tube diameter, which are measured by a caliper or machine vision system.

To avoid the determination error caused by these issues, two methods were used to improve the accuracy of the identification. First, the data file of the test tubes will be created by the results measured by the machine vision system. Second, because the error ranges of the test tube diameter and length are smaller than that of the cap diameter, the weight factors for the fuzzy determination parameters for the diameters and lengths of the test tubes are set to larger values compared to the weight factor assigned to the cap diameter.

6.6.2 Testing all available test tube types

This experiment is conducted to verify the system capability of identifying the types of test tubes. All types of test tubes, which were collected from the inspection line of the Core Lab, were tested in this experiment. The data file was created using the machine vision measurement results rather than the original results measured by caliper. Every type of test tubes was tested 30 times. The test results were recorded and analyzed.

6.6.2.1 Experiment set up

Fifteen types of test tubes with caps listed in Table 6-1 were tested in this experiment. The test tubes are covered with different layers of labels from 1 to 3 randomly as shown in Fig. 6-11.

The functional prototype shown in Fig. 6-9 identifies the type of each test tube by machine vision and fuzzy logic determination.

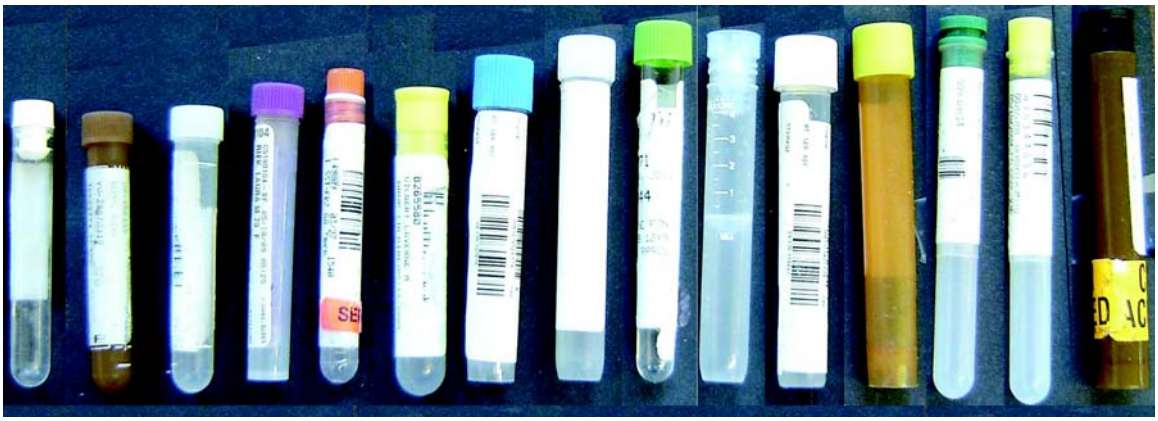

Fig. 6-11 15 types of test tubes with caps were tested in the experiments

6.6.2.2 Experiment process

During this experiment, each type of test tube was tested 30 times. The test tubes were remounted randomly after every determination to simulate variations of the holding position. Every time the test operated followed the same steps.

First, test tubes are fixed on the testing stage randomly. The shield box is closed to prevent the environment noise. The light sources are turned on to illuminate the samples, waiting for several seconds, and making sure the light output is stable.

The program runs once to identify the type of test tubes. Test results are shown on the screen of a computer and recorded to a file. After every test, the test tube is removed from the testing position and remounted for a next test.

6.6.2.3 Results and analysis

After a total of 420 measurements, the test results were collected and analyzed. When the identification failed, the wrongly identified tube type together with the number of misidentifications was recorded and listed in Table 6-2.

Table 6-2 Results of system verification

Type of test tube	Testing number	Number of success	Ratio of success	Wrong type and number
1	35	34	97.14%	13(1)
2	35	35	100%	
3	35	35	100%	
4	35	35	100%	
5	35	35	100%	
6	35	35	100%	
7	35	35	100%	
8	35	35	100%	
9	35	34	97.14%	4(1)
10	35	35	100%	
11	35	35	100%	
12	35	34	97.14%	9(1)
13	35	35	100%	
14	35	35	100%	
15	35	35	100%	
Total	525	522	99.43%	

The results of the experiment are listed in Table 6-2. From the results, the identification system can detect the type of tube with a reasonable reliability.

6.7 Conclusions and future work

In this chapter, a machine vision system, which can identify the type of test tubes, is introduced. The detection principle is presented, and the mathematic methods are explained.

A functional prototype of machine vision system was set up, and a LabVIEW program was coded to identify the types of test tubes. A dimension data file of test tubes was created. This system consists of 6 parts, a camera and its support stage, light sources,

background, a robot system, a shielding box and a computer system. The digital camera captures the image of a test tube and sends it to a computer. A LabVIEW program running on the computer extracts the features of the test tube by detecting the edges of the tube profile while compensating the optical distortion from the perspective. Next, a fuzzy logical determination identifies the type of the test tube based on the measured features and a dimension data file of test tubes. Final results are sent out to another computer.

A series of verification experiments were conducted. From the experiment results, the system worked well for the 15 different types of tubes collected at ARUP.

In future work, efforts in several aspects may improve the performance of system. A high-resolution digital camera will increase the precision of the detection. A well-designed lens system for the digital camera can reduce the aberration of the image. Using an invisible light source and detector may eliminate the effect of sample color.

6.8 References

Baldwin, J. F. (1996). *Fuzzy logic*, UNICOM; J. Wiley and Sons, Chichester, West Sussex, England ; New York.

Bir, B., Yingqiang, L., Jones, G., and Jing, P. (1999). "Adaptive target recognition." *Proceedings of IEEE Workshop on Computer Vision : Beyond the Visible Spectrum - Methods and Applications,* IEEE Comput. Soc, Los Alamitos, CA, USA, 71-81.

Bockstein, I. M. (1986). "Color equalization method and its application to color image processing." *Journal of the Optical Society of America A (Optics and Image Science)*, 3(1986), 735-737.

Brejl, M., and Sonka, M. (1998). "Edge-based image segmentation: machine learning from examples." *Proceedings of ICNN '98 - International Conference on Neural Networks,* IEEE, New York, NY, USA, 814-819.

Canny, J. (1986). "A computational approach to edge detection." *IEEE Transactions on Pattern Analysis and Machine Intelligence*, PAMI-8(1987), 679-698.

Carbonetto, P., Dorko, G., Schmid, C., Kuck, H., and De Freitas, N. (2008). "Learning to recognize objects with little supervision." *International Journal of Computer Vision*, 77(2008), 219-237.

Caria, M. (2000). *Measurement analysis: an introduction to the statistical analysis of laboratory data in physics, chemistry and the life sciences*, Imperial College Press, London.

Chu, B., Jung, K., Chu, Y., Hong, D., Lim, M.-T., Park, S., Lee, Y., Lee, S.-U. K., Min Chul, K., and Kang Ho, K. (2009). "Robotic automation system for steel beam assembly in building construction." *4th International Conference on Autonomous Robots and Agents, ICARA 2009,* Inst. of Elec. and Elec. Eng. Computer Society, Wellington, New Zealand, 38-43.

Cypher, R., and Sanz, J. L. C. (1989). "SIMD architectures and algorithms for image processing and computer vision." *IEEE Transactions on Acoustics, Speech and Signal Processing*, 37(1990), 2158-2174.

Dainty, P., Boyce, J. F., Dimitropoulos, C. H., Edmundson, P., Toulson, D. L., and Bernhardt, M. (1999). "Dual-band ATR for forward-looking infrared images." *Proceedings of IEEE Workshop on Computer Vision : Beyond the Visible Spectrum - Methods and Applications,* IEEE Comput. Soc, Los Alamitos, CA, USA, 23-29.

Davies, E. R. (2005). *Machine vision : theory, algorithms, practicalities*, 3rd Ed., Elsevier, Amsterdam ; Boston.

Davies, E. R. (2008). "A generalised approach to the use of sampling for rapid object location." *International Journal of Applied Mathematics and Computer Science*, 18(1), 7-19.

Deriche, R. (1988). "Fast algorithms for low-level vision." *9th International Conference on Pattern Recognition (IEEE Cat. No.88CH2614-6),* IEEE Comput. Soc. Press, Washington, DC, USA, 434-438.

Fathy, M., Siyal, M. Y., and Darkin, C. G. (1994). "A low-cost approach to real-time morphological edge detection." *Proceedings of TENCON'94 - 1994 IEEE Region 10's 9th Annual International Conference on: `Frontiers of Computer Technology'* , IEEE, New York, NY, USA, 759-762.

Flemmer, R. C., and Bakker, H. (2009). "Generalised object recognition." *2009 4th International Conference on Autonomous Robots and Agents* , IEEE, Piscataway, NJ, USA, 363-368.

Georgieva, A., and Jordanov, I. (2009). "Intelligent Visual Recognition and Classification of Cork Tiles With Neural Networks." *IEEE Transactions on Neural Networks*, 20(4), 675-685.

Habets, R. (2002). "Machine vision for automatic inspection in food processing industry." *ACIVS'2002: Advanced Concepts for Intelligent Vision Systems*, Univ. Gent, Gent, Belgium, 6-10.

Harris, J. (2006). *Fuzzy logic applications in engineering science*, Springer, Dordrecht, Netherlands.

He, X., Jia, W., and Wu, Q. (2008). "An approach of canny edge detection with virtual hexagonal image structure." *2008 10th International Conference on Control, Automation, Robotics and Vision, ICARCV 2008*, Inst. of Elec. and Elec. Eng. Computer Society, Hanoi, Vietnam, 879-882.

Hou, Z. J., and Wei, G. W. (2002). "A new approach to edge detection." *Pattern Recognition*, 35(2002), 1559-1570.

Jimenez, A. R., Ceres, R., and Pons, J. L. (1999). "A machine vision system using a laser radar applied to robotic fruit harvesting." *Proceedings of IEEE Workshop on Computer Vision : Beyond the Visible Spectrum - Methods and Applications*, IEEE Comput. Soc, Los Alamitos, CA, USA, 110-119.

Joo, H., and Haralick, R. M. (1989). "Understanding the application of mathematical morphology to machine vision." *1989 IEEE International Symposium on Circuits and Systems (Cat. No.89CH2692-2)*, IEEE, New York, NY, USA, 977-982.

Khabou, M. A., Gader, P. D., and Keller, J. M. (1999). "Morphological shared-weight neural networks: a tool for automatic target recognition beyond the visible spectrum." *Proceedings of IEEE Workshop on Computer Vision : Beyond the Visible Spectrum - Methods and Applications*, IEEE Comput. Soc, Los Alamitos, CA, USA, 101-109.

Kochan, A. (2002). "Machine vision guides the automotive industry." *Sensor Review*, 22(2002), 119-124.

Lindeberg, T. (1998). "Edge detection and ridge detection with automatic scale selection." *International Journal of Computer Vision*, 30(1999), 117-154.

Manjunath, B. S., and Chellappa, R. (1991). "A computational approach to boundary detection." *Proceedings 1991 IEEE Computer Society Conference on Computer Vision and Pattern Recognition (91CH2983-5)*, IEEE Comput. Sco. Press, Los Alamitos, CA, USA, 358-363.

Mehrotra, R., and Shiming, Z. (1996). "A computational approach to zero-crossing-based two-dimensional edge detection." *Graphical Models and Image Processing*, 58(1996), 1-17.

National_Instruments. (2008). "NI Vision Concepts Manual."

Scribner, D., Warren, P., and Schuler, O. (2000). "Extending color vision methods to bands beyond the visible." *Machine Vision and Applications*, 11(6), 306-312.

Silva, L., Bellon, O. R. P., and Gotardo, P. F. U. (2001). "Edge-based image segmentation using curvature sign maps from reflectance and range images." *Proceedings 2001 International Conference on Image Processing*, IEEE, Piscataway, NJ, USA, 730-733.

Strand, T. C. (1988). "Optical processing for machine vision." *1988 IEEE International Symposium on Circuits and Systems. Proceedings (Cat. No.88CH2458-8)*, IEEE, New York, NY, USA, 1071-1073.

Strehl, A., and Aggarwal, J. K. (1999). "Detecting moving objects in airborne forward looking infra-red sequences." *Proceedings of IEEE Workshop on Computer Vision : Beyond the Visible Spectrum - Methods and Applications*, IEEE Comput. Soc, Los Alamitos, CA, USA, 3-12.

Strzecha, K., Fabijanska, A., and Sankowski, D. (2006). "Application of the edge-based image segmentation." *Perspective Technologies and Methods in MEMS Design - 2nd International Conference of Young Scientists, MEMSTECH 2006*, Institute of Electrical and Electronics Engineers Inc., Lviv-Polyana, Ukraine, 28-31.

CHAPTER 7

CONCLUSIONS AND FUTURE WORK

7.1 Conclusions

Detecting the level or volume of biomedical samples in opaque tubes is one of the most important steps in an automated testing process.

A method based on the different optical properties of labels, test tube and aqueous medical samples was developed. It uses two laser beams with 980 nm and 1550 nm peak wavelengths as the light sources. By comparing the power ratio of the transmitted light, this method can eliminate the effect of labels.

In this research, a model was created that simulated the scanning process of samples with a meniscus. A ray tracing method was used to calculate the change of transmitted power during the scanning process. The simulation results were verified by an experiment.

Two application devices were designed based on the optical method. The Max/Min Level Detection System can identify the presence of the aqueous medical sample in standard test tubes, which were covered by up to six layers of labels, at two fixed position. The measurement result can reach ±0.1 mL uncertainty of measurement with a level of confidence of 99.73%. The Variable Volume Detection System can detect the surface of the aqueous medical sample by scanning the entire height of the test tubes.

Combined with the inner geometric size of the test tube, it can determine the volume of the liquid sample in the test tube.

Based on the optical effect of the meniscus, a method was developed to improve the measurement accuracy of the Variable Volume Detection System. The top edge and the bottom of the meniscus are acquired by finding the intersection point of the fitted lines.

To retrieve the inner geometric size of test tubes, a Machine Vision system was developed to identify the type of test tubes. This system measures the feature characteristics of test tubes by edge detection and modification. Using a Fuzzy detection method, the types of test tubes are identified based on the measurement result and the pre-measured feature characteristics of different test tubes.

7.2 Future work

For the Variable Volume Detection System, several improvements are suggested. The first suggestion is the elimination of the offset between the detection and reference beam. This can be achieved with a dual-band detector whose two photo diodes are sensitive for one wavelength but very insensitive for the second wavelengths and also vice versa. By eliminating the offset, the lift-up distance of the detection system decreases, and the detection times become shorter accordingly. By using a dual band detector, one detector and its optical accessories can be omitted. Thus, the cost of hardware will drop too. Furthermore, a single beam detection system will not require the storage of the transmitted powers together with the position of the tube. This eliminates the need for complex array manipulations. After finishing the new design, the detection

system will need to be integrated with a robotic device that can be installed on the track at ARUP.

Another possible improvement is the Machine Vision System whereby the system would work on transmitted rather than reflected light. If the light source operates in the infrared range between 1400 and 1600 nm, due to the large attenuation by the liquid, the profile of the liquid will be projected to a CCD sensor. By analyzing the geometric size of the projection image, the cross-section size of the liquid along the axis of the test tube can be measured. Furthermore, the volume of the liquid can be calculated by the measurement results of the 2D outline. This method can decrease the detection time of the system by integrating two detection steps into one.

To increase the robustness of the detection system, a white light could be used as a light source. By analyzing the power change of the light at different wavelengths instead of only two wavelengths, the liquid presence and interferences contained in the liquid can be detected with higher accuracy and reliability.